AN INVESTIGATION OF NON-STANDARD ANGLE COMPOSITE LAMINATE DESIGN

A dissertation
presented to
the Academic Faculty

by

Gaurav M. Batra

In Partial Fulfillment
of the Requirements for the Degree
Master of Science in Mechanical Engineering in the
School of Mechanical Engineering

Georgia Institute of Technology
May 2018

AN INVESTIGATION OF NON-STANDARD ANGLE COMPOSITE LAMINATE DESIGN

Approved by:

Dr. Jonathan S. Colton, Advisor
School of Mechanical Engineering
Georgia Institute of Technology

Dr. Kyriaki Kalaitzidou
School of Mechanical Engineering
Georgia Institute of Technology

Dr. John Muzzy
School of Chemical and Biomolecular Engineering
Georgia Institute of Technology

Date Approved: February 16, 2018

ACKNOWLEDGMENTS

This project has been incredibly challenging and rewarding. I would like to thank my advisor Dr. Jonathan Colton for an amazing opportunity. His guidance throughout the project has been invaluable. My approach to engineering and problem solving in general has been greatly enriched as a result of his insight. I would like to thank Dr. Abe Gissen from Boeing for his input on the project. I would like to thank the GT-Boeing Strategic University Partnership Program for funding this project. I would like to thank my lab-mates Ahmed Aly and Su Yu for their input and availability in times of stress. This project would not have been possible without their support. I would like thank the undergraduate assistants Matias Giradi, Harshkumar Tapara, and Kaie Westmass for their untiring efforts. I would like to thank my thesis committee members Dr. Kyriaki Kalaitzidou and Dr. John Muzzy.

I would like to thank my friends from the graduate student community at Georgia Tech. Their willingness to share knowledge and drive to learn have inspired me beyond words. Finally, I'd like to thank my family; no words can convey my gratitude to my parents and sister.

TABLE OF CONTENTS

LIST OF TABLES

LIST OF FIGURES

LIST OF SYMBOLS AND ABBREVIATIONS

NS	Non-Standard
VAT	Variable Angle Tow
OHC	Open Hole Compression
$C_{\alpha\beta}$	Elastic Tensor
CLT	Classical Laminate Theory
U_i	Stiffness Invariant
[A]	In-plane laminate stiffness matrix
[B]	Coupling Stiffness matrix
[D]	Bending Stiffness matrix
N_{ij}	Force Resultant
M_{ij}	Moment Resultant
$[\epsilon^0]$	Mid-plain strains of laminate
$[\kappa]$	Curvature of laminate
S_{LC}	Longitudinal Compressive Strength
S_{Lt}	Longitudinal Tensile Strength

S_{Tt}	Transverse Tensile Strength
S_{LTS}	Shear Strength
FPF	First Ply Failure
$[T_1]$	Rotation Tensor

SUMMARY

Carbon Fiber Reinforced Plastics (CFRP) have become indispensable structural materials in the aerospace industry. They offer much higher specific stiffness and strength compared to the aluminum alloys that they have come to replace. The ability to tailor the stiffness and strength of composite laminates is a unique advantage over metals allowing for optimization at the material level.

The ability to tailor the stiffness and strength for applications has been limited by the standardization of laminate design by the aerospace industry. Laminate design has been standardized into a set of rules, which limit the options available to a designer. Current laminate design allows for alignment of fiber reinforcement along only four standard directions. Other restrictions such as symmetry about the mid plane and balance are also strictly enforced. This thesis studies the effects of using non-standard (NS) angles for the ply orientation when designing a laminate.

To develop NS designs that can be easily compared with standard designs, this study proposes a stiffness matching method. This method allows one to design non-standard laminates that match the in-plane stiffness of standard composite layups. This method has been validated against a stiffness matching method proposed prior to this work.

NS designs that match the stiffness of a typical wing skin layup were developed based on the stiffness matching method proposed in this thesis. The theoretical strengths of these NS designs were calculated based on First Ply Failure (FPF) theory. Based on the significantly improved theoretical strengths of the NS designs when compared to the standard wing skin design, physical samples of the standard and NS designs were fabricated and tested.

As notched compressive strength is often the limiting factor in composite structures, Open Hole Compression (OHC) testing has been carried out on non-standard and standard designs. The failure modes and failure strengths for the designs were analyzed. The NS designs were observed to be weaker due to fiber discontinuity. Modifications to the testing method have been proposed for accurate characterization of the strength of NS laminates

CHAPTER 1

INTRODUCTION

1.1 Laminate Design in the Aerospace Industry

Composite materials have been used by mankind for centuries. From the composite bow used by the Mongols to tow steered composites at the cutting edge today, the use of composites as structural materials has grown as the understanding of their capabilities and failings has improved.

As composites started replacing metals in aircraft structures, laminates were designed to mimic the behavior of metals, which are isotropic materials. This philosophy of using "quasi-isotropic" laminates that behave similar to metals has resulted in engineers treating composites as 'black aluminum' [25]. This practice has worked well to ease the transition from metal to composite structures. These practices however limit the extent to which composites can be tailored to best fit their intended uses.

In the 1960's, the aerospace industry agreed upon a set of rules for the design of laminate materials [1]. These rules have been found to be robust and act as vital guidelines for designers. These rules require all laminate designs to maintain symmetry and balance, and exclusively use standard angled fiber reinforcement. These rules have been found to limit the potential of laminate materials [1]. This work will focus on the orientation of the fiber reinforcement within laminates.

At present, one of the fundamental rules of laminate design is the use of four standard angles when designing a composite layup, as shown in Figure 1.1. These angles are 0˚, 45˚, -45˚ and 90° [2], with 0˚ being the expected primary loading direction. A typical standard angled laminate is shown in Figure 1.1. The laminate in Figure 1.1 follows all of the rules prescribed by the aerospace industry. The fiber orientations are aligned along the standard angles. The laminate is "balanced," i.e., for every ply with an off-axis orientation θ, there is a corresponding ply with an orientation $-\theta$. The laminate is also symmetric about the mid-plane.

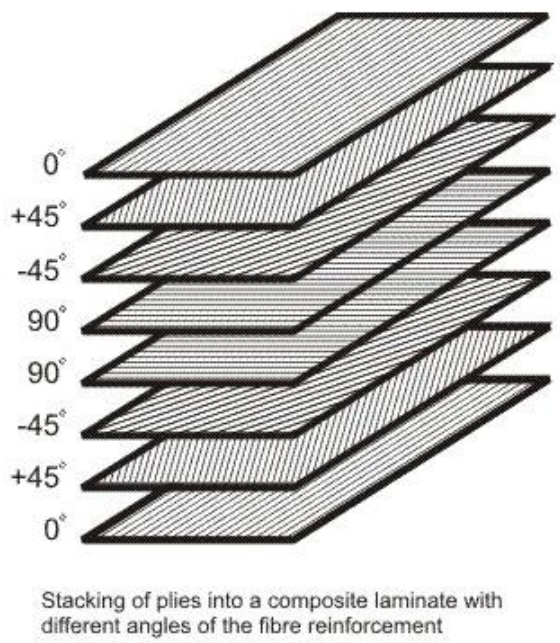

Figure 1.1 Standard angle laminate

These designs based on simple 0˚ ±45˚ /90˚ configurations were also used to broadly match the stiffness of aluminum alloys [28]. As effective as these standard practices are, the stringent use of only four angles limits the range of possible stiffness and strength combinations available when designing a composite material [7].

Lately there has been an increasing interest in moving past the entrenched rules towards non-standard laminates, those that do not follow the 0˚ +/-45˚ 90˚ laminate layup rules. Multiple studies have found various benefits of using non-standard angles [1], [7] and [30]. This thesis is a step in that direction.

Notches and holes in composites present challenges. Fastener holes often limit the operating strain in structures [27]. Drilled holes compromise the structure of composites as they lead to delamination and breakage of the fibers as the drill bit enters and exits the part [4]. On average, more than 12,000 holes are drilled into a single wing set during manufacture [13]. Hence, the strength of composite materials with stress concentrations is a central design issue often dictating the design allowables for the entire structure [20]. Any shift away from standard designs must consider the notched strength of the proposed designs and compare them with existing designs.

The current practice of dealing with notches and holes in composite structures is based on practices used for metals, whereby reinforcement and increased thickness around holes reduce stress concentrations. Figure 1.2 shows an example of annular reinforcement rings used to reinforce holes in laminated plates. These rings add additional weight and complexity to the structure. Stronger laminates could help eliminate these additional parts. The benefits of improved strength are two-fold: (a) lighter structures make the overall aircraft more efficient and (b) reduced material costs.

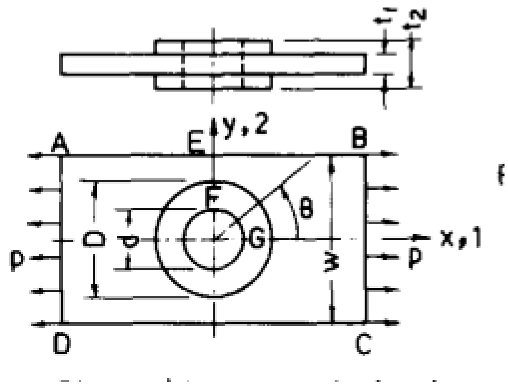

Figure 1.2 Reinforcement ring around a hole in a laminate plate [5]

These practices curtail the ability to utilize the unique opportunities presented by composites. The ability to orient fibers along the load paths that are present near notches has not been utilized to the maximum possible extent. Current laminates are restricted to the four standard angles, which may or may not align well with the stresses present at a notch.

To better tailor laminates for improved performance, two approaches are currently being investigated. The first is the use of angles other than standard angles, termed Non-Traditional/Non-Standard (NS) angles. NS designs are laminate designs in which the fiber reinforcement orientations are not constrained to the four standard directions [1]. Angles that conform better to the part geometries should improve fiber continuity. NS angles, such as ±23˚, can be paired with other angles, like ±80˚, to produce laminates that are better tailored for the specific part functionality

These laminates could be used to align the fibers with the shape of cut outs in any structure. This will allow better tailoring of the fibers to the stresses concentrated at the notch, thereby allowing for purposefully designed laminates for holes and notches. Based on the part geometry and application more suitable fiber orientations that are not limited to the four standard angles can be created. This opens up more opportunities to leverage the flexibility offered by laminate materials in terms of directional stiffness and strengths.

The second method is the use of tow steering, seen in Variable Angle Tow (VAT) composites. VAT composites are laminated materials in which the fiber reinforcement orientation varies over the plane of each ply, they exhibit variable stiffness [23]. Figure 1.3 shows the structure of a VAT laminate.

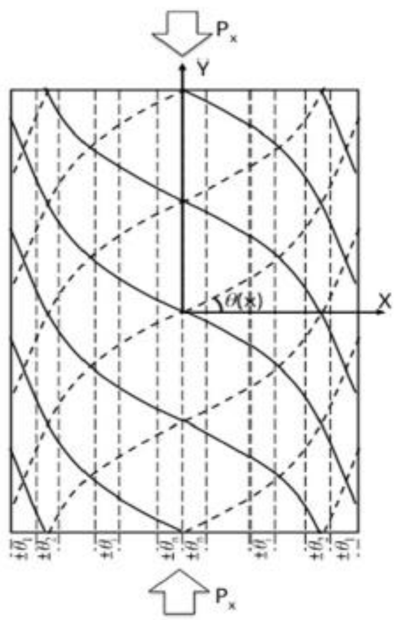

Figure 1.3 Variable angle tow composite schematic [6]

Even though VAT composites potentially offer upto 38% of weight savings over conventional designs [2] and have the maximum potential for tailoring stiffness and strength to expected load paths, their mechanics and analysis are more complex than unidirectional fiber reinforced laminated composites. Hence, extensive research is still required before they can be used as structural materials.

When stiffness is considered, NS angle composites allow for a larger design space when compared to standard angle composites [7]. This is demonstrated in Figure 1.4 where the range for possible in-plane responses for standard and NS designs are compared. The design space for a laminate can be defined in multiple ways. This thesis considers the range of in-plane stiffness responses. These responses depend on the orientation of fiber reinforcement, the stacking sequence of plies, and the individual contributions of each orientation towards the total laminate thickness.

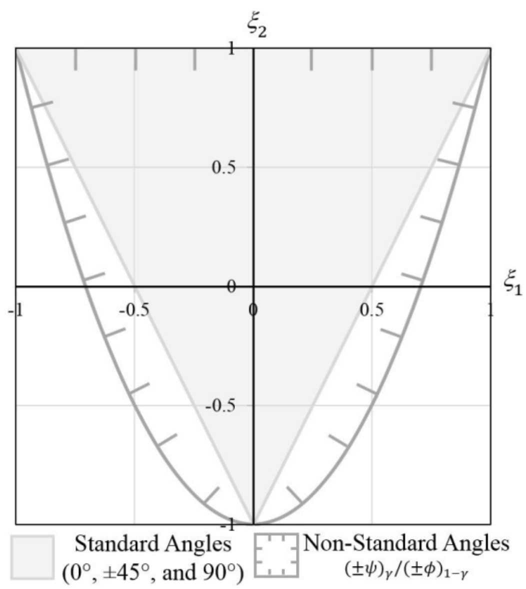

Figure 1.4 Comparison of in-plane stiffness design space [7]

However, the NS design space is more difficult to navigate as the possible number of laminate designs are infinite and a reasonable design space is required. To help transition from the standard angle design space to this larger possible design space, a benchmark for comparing current designs to possible future designs is required. Butler et al. [7] developed a mathematical formulation that computes a range of NS designs that match the in-plane stiffness of any given design. This is applied to three layups that are widely seen across the aerospace industry. It allows for a direct comparison between traditional and non-traditional layups and formed the basis of this thesis. NS designs that match the stiffness of standard designs will be able to perform the same functions as standard designs. Their only difference lies in the respective laminate strengths. NS designs can replace existing standard designs and help transition away from standard designs in the same manner that the “black aluminum” treatment of composites has helped in the transition away from metallic structures.

The strength of stiffness-matched NS designs with the strength of standard designs will be compared to the respective standard designs. Both sets of designs will have the same thickness, i.e., components made up of these laminates will have the same mass and stiffness. Hence the strengths of layups with the same mass and stiffness will be compared, thereby allowing one to determine if NS designs are stronger or weaker than standard designs. Stronger NS designs will allow for reduced ply and laminate thickness resulting in weight savings, which also leads to material cost reduction.

The primary goal of this thesis is to assess non-standard angle laminate designs and compare them to existing standard designs. The properties used for comparing the designs in this work are the stiffness and strength of the laminates. To aid this goal, NS designs that match the stiffness of existing standard designs were used.

Studies conducted on NS laminates by Butler [7] and by Tsai [1] highlight multiple advantages of using NS designs. However, the studies do not extend to the strength of these designs. The strength of these NS designs will allow one to estimate any change in the overall weight of structures made up from NS laminates when compared to existing standard designs.

1.2 Thesis Overview

Current standard laminate design practices have been very effective. These practices have made laminate design and analysis accessible. First, laminate theory will be presented. Next, the rationale behind standard laminate design will be discussed. This will help one appreciate the possible paths that can be taken, so that one may move beyond standard rules to a more optimal set of laminate design practices.

Chapter 2 provides a review of composite mechanics. The framework of this theory is used extensively in all subsequent chapters to develop and analyze layup designs. The motivations for stiffness matching are discussed in detail. Common methods used to perform preliminary analysis on layup designs are then discussed. These methods will be applied to compare existing standard designs to NS designs in chapter 4. The NS designs will be based on solutions from stiffness matching.

Chapter 3 details a method developed to design non-traditional laminates that match the in-plane stiffness of standard laminates. Stiffness matching has been performed to limit the possible designs being compared to standard designs. NS designs that match the stiffness of standard layups can be used to replace existing parts made of standard layups without affecting the overall aircraft design. Furthermore, it allows one to maintain constant stiffness regardless of laminate thickness. A detailed inquest into this method is carried out. The results of the method developed are checked against those found by Butler et al.[7] and good agreement is seen between both. This method is then extended to perform stiffness matching. This allows one to better control the thickness of a laminate which aids in reducing material costs. Detailed discussions on the benefits of stiffness matching are presented in the conclusions.

Initially, the method for stiffness matching are developed for a special case when both standard and NS designs have the same thickness, i.e., the same number of plies. This method is extended to perform stiffness matching when the NS design may or may not have the same thickness as the standard design. The solutions for both formulations are found to be identical, i.e., the solutions for stiffness matching are independent of the number of plies in the NS design.

Chapter 4 introduces the concept of stress distributions developed in a laminate under loading. This forms the framework for evaluating the First Ply Failure (FPF) loads for the layups being studied. The FPF approach is utilized to predict the ultimate strength of NS designs detailed in chapter 3 and contrasts them with the predicted ultimate performance of standard angle laminates. Theoretical strengths will help in performing an initial assessment of the performance of NS designs when compared to a standard design of the same stiffness.

Chapter 5 discusses experiments performed to investigate the Open Hole Compression (OHC) strength of the NS layups. OHC strength is used by the aerospace industry as the maximum allowable stress for most composite structures under compression. Experimental values for the OHC strength of various NS and standard layups are measured and analyzed.

Chapter 6 presents a discussion of the experimental results and the experimental techniques themselves from which the conclusions have been drawn. Finally, suggestions for future work are presented.

CHAPTER 2

BACKGROUND

In order to better understand the project scope, the differences between traditional isotropic materials and orthotropic materials are presented. Based upon this, a review of composite laminate theory is presented. Then, methods based on the framework of laminate theory, which are utilized to characterize the stiffness and strength of laminates, are described. Finally, meaningful NS designs will be developed, analyzed using the methods mentioned above, and contrasted with existing standard laminate designs.

Continuous fiber reinforced composites are materials that primarily consist of two separate materials. A fiber, which acts as reinforcement, carries majority of the load and the matrix, which is typically a polymer, holds the fibers together in a structural unit, protects them from external damage, and distributes the loads to the fibers, as shown in Figure 2.1 [4].

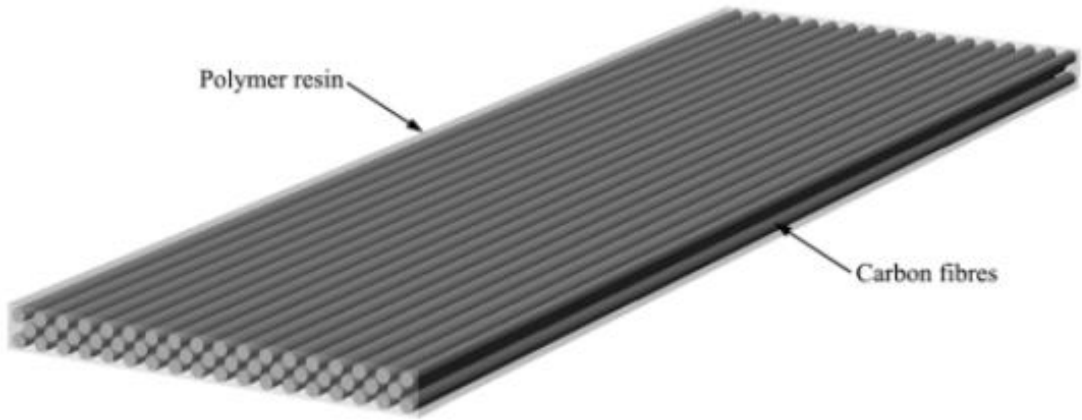

Figure 2.1 Carbon fiber reinforced composite [9]

As fiber-reinforced materials are not isotropic, the concept of stiffness is more complex and not intuitive when compared to most engineering materials. This isotropy is a tacit assumption used for designers and researchers when using traditional engineering materials. As isotropic material models are sufficient to model the overwhelming majority of materials, the transition to working with orthotropic material models in which stiffness is a function of the material orientation can be challenging and counter intuitive.

The stress-strain relationship for a linear-elastic isotropic material according to classical plate theory is given in Equation 1, where E is Young's Modulus and ν is Poisson's ratio. But, when dealing with laminated composites, this relationship does not apply. As it can be seen from Equation 1, only two elastic constants are required and there are no terms that take into account the orientation of an anisotropic material.

$$\begin{bmatrix}\boldsymbol{\sigma_{11}}\\\boldsymbol{\sigma_{22}}\\\boldsymbol{\sigma_{12}}\end{bmatrix}=\frac{\boldsymbol{E}}{\mathbf{1}-\boldsymbol{\nu}^{\mathbf{2}}}\begin{bmatrix}\mathbf{1}&\boldsymbol{\nu}&\mathbf{0}\\\boldsymbol{\nu}&\mathbf{1}&\mathbf{0}\\\mathbf{0}&\mathbf{0}&\mathbf{1}-\boldsymbol{\nu}\end{bmatrix}\begin{bmatrix}\boldsymbol{\epsilon_{11}}\\\boldsymbol{\epsilon_{22}}\\\boldsymbol{\epsilon_{12}}\end{bmatrix} \qquad (\mathbf{1})$$

The stiffness of any linear elastic material can be considered as a special case of a general linear elastic anisotropic material. To describe the stiffness of an anisotropic material, a tensor known as the elastic tensor (Equation 2) is used. The elements of this tensor are elastic constants that describe the relationships between different components of stress and strain. This tensor is denoted by [C] [10]. The stress strain relationship for anisotropic materials is described by the Equation 3 [10]. The 1, 2, and 3 directions denote the normal response whereas the 4, 5, and 6 directions denote the shear response.

$$\boldsymbol{C_{\alpha\beta}}=\begin{bmatrix}\boldsymbol{C_{11}}&\boldsymbol{C_{12}}&\boldsymbol{C_{13}}&\boldsymbol{C_{14}}&\boldsymbol{C_{15}}&\boldsymbol{C_{16}}\\\boldsymbol{C_{21}}&\boldsymbol{C_{22}}&\boldsymbol{C_{23}}&\boldsymbol{C_{24}}&\boldsymbol{C_{25}}&\boldsymbol{C_{26}}\\\boldsymbol{C_{31}}&\boldsymbol{C_{32}}&\boldsymbol{C_{33}}&\boldsymbol{C_{34}}&\boldsymbol{C_{35}}&\boldsymbol{C_{36}}\\\boldsymbol{C_{41}}&\boldsymbol{C_{42}}&\boldsymbol{C_{43}}&\boldsymbol{C_{44}}&\boldsymbol{C_{45}}&\boldsymbol{C_{46}}\\\boldsymbol{C_{51}}&\boldsymbol{C_{52}}&\boldsymbol{C_{53}}&\boldsymbol{C_{54}}&\boldsymbol{C_{55}}&\boldsymbol{C_{56}}\\\boldsymbol{C_{61}}&\boldsymbol{C_{62}}&\boldsymbol{C_{63}}&\boldsymbol{C_{64}}&\boldsymbol{C_{65}}&\boldsymbol{C_{66}}\end{bmatrix} \qquad (2)$$

$$\begin{bmatrix}\sigma_1\\\sigma_2\\\sigma_3\\\sigma_4\\\sigma_5\\\sigma_6\end{bmatrix}=\begin{bmatrix}C_{11}&C_{12}&C_{13}&C_{14}&C_{15}&C_{16}\\C_{21}&C_{22}&C_{23}&C_{24}&C_{25}&C_{26}\\C_{31}&C_{32}&C_{33}&C_{34}&C_{35}&C_{36}\\C_{41}&C_{42}&C_{43}&C_{44}&C_{45}&C_{46}\\C_{51}&C_{52}&C_{53}&C_{54}&C_{55}&C_{56}\\C_{61}&C_{62}&C_{63}&C_{64}&C_{65}&C_{66}\end{bmatrix}\begin{bmatrix}\epsilon_1\\\epsilon_2\\\epsilon_3\\2\epsilon_4\\2\epsilon_5\\2\epsilon_6\end{bmatrix} \qquad (3)$$

Based on the properties of different materials, the elastic tensor can be simplified and relations between elements can be identified such that the number of independent elastic constants required to describe a material can be reduced from the 36 required for a general anisotropic material. Isotropic materials have only two independent elastic constants and their stiffness tensor can be simplified into the form shown in Equation 4.

$$C_{\alpha\beta} = \begin{bmatrix} C_{11} & C_{12} & C_{12} & 0 & 0 & 0 \\ C_{12} & C_{11} & C_{12} & 0 & 0 & 0 \\ C_{12} & C_{12} & C_{11} & 0 & 0 & 0 \\ 0 & 0 & 0 & \frac{C_{11} - C_{12}}{2} & 0 & 0 \\ 0 & 0 & 0 & 0 & \frac{C_{11} - C_{12}}{2} & 0 \\ 0 & 0 & 0 & 0 & 0 & \frac{C_{11} - C_{12}}{2} \end{bmatrix} \tag{4}$$

For unidirectional fiber reinforced composites, the special case of a transversely isotropic material is used. Transversely isotropic materials are defined by an axis of material symmetry, i.e., the direction with respect to which the material has identical properties. The axis of symmetry is the orientation of the fiber reinforcement, e.g., the z axis. The other two directions, x and y, are perpendicular to this axis, i.e., the z axis, and to each other. The x-y plane is referred to as the plane of isotropy [32]. Hence, a transverse isotropic model describes a material that is isotropic in one plane and has a different stiffness in the direction perpendicular to the isotropic plane. This model requires five independent elastic constants to populate the stiffness tensor and is shown in Equation 5

[10]. Figure 2.1 demonstrates this property of unidirectional composites as the material is seen to be isotropic in the plane perpendicular to fiber direction.

$$C_{\alpha\beta} = \begin{bmatrix} C_{11} & C_{11} - 2C_{66} & C_{13} & 0 & 0 & 0 \\ C_{11} - 2C_{66} & C_{11} & C_{13} & 0 & 0 & 0 \\ C_{13} & C_{13} & C_{33} & 0 & 0 & 0 \\ 0 & 0 & 0 & C_{44} & 0 & 0 \\ 0 & 0 & 0 & 0 & C_{44} & 0 \\ 0 & 0 & 0 & 0 & 0 & C_{66} \end{bmatrix} \tag{5}$$

As classical plate theory is only valid for isotropic materials, a different theory is utilized for anisotropic materials. The mathematical framework used to deal with these anisotropic materials for the case when layers composed of differently oriented fiber reinforcements are stacked on top of each other is presented in the following section. This framework is called Classical Laminate Theory (CLT). CLT was developed to model ply-wood [1]. It has found extensive application in modeling the stresses and strains developed in carbon fiber composites.

2.1 Classical Laminate Theory Review

The methods used in this thesis to perform stiffness matching and estimate strength heavily depend on the framework of Classical Laminate Theory (CLT). A review of CLT is presented below. As unidirectional fiber-reinforced, composites are transversely isotropic materials, classical plate theory, which is typically used for structures made of metals or other isotropic materials, cannot be used to describe their stress-strain relationship. CLT is used to accurately describe the response of a laminate in which layers with fibers running along different orientations are stacked on top of each other. CLT considers the transversely isotropic nature of each ply to model the stresses and strains in each ply when a laminate is subjected to mechanical or thermal loading.

2.1.1 Assumptions in Classical Laminate Theory:

The following are the assumptions used in CLT [10]:

1) The laminate consists of perfectly bonded layers (or plies).
2) The normals to the mid-plane of the laminate remain straight and normal to the deformed mid-plane after deformation (Kirchhoff hypothesis for plates and Kirchhoff-Love hypothesis for shells).
3) The normals to the mid-plane of the laminate do not change length (constant thickness).

2.1.2 Co-ordinate Systems used for Classical Laminate Theory:

The global co-ordinate system, also referred to as the balancing axes for CLT are denoted by (x, y, z) with x and y as the in-plane axes and z as the thickness direction. The origin lies on the mid-plane of the laminates shown in Figure 2.2.

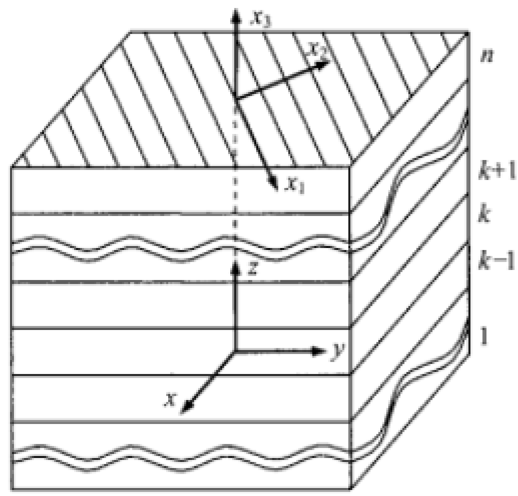

Figure 2.2 Co-ordinate system for classical laminate theory [10]

Each ply is assigned a number, the bottom most ply being ‘1’ and the top most being ‘N’. Each ply has its own local or material co-ordinate system, which is defined by ‘1’ being the fiber direction for that ply and ‘2’ being the direction perpendicular to the fiber direction, as shown in Figure 2.3.

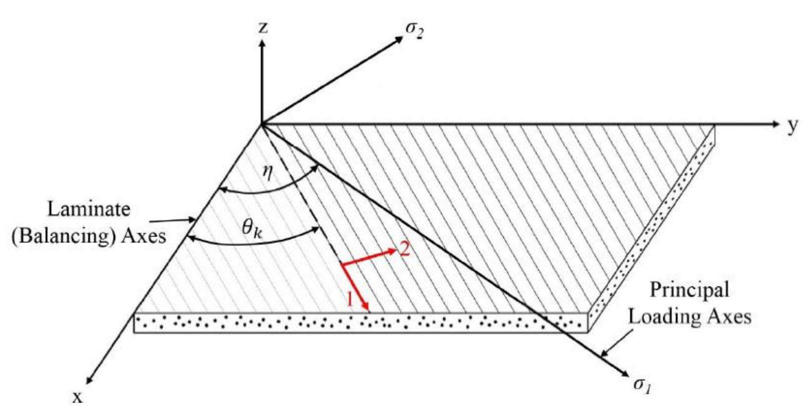

Figure 2.3 Material co-ordinate system [7]

The building block for CLT is the [Q] matrix. It contains the material properties of a single ply in its material co-ordinate system, i.e., the co-ordinate. Based on this matrix, the stiffness responses for laminates composed of multiple plies stacked in arbitrary orientations can be formulated. The responses of laminates made from multiple plies stacked on top of each other will be described later in this chapter.

The [Q] matrix is detailed in Equation 6. Here E_{11} is the Young's modulus along the fiber direction, E_{22} is the in-plane Young's modulus perpendicular to the fiber direction, and G_{12} is the shear modulus [10]. It must be noted that it is a symmetric matrix.

$$[Q] = \begin{bmatrix} \frac{E_{11}}{1-\nu_{12}.\nu_{21}} & \frac{\nu_{12}\,E_{22}}{1-\nu_{12}.\nu_{21}} & 0 \\ Q_{12} & \frac{E_{22}}{1-\nu_{12}\nu_{21}} & 0 \\ 0 & 0 & G_{12} \end{bmatrix} \tag{6}$$

The invariants of the [Q] matrix are called stiffness invariants. They are independent of material orientation and simplify the rotation of this matrix that is used extensively throughout CLT. These invariants can be calculated as shown in Equations 7-11.

$$U_1 = \frac{1}{8}(3Q_{11} + 3Q_{22} + 2Q_{12} + 4Q_{66}) \tag{7}$$

$$U_2 = \frac{1}{2}(Q_{11} - Q_{22}) \tag{8}$$

$$\mathrm{U}_3 = \frac{1}{8}(\mathrm{Q}_{11} + \mathrm{Q}_{22} - 2\mathrm{Q}_{12} - 4\mathrm{Q}_{66}) \tag{9}$$

$$\mathrm{U}_4 = \frac{1}{8}(\mathrm{Q}_{11} + \mathrm{Q}_{22} + 6\mathrm{Q}_{12} - 4\mathrm{Q}_{66}) \tag{10}$$

$$\mathrm{U}_5 = \frac{1}{8}(\mathrm{Q}_{11} + \mathrm{Q}_{22} - 2\mathrm{Q}_{12} + 4\mathrm{Q}_{66}) \tag{11}$$

This [Q] matrix can be rotated according to individual ply orientations to give the $[\overline{Q}]$ matrix, which represents the stiffness matrix for an individual ply in the global co-ordinate system. The elements of the $[\overline{Q}]$ can be calculated by Equations 12-17.

$$\overline{Q}_{11} = Q_{11}\,cos^4\theta + 2(Q_{12} + 2Q_{66})sin^2\theta cos^2\theta + Q_{22}sin^4\theta \tag{12}$$

$$\overline{Q}_{12} = Q_{12}\,(sin^4\theta + cos^4\theta) + (Q_{11} + Q_{22} - 4Q_{66})sin^2\theta cos^2\theta \tag{13}$$

$$\overline{Q}_{22} = Q_{11}\,sin^4\theta + 2(Q_{12} + 2Q_{66})sin^2\theta cos^2\theta + Q_{22}cos^4\theta \tag{14}$$

$$\overline{Q}_{16} = (Q_{11} - Q_{12} - 2Q_{66})sin\theta cos^3\theta + (Q_{12} - Q_{22} + 2Q_{66})sin^3\theta cos\theta \tag{15}$$

$$\overline{\mathrm{Q}}_{26} = (\mathrm{Q}_{11} - \mathrm{Q}_{12} - 2\mathrm{Q}_{66})\sin^3\theta\cos\theta + (\mathrm{Q}_{12} - \mathrm{Q}_{22} + 2\mathrm{Q}_{66})\sin\theta\cos^3\theta \tag{16}$$

$$\overline{\mathrm{Q}}_{66} = (\mathrm{Q}_{11} + \mathrm{Q}_{22} - 2\mathrm{Q}_{12} - 2\mathrm{Q}_{66})\sin^2\theta\cos^2\theta + \mathrm{Q}_{66}(\sin^4\theta + \cos^4\theta) \tag{17}$$

Another method for computing the $[\overline{Q}]$ matrix is through the use of stiffness invariants, which are shown in Equations 18-23.

$$\overline{\mathrm{Q}}_{11} = \mathrm{U}_1 + \mathrm{U}_2\cos(2\theta) + \mathrm{U}_3\cos(4\theta) \tag{18}$$

$$\overline{Q}_{22} = U_1 - U_2\cos(2\theta) + U_3\cos(4\theta) \tag{19}$$

$$\overline{Q}_{12} = U_4 - U_3\cos(4\theta) \tag{20}$$

$$\overline{Q}_{66} = U_5 - U_3\cos(4\theta) \tag{21}$$

$$\overline{Q}_{16} = \frac{1}{2}U_2\sin(2\theta) + U_3\cos(4\theta) \tag{22}$$

$$\overline{Q}_{26} = \frac{1}{2}U_2\sin(2\theta) - U_3\cos(4\theta) \tag{23}$$

where θ is the angle of the fibers with respect to the global x-axis.

For each lamina $[\overline{Q}]$ must be computed and the elements of these rotated matrices are then used to calculate the laminate level stiffness matrices There are three laminate level stiffness matrices, [A], [B], and [D].

The [A] matrix describes the in-plane extensional response whereas the [D] matrix describes the bending response of a laminate. The [B] matrix is the coupling stiffness matrix and describes the coupling between in-plane and out of plane responses [10]. These can be computed for any laminate as shown in Equations 24-26.

$$A_{mn} = \sum_{j=1}^{N} (\overline{Q_{mn}})_j (h_j - h_{j-1}) \tag{24}$$

$$B_{mn} = \frac{\sum_{j=1}^{N} (\overline{Q_{mn}})_j (h_j^2 - h_{j-1}^2)}{2} \tag{25}$$

$$D_{mn} = \frac{\sum_{j=1}^{N} (\overline{Q_{mn}})_j (h_j^3 - h_{j-1}^3)}{3} \tag{26}$$

where N is the total number of plies, h_j is the top z co-ordinate of the j^{th} layer, and $(\overline{Q_{mn}})_j$ is the element corresponding to the rotated Q matrix of the j^{th} ply

The stiffness of the laminate is represented by these matrices and the equivalent in-plane Young's and shear moduli of the laminate can be calculated from Equations 27-29.

$$E_{xx} = (A_{11} - \frac{A_{12}^2}{A_{22}}) \frac{1}{N * \text{thickness of ply}} \tag{27}$$

$$\mathrm{E_{yy}} = (\mathrm{A_{22}} - \frac{\mathrm{A_{12}^2}}{\mathrm{A_{11}}}) \frac{1}{\mathrm{N} * \text{thickness of ply}} \quad (28)$$

$$G_{xy} = \frac{A_{66}}{N * thickness\ of\ ply} \quad (29)$$

2.1.3 Force and moment resultants:

The in-plane forces per unit length [N] can be described as the through thickness integral of the planar stresses in the laminate, described in Equations 30-32.

$$N_{xx} = \int_{-h/2}^{h/2} \sigma_{xx} dz \quad (30)$$

$$N_{yy} = \int_{-h/2}^{h/2} \sigma_{yy} dz \quad (31)$$

$$N_{xy} = \int_{-h/2}^{h/2} \sigma_{xy} dz \quad (32)$$

The constitutive equations relating the stress resultants to the strains and curvatures are shown in Equation 33.

$$\begin{bmatrix} N_{xx} \\ N_{yy} \\ N_{xy} \end{bmatrix} = [A] \begin{bmatrix} \epsilon_{xx} \\ \epsilon_{yy} \\ \epsilon_{xy} \end{bmatrix} + [B] \begin{bmatrix} \kappa_{xx} \\ \kappa_{yy} \\ \kappa_{xy} \end{bmatrix} \tag{33}$$

The moment per unit length [M] can be described as the through thickness integral of the planar moments in the laminate, as shown in Equations 34-36.

$$M_{xx} = \int_{-h/2}^{h/2} \sigma_{xx} z dz \tag{34}$$

$$M_{yy} = \int_{-h/2}^{h/2} \sigma_{yy} z dz \tag{35}$$

$$M_{xy} = \int_{-\frac{h}{2}}^{\frac{h}{2}} \sigma_{xy} z dz \tag{36}$$

The constitutive equations relating the moment resultants to the strains and curvatures are shown in Equation 37

$$\begin{bmatrix} \mathrm{M_{xx}} \\ \mathrm{M_{yy}} \\ \mathrm{M_{xy}} \end{bmatrix} = [\mathrm{B}] \begin{bmatrix} \epsilon_{xx} \\ \epsilon_{yy} \\ \epsilon_{xy} \end{bmatrix} + [\mathrm{D}] \begin{bmatrix} \mathrm{k_{xx}} \\ \mathrm{k_{yy}} \\ \mathrm{k_{xy}} \end{bmatrix} \tag{37}$$

where

N_{xx}= force resultant in the x-direction (per unit width)

N_{yy}= force resultant in the y-direction (per unit width)

N_{xy}= shear force resultant (per unit width)

M_{xx}= bending moment resultant in the yz plane (per unit width)

M_{yy}= bending moment resultant in the xz plane (per unit width)

M_{xy}= twisting moment resultant (per unit width).

Also, the strain and curvature vectors that define the midplane strains and curvatures developed in the laminate are

$\begin{bmatrix} \epsilon_{\mathrm{xx}} \\ \epsilon_{yy} \\ \epsilon_{\mathrm{xy}} \end{bmatrix}$= mid-plane stains of the laminate

and

$\begin{bmatrix} \kappa_{xx} \\ \kappa_{yy} \\ \kappa_{xy} \end{bmatrix}$= curvatures of the laminate.

These matrices and vectors can be assembled into one system of equations as shown in Equation 38. Equation 38 describes the response of a laminated plate under mechanical loading.

$$\begin{bmatrix} N \\ M \end{bmatrix} = \begin{bmatrix} A & B \\ B & D \end{bmatrix} \begin{bmatrix} \epsilon^o \\ \kappa \end{bmatrix} \tag{38}$$

Based on this framework, a stiffness matching method is developed in Chapter 3. Furthermore, these equations are utilized to predict the strength of selected laminate designs.

2.2 Common Laminate Design Practices

Laminated composite structures provide improved design flexibility as compared to metallic materials, with the possibility of tailoring their stiffness and strength by selecting fiber orientations. Therefore, dedicated design methods that take into account composite materials specificities are required [15].

All laminates are currently designed based on a fixed set of rules. The rules, which are presented below, simplify the process used by designers to define the layups of the layers that form laminates. Standard layups currently in use by industry are based on these guidelines. As NS designs are currently unconstrained by any rules, it is important to understand the deviations from existing practice so as to better leverage existing knowledge. When a laminate is designed, the inputs, such as the required stiffness, damage tolerance, and strength, are considered. These are used to guide the selection of fiber angles in each ply, their stacking sequence, and the thickness ratios.

However, as an infinite number of angles in infinite combinations can be used, this problem is very hard to tackle and optimize. Therefore, laminate design was standardized in the aerospace industry from very early on. These standardized rules make laminate design accessible and introduces robustness. The well-known rules are listed below:

1) Laminates must have mid-plane symmetry (to avoid warpage from curing).
2) Only four angles may be used: 0°, 45°, -45°, and 90°.
3) The 10% rule that requires each of the four ply orientations to be at least 10% of the total laminate thickness.
4) Laminates must be balanced, i.e., the off-axis plies of 45˚ and -45˚ must be selected in pairs. Thus, the in-plane stiffness of the laminate must remain orthotropic. There will be no shear coupling components, i.e., A16 and A26 are zero [1].

These rules simplify the design problem and the behavior of the laminates themselves. However, these rules discretize the design space, i.e., limit the number of options from which a designer can select.

Based on the type of component being manufactured, the relative thickness ratios of standard angles are varied. For wing skins, the standard angles 0°/±45°/90° are used in relative ratios of 44/44/12, respectively. The percentages for stiffeners are 60/30/10 and for spars the percentages are 10/80/10 [7]. In this thesis, the strength of NS designs will be compared to a standard wing skin design that is based on these rules.

2.3 Stiffness Matching

Stiffness matching allows for easy comparison between standard and NS designs in the strength domain. Further, stiffness matching allows for existing designs to be replaced with non-standard laminates without affecting the larger scale design of the aircraft. Stiffness matching allows one to develop NS laminate designs that are directly comparable to standard designs.

Two primary factors considered when designing composite laminates are stiffness and ultimate strength. The stiffness defines the response to loads encountered by a component during its service life, whereas the ultimate strength defines the safety of the design. Both of these factors must be considered when comparing standard and non-standard angle composites.

The stiffness and strength of laminates are intertwined, on the lamina level in the direction of the maximum stiffness, i.e., along the fiber reinforcement, which is also the direction along which maximum stiffness is seen. As most components must be able to withstand loading from multiple directions, tradeoffs must be made so that the laminate can perform adequately when loaded in multiple directions. The interaction between strength and stiffness is more complex when multi-directional laminates are used and performance in one domain may not necessarily translate to good performance in another.

The shift towards non-standard angle composites cannot come at any cost to performance in either the stiffness or strength domains. To facilitate the transition from standard angle composites, a good starting point was identified by Butler et al. [7] with the design of NS laminates with the same performance in the stiffness domain as existing, traditional laminates.

If the stiffness of standard and non-standard angle laminates are kept constant and other variables such as ultimate strength, formability, and manufacturing costs are compared, then designers can identify the most optimal laminates within a range of designs that provide the same in-plane response under loading.

Butler et al. [7] performed stiffness matching for layups used in three types of components: wing skins, spars, and stiffeners. The NS designs developed by Butler's stiffness matching method are shown in Figure 2.4. They found that non-standard angles offer greatly improved forming compatibility, i.e., the plies can be more easily formed into complex shapes when compared to standard angle composites before curing, while maintaining the same post cured in-plane stiffness as standard angles composites. This improved compatibility between the pairs of non-standard angles reduces the likelihood of fiber wrinkle defects. An alternate method for stiffness matching has been developed in this thesis and has been used to develop NS designs that have been compared with a standard wing skin layup in terms of strength.

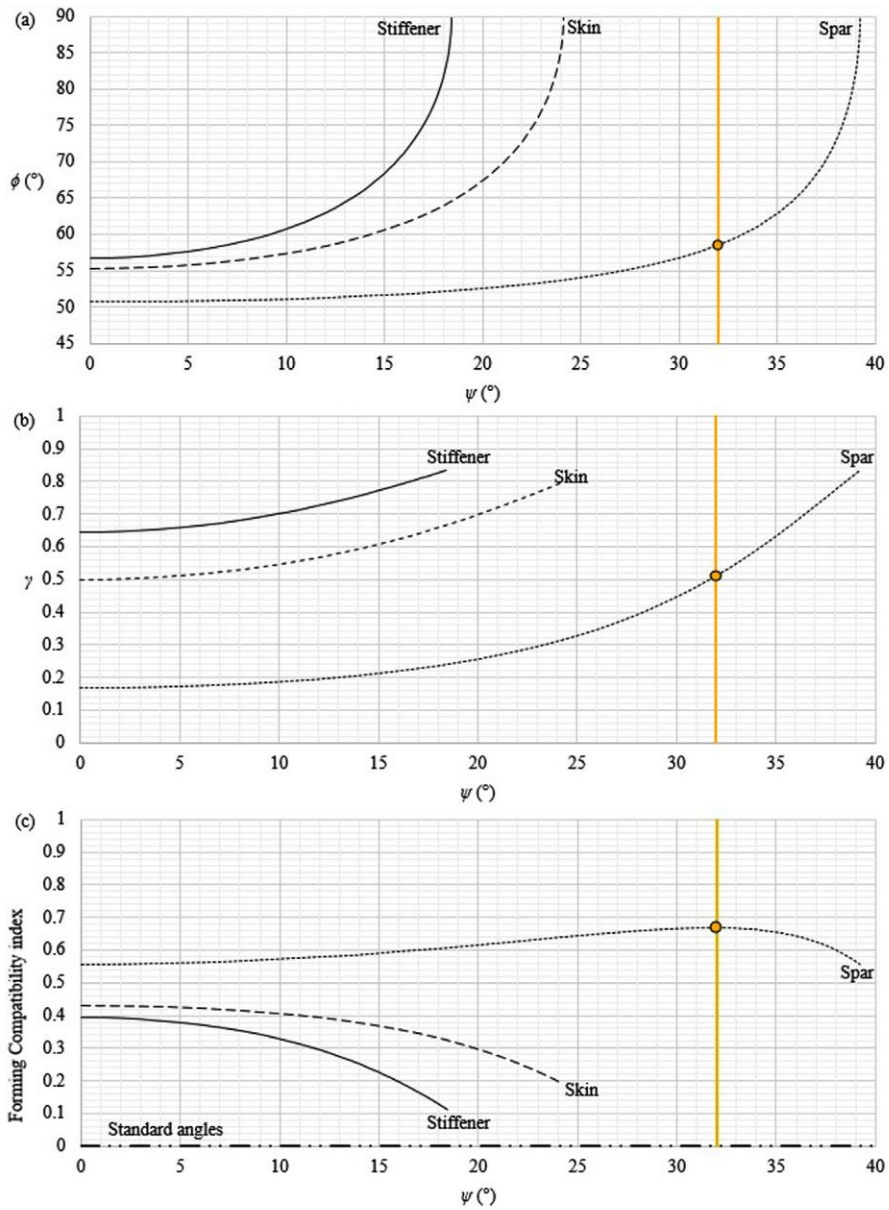

Figure 2.4 Angle pairs and relative rations for non-standard layups [7]

2.4 Strength of Laminates

Strength design is often employed for composite aircraft structures. A primary concern when designing aircraft is to minimize weight. For this reason, the stresses experienced by the structure are of the same order of magnitude as the material strength [10]. The comparison of the strengths of NS designs to standard designs of the same stiffness highlights any potential weight savings.

The complexity of designing with composites is in part due to the large number of damage mechanisms that influence the properties of the material when it undergoes loading [30]. Structural analysis is generally performed by comparing the stresses developed at the location of interest as a result of the applied loads within allowable maximum limits [11]. For isotropic materials, the Von Mises and Tresca yield criteria are widely used. Continuous fiber composites are not isotropic, hence different failure criteria must be used.

A multitude of failure theories have been proposed for fiber reinforced composites, for example maximum stress [10], Tsai-Wu [35], and Tsai-Hill [8]. However, the failure mechanisms of composite structures are not completely understood yet [10]. As there is still much to be learned regarding the failure mechanisms of composites, the selection of failure criteria has a vital impact on the accuracy of the predictions of any structural analysis performed on laminates. This thesis utilizes the maximum stress theory because it is readily implemented and reasonable agreement is seen with experimental data.

2.4.1 Maximum Stress Criterion:

Maximum stress theory compares stress in each material direction independently with material strength [33]. For this theory to be applied, the stresses in each ply must be calculated according to CLT and then the stresses for each ply that are found in global co-ordinates must be rotated to its material co-ordinate system and checked against the allowable limits to determine if a laminate design is safe for a particular load. Failure is said to occur if any of the conditions in Equations 39-41 is violated.

$$-S_{Lc} < \sigma_{11} < S_{Lt} \tag{39}$$

$$-S_{Tc} < \sigma_{22} < S_{Tt} \tag{40}$$

$$-S_{LTs} < \tau_{12} < S_{LTs} \tag{41}$$

2.4.2 First Ply Failure Theory

The initial failure of the first ply within a laminate under loading can be predicted by applying first ply failure theory [31]. The FPF load indicates the minimum load at which damage occurs within a laminate. The first ply failure approach utilizes the constitutive relations from CLT to calculate the global stresses sustained by each ply based on applied loading. These stresses are transformed from the global co-ordinate system to the local co-ordinate system of each ply as shown in Equation 42

$$\begin{bmatrix} \sigma_1 \\ \sigma_2 \\ \sigma_6 \end{bmatrix} = [T_1] \begin{bmatrix} \sigma_x \\ \sigma_y \\ \tau_{xy} \end{bmatrix} \tag{42}$$

where $[T_1]$ represents the transformation matrix detailed in Equation 43

$$[T_1] = \begin{bmatrix} m^2 & n^2 & 2mn \\ n^2 & m^2 & -2mn \\ -mn & mn & m^2 - n^2 \end{bmatrix} \tag{43}$$

where $m = \sin\theta$ and $n = \cos\theta$ reference [10].

Individual ply stresses in the material co-ordinate system are used as inputs for the most appropriate failure criteria and the progression of the failure of plies can be predicted to determine which plies fail first. As a result, an assessment of the safety of the design can be made. In general, a laminate under study is loaded incrementally and the stresses of each ply are checked against the failure criteria at each load step. Once a failure criteria is exceeded, the lamina that exceeds the allowable material strength is said to have failed. The progression of failure can be studied by extending this method. Once FPF occurs, the stiffness of the failed ply is degraded. The load applied to the laminate is increased to arrive at the ultimate failure load at which all plies have failed. This process is shown in Figure 2.5.

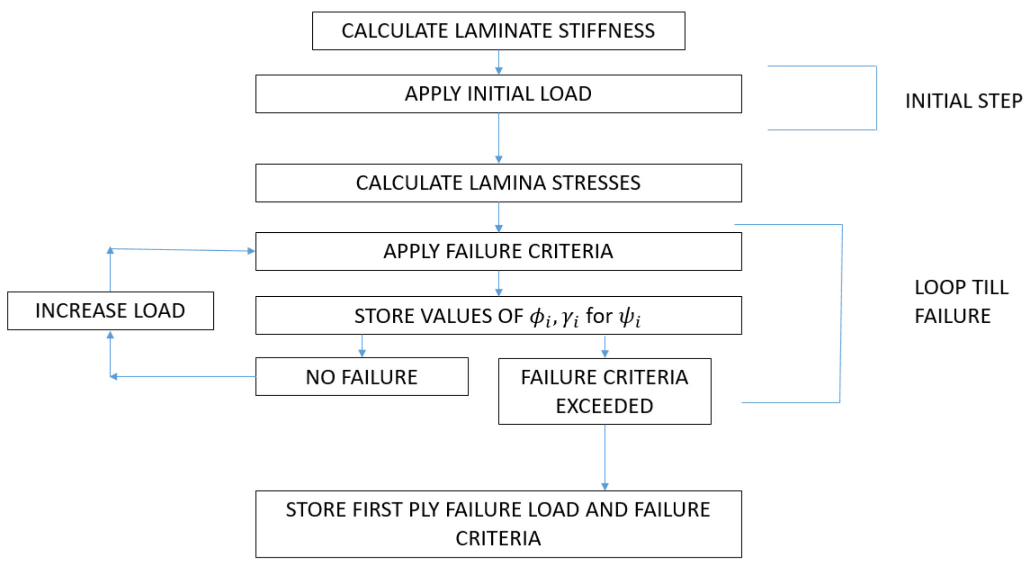

Figure 2.5 Analysis of laminate strength and load-deformation behavior [33]

Coupling the first ply failure theory with the maximum stress criterion enables one to predict the failure of standard as well as NS Layups. The predicted strengths have been used to highlight the advantages of NS designs in Section 4.3.

2.5 Chapter Summary

In this chapter, the theoretical framework of classical laminate theory was reviewed. This theory helps one to characterize the stiffness of a laminate and define the constitutive relationships for laminate materials. The common laminate design rules and the importance of rules such as symmetry and balance were discussed. As these rules define standard laminate design, one can now understand the effect of standard rules on laminate mechanics.

CHAPTER 3

STIFFNESS MATCHING METHOD

Stiffness matching provides a range of non-standard layup designs that match the stiffness of a certain standard layup. These designs can be subjected to various tests to compare them with the existing standard design.

Butler et al. developed a stiffness matching method [7]. The stiffness matching method outlined below takes inspiration from Butler et al. to compute the range of non-standard laminates which match the stiffness of an arbitrary laminate. The method presented in this thesis uses an alternate approach but arrives at the same results seen by Butler et al.

The motivation behind developing this method is two-fold. The code developed to implement this method can be altered for further investigations into NS layups and allows one to compute the exact angle pairs and thickness ratios, which is not possible when one refers to the chart presented in Butler's study.

As seen in the CLT review in Section 2.1, the in-plane response of a laminate is defined by the [A] and [B] matrices and is given by Equation 33.

$$\begin{bmatrix} N_{xx} \\ N_{yy} \\ N_{xy} \end{bmatrix} = [A] \begin{bmatrix} \epsilon_{xx} \\ \epsilon_{yy} \\ \epsilon_{xy} \end{bmatrix} + [B] \begin{bmatrix} \kappa_{xx} \\ \kappa_{yy} \\ \kappa_{xy} \end{bmatrix} \tag{33}$$

As the B matrix can be assumed to be zero for symmetric laminates, this system of equations reduces to Equation 44.

$$\begin{bmatrix} N_{xx} \\ N_{yy} \\ N_{xy} \end{bmatrix} = [A] \begin{bmatrix} \epsilon_{xx} \\ \epsilon_{yy} \\ \epsilon_{xy} \end{bmatrix} \tag{44}$$

It can be seen that to match the in-plane response of a standard angle laminate. A symmetrical NS laminate must have an identical [A] matrix.

The method, based on the assumptions presented below, requires NS layups to match the [A] matrix of an arbitrary standard angle composite. The applications and limitations of this method are discussed in Section 3.6.

3.1 Formulation of In-Plane Stiffness Matching Method

To match the in-plane stiffness of a standard angled laminate with a set of NS designs, first the in-plane stiffness of the standard design is required. In this thesis, the standard wing skin layup is utilized as the standard angle layup. The standard wing skin layup is outlined in Table 3.1 and discussed in Section 3.2. Once the stiffness required from NS designs, i.e., the A matrix of the standard angles, has been calculated, then the number of angles in the NS design used must be constrained. Standard angle designs have four angles, i.e., 0˚, 45˚, -45˚, 90˚. To allow for validation of the results against the study conducted by Butler et al. [7], the same number of NS angles, i.e., two, has been used.

The following assumptions are used to develop the stiffness matching method.

1. Each ply within the laminate has the same thickness.
2. The NS angle laminate consists of a pair of angles being $\pm\psi, \pm\varphi$.
3. The thickness proportion of plies with angles $\pm\psi$ is γ.

4. The standard and non-standard angled laminates are made up of the same material.
5. The NS laminates are symmetric.

Now that the design space has been adequately constrained, stiffness matching can be performed within this space by utilizing the framework of CLT. Equation 24 is presented again

$$\mathrm{A_{mn}} = \sum_{\mathrm{j=1}}^{\mathrm{N}} (\overline{Q_{mn}})_{\mathrm{j}} (h_j - h_{j-1}) \tag{24}$$

where i, j =1, 2, 6 and N is the total number of plies. Substituting the values of the indices results in Equations 45-48.

$$\mathrm{A_{11}} = \sum_{\mathrm{k=1}}^{\mathrm{N}} (\mathrm{U_1} + \mathrm{U_2}\cos(2\theta_k) + \mathrm{U_3}\cos(4\theta_k))(t_{ply}) \tag{45}$$

$$\mathrm{A_{12}} = \sum_{\mathrm{k=1}}^{\mathrm{N}} (\mathrm{U_4} - \mathrm{U_3}\cos(4\theta_k))\,(t_{ply}) \tag{46}$$

$$\mathrm{A_{22}} = \sum_{\mathrm{k=1}}^{\mathrm{N}} (\mathrm{U_1} - \cos(2\theta_k) + \mathrm{U_3}\cos(4\theta_k))(t_{ply}) \tag{47}$$

$$\mathrm{A_{66}} = \sum_{\mathrm{k=1}}^{\mathrm{N}} (\mathrm{U_5} - \mathrm{U_3}\cos(4\theta_k))(t_{ply}) \tag{48}$$

As [A] is symmetric, Equation 49 results.

$$A_{21} = A_{12} \tag{49}$$

Now let the standard angled laminates have an A matrix denoted by $[A^S]$ and the non-standard angled laminates have an A matrix $[A^N]$. For in-plane stiffness matching, the condition detailed in Equation 50 must be enforced.

$$[A^S] = [A^N] \tag{50}$$

As the non-standard angle $\pm\psi$ has a thickness fraction γ, the latter non-standard angle $\pm\varphi$ will have a thickness fraction of $1-\gamma$. The number of plies with angle $\pm\psi$, denoted by N_ψ, is given by Equation 51.

$$N_\psi = N * \gamma \tag{52}$$

Similarly, the number of plies with angle $\pm\phi$, denoted by N_ϕ is given by Equation 52.

$$N_\phi = N * (1-\gamma) \tag{52}$$

These three parameters, ψ, ϕ, γ, allow one to begin the process of arriving at a non-standard layup that matches a given stiffness. Now because cos (θ) is an even function, i.e., $\cos(\theta) = \cos(-\theta)$, the non-standard angles may be either positive or negative. Keeping in mind the assumption that the NS laminate is symmetric about the mid plane and that balance must be maintained as much as possible, one can arrive at a discrete design.

For a non-standard angled laminate, the elements of the A matrix can be calculated as demonstrated by Equations 53-56.

$$A_{11}^{N} = \mathrm{N}\gamma(\mathrm{U}_1 + \mathrm{U}_2\cos(2\psi) + \mathrm{U}_3\cos(4\psi))\left(t_{ply}\right) + \mathrm{N}(1-\gamma)(\mathrm{U}_1 + \mathrm{U}_2\cos(2\phi) + \mathrm{U}_3\cos(4\phi))\left(t_{ply}\right) \tag{53}$$

$$A_{22}^{N} = \mathrm{N}\gamma(\mathrm{U}_1 - U_2\cos(2\psi) + \mathrm{U}_3\cos(4\psi))\left(t_{ply}\right) + N(1-\gamma)(\mathrm{U}_1 - U_2\cos(2\phi) + \mathrm{U}_3\cos(4\phi))(t_{ply}) \tag{54}$$

$$A_{12}^{N} = \mathrm{N}\gamma(\mathrm{U}_4 - \mathrm{U}_3\cos(4\psi))\ (t_{ply}) + \mathrm{N}(1-\gamma)(\mathrm{U}_4 - \mathrm{U}_3\cos\left(4\phi_j\right))\ (t_{ply}) \tag{55}$$

$$A_{66}^{N} = \mathrm{N}\gamma\left(\mathrm{U}_5 - \mathrm{U}_3\cos\left(4\psi_j\right)\right)\left(t_{ply}\right) + N(1-\gamma)(\mathrm{U}_5 - \mathrm{U}_3\cos(4\phi_j))(t_{ply}) \tag{56}$$

The elements of $[A^S]$, which are calculated based on the material, type of standard layup, and number of plies in the standard layup, can be equated to the symbolic equations for the elements of $[A^N]$, as shown in Equations 57 and 58.

$$A_{11}^{s} = A_{11}^{N} \tag{57}$$

$$A_{22}^{s} = A_{22}^{N} \tag{58}$$

By setting the value of ψ at finite increments between 0˚ and 90˚ and solving these two equations for φ and γ, the range of laminate designs with a pair of angles that match a given stiffness results. It must be noted that every angle ψ does not have a possible complementary angle ϕ; hence the range of designs is bound by the input stiffness and varies depending on the stiffness of the standard angled laminate used.

3.2 Stiffness Matching for a Standard Wing Skin Layup

A standard wing skin layup as described in [7] will be used as the input to compute the range of possible NS designs that will match its in-plane stiffness. To facilitate an easy comparison between the standard wing skin and NS designs, it was decided to use the same number of plies for both standard and NS designs. For wing skins, the standard angles 0°/±45°/90° are used in relative ratios of 44/44/12 [7]. The closest physically realizable approximation of these ratios was used while keeping the numbers of plies to a minimum. The standard wing skin design hence has a minimum total of eighteen plies, which was fixed as the total number of plies for NS designs. The standard wing skin layup based on these considerations is shown in Table 3.1. The layup in Table 3.1 was used as the input for a MATLAB code that implements the stiffness matching method described in Section 3.1. The MATLAB code is presented in Appendix A.

Table 3.1 Standard Wing Skin Design

Standard Wing Skin Design	
Ply Number	Ply Orientation (Degrees)
1	0
2	0
3	0
4	0
5	45
6	-45
7	45
8	-45
9	90
10	90
11	-45
12	45
13	-45
14	45
15	0
16	0
17	0
18	0

Figure 3.1 show the pairs of angles, i.e., ±ψ° and ±φ°, as well as a plot of ψ° vs γ that match the stiffness of an NS design to a standard wing skin layup shown in Table 3.1 and when the number of plies of standard angle and NS laminates is the same.

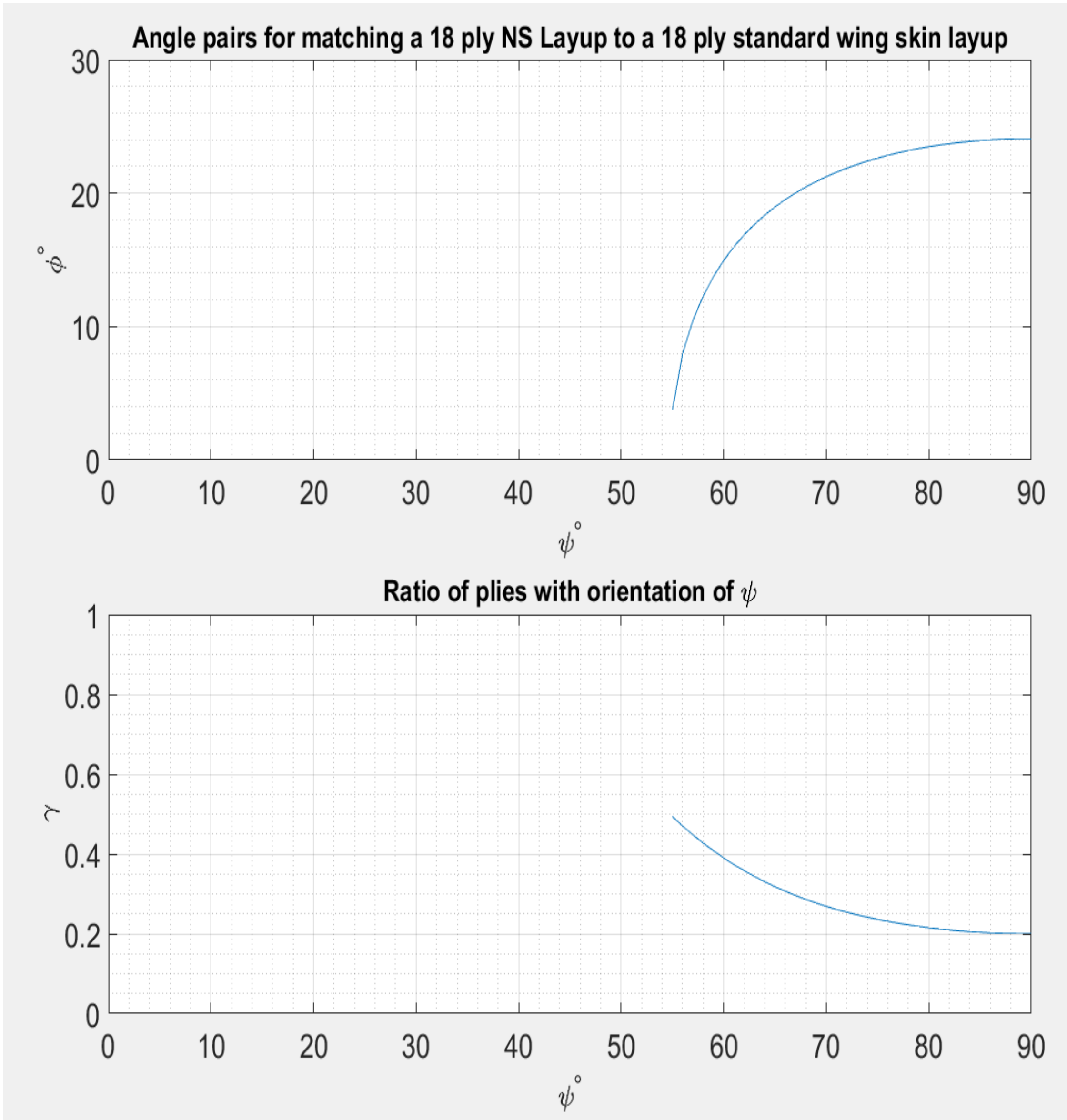

Figure 3.1 Designs for stiffness matched non-standard laminates

The results in Figure 3.1 have been compared to the results presented by Butler et al. in Figure 2.3 and in Table 3.2. Good agreement between both is seen. From Figure 3.1, NS layups that match the in-plane stiffness of the standard wing skin design shown in Table 3.1 can be designed. The NS designs selected for detailed study are shown in Tables 3.3-3.5.

3.3 Validation of Method

As the method developed in this thesis differs from the method proposed by Butler, the results of both methods have been compared to check its validity. The angle pairs and thickness ratios resulting in this thesis' method were compared to the results presented by Butler et al. [7] and are shown in Table 3.1

Based on the method in Section 3.1, NS designs that match the stiffness of the standard wing skin layup can be defined. To define a NS design, one must select a value for the primary angle, i.e., the angle closer to zero degrees denoted by ϕ_i.This angle can be considered as the 'input parameter.' For every primary angle there is a corresponding complimentary angle, i.e., the angle closer to ninety degrees ψ_i. The thickness fraction of the complimentary angle ψ_i, γ_i can be found from Figure 3.1. Hence ψ_1 ,γ_1 can be considered as 'output parameters,' which depend on the input parameter. Using these three parameters, an NS design that matches the stiffness of a standard design can be defined.

On using the same value for the 'input parameter,' i.e., the primary angle for both methods, one can compare the 'output parameters,' i.e., the complimentary angle and the thickness ratio of the complimentary angle calculated according to the method proposed by Butler et al.[7] and the method shown in Section 3.1. Several values of the primary angle for the standard wing skin layup have been used as an input, the complimentary angle and thickness fractions of the primary and complimentary angles calculated according to the method proposed by Butler et al. and the method shown in Section 3.1 are compared in Table 3.2.

Table 3.2 Comparison of NS designs from Butler's method and A based method

Method	Primary Angle (Degrees)	Thickness Fraction	Complimentary Angle (Degrees)	Thickness Fraction
Butler	4.00	0.51	55.00	0.49
A matrix	3.75	0.49	55.00	0.51
Butler	10.00	0.57	57.00	0.43
A matrix	10.48	0.55	57.00	0.45
Butler	15.00	0.60	60.50	0.40
A matrix	14.86	0.61	60.00	0.39
Butler	20.00	0.70	67.00	0.30
A matrix	20.02	0.70	67.00	0.30
Butler	24.00	0.80	85.00	0.20
A matrix	24.00	0.80	86.00	0.20

3.4 Stiffness Matching for Dissimilar Number of Ply Counts

3.4.1 Motivation

This section extends the method developed in Section 3.1 to compute designs for non-standard angled laminates that do not have the same thickness as the standard angled input laminates. The reasons for this are two-fold. First, one needs to ensure that the non-standard layups are balanced and symmetric. For a balanced, non-standard angle composite, an even number of plies for each non-standard angle is required on both sides of the plane of symmetry. For a typical wing skin layup with the angles 0°, ±45°, 90° and the corresponding thickness fractions 12/44/44, the closest approximation to these ratios results in a total of eighteen plies. With a total of eighteen plies, there are nine plies above and below the plane of symmetry. For a laminate to be balanced, for each ply with an orientation θ there must be another ply with the orientation $-\theta$. To maintain symmetry and balance, an even number of plies is required on each side of the plane of symmetry. The NS 18 ply laminate designs do not have an even number of plies on both sides of the plane of symmetry, one cannot design a balanced laminate. If the NS design can be modified to have an even number of plies on both sides of the plane of symmetry, then a balanced and symmetric NS layup can be designed.

The second motivation is that the ability to incrementally increase or decrease the number of plies in a laminate while maintaining the stiffness gives the designer greater flexibility to make more measured changes to a laminate design. This can also help to reduce the number of plies while maintaining stiffness.

Even though the NS designs have the same stiffness as standard angle composites, they may or may not have the same strength. The strength of NS designs still requires rigorous investigation as the failure mechanisms of NS designs are not well understood. Higher strengths will allow for potential weight savings. To implement any possible weight savings two approaches may be used, the use of thinner plies or a reduced ply count.

In recent years, important progress has been made in the development of composite laminates using thinner plies. Nowadays, thin-ply composite materials are commercially available down to about 20 μm per ply depending on the type of fiber [19]. This work will look at reduced ply counts. Reduced ply counts have the benefit of reduced layup time as well as the ability to use existing material for experimental validation.

When trying to achieve stiffness matching for dissimilar ply counts, the matching of $[A^N]$ and $[A^S]$ may or may not result in stiffness matching because the equivalent modulus depends on both the [A] matrix and the number of plies within the laminate. Hence, a more rigorous approach is required in which the $[A^S]$ matrix must be scaled to obtain values of individual elements to which the elements of the $[A^N]$ must be equated.

It was found that dividing the $[A^S]$ by the number of plies in the standard layup and then multiplying it by the number of plies in the non-standard layup gives the correctly scaled matrix that can be used to equate the elements of the $[A^N]$ matrix. The proof of this is presented in Section 3.4.2.

3.4.2 Formulation for Performing Stiffness Matching Independent of Ply Count

To maintain the same stiffness, i.e., the same effective modulus, the condition $E_{xx}^{S} = E_{xx}^{N}$ must be enforced. Let 'n' be the number of plies in the non-standard angle layup. This allows one to test the solution for its dependence on the number of plies in the NS layup. Substituting the corresponding elements of both laminates into Equation 27 produces Equation 59.

$$(A_{11}^{S} - \frac{(A_{12}^{S})^{2}}{A_{22}^{S}}) \frac{1}{N * thickness\ of\ ply} = (A_{11}^{N} - \frac{(A_{12}^{N})^{2}}{A_{22}^{N}}) \frac{1}{n * thickness\ of\ ply} \tag{59}$$

Comparing the corresponding elements of the [A] matrices results in Equation 60.

$$A_{11}^{S} \frac{1}{N * thickness\ of\ ply} = A_{11}^{N} \frac{1}{n * thickness\ of\ ply} \tag{60}$$

On simplification, a more compact relationship between the elements of the [A] matrices results in Equation 61.

$$A_{11}^{S} \frac{n}{N} = A_{11}^{N} \tag{61}$$

Similarly, comparing the other elements of the [A] matrix results in

$$\frac{(A_{12}^{S})^{2}}{A_{22}^{S}} \frac{1}{N} = \frac{(A_{12}^{N})^{2}}{A_{22}^{N}} \frac{1}{n}$$

upon rearranging,

$$\frac{(A_{12}^{S})^2}{A_{22}^{S}}\frac{n}{N} = \frac{(A_{12}^{N})^2}{A_{22}^{N}}$$

further manipulation results in

$$\frac{\left(A_{12}^{S} * \frac{n}{N}\right)^2}{A_{22}^{S}} * \frac{N^2}{n^2} * \frac{n}{N} = \frac{(A_{12}^{N})^2}{A_{22}^{N}}$$

additional simplification results in

$$\frac{\left(A_{12}^{S} * \frac{n}{N}\right)^2}{A_{22}^{S}} * \frac{N}{n} = \frac{(A_{12}^{N})^2}{A_{22}^{N}}$$

comparing corresponding terms results in

$$\left(A_{12}^{S} * \frac{n}{N}\right)^2 = (A_{12}^{N})^2$$

finally, leading to Equation 62.

$$A_{12}^{S} * \frac{n}{N} = A_{12}^{N} \tag{62}$$

Performing similar manipulations with the remaining corresponding elements of the [A] matrices

$$\frac{1}{A_{22}^{S}} * \frac{N}{n} = \frac{1}{A_{22}^{N}}$$

results in Equation 63.

$$A_{22}^{s} * \frac{n}{N} = A_{22}^{N} \tag{63}$$

Now, the only unconstrained pair of corresponding elements are the elements defining the shear response of the laminate. Hence, to constrain these elements of the [A] matrix, one utilizes the effective shear moduli of the respective laminates. For $G_{xy}^{S} = G_{xy}^{N}$, i.e., identical in-plane shear response, one uses the Equation 29. Substituting the elements of both laminates and then equating them to each other as carried out previously results in Equation 64.

$$\frac{A_{66}^{S}}{N * thickness\ of\ ply} = \frac{A_{66}^{N}}{n * thickness\ of\ ply} \tag{64}$$

Simplification results in Equation 65.

$$A_{66}^{s} * \frac{n}{N} = A_{66}^{N} \tag{65}$$

As the same relationship is seen between corresponding elements of the [A] matrix, this relationship can be extended to the entire matrix. Hence, to achieve the stiffness matching of laminates with different numbers of plies, one needs to alter the previous calculations by scaling the A matrix of the standard angle laminates before equating it to the symbolic equations consisting of the non-standard angled laminate angles using Equation 66.

$$[A^S] * \frac{n}{N} = [A^N] \tag{66}$$

Performing the same set of calculations for stiffness matching as above but now with the scaled A matrix for standard angle composites yields the angle pairs and ratios for stiffness matching laminate designs. As a NS laminate with a smaller thickness than the standard angle design would aid in reducing overall weight, the number of plies in the NS designs was initially reduced compared to standard design, i.e., the stiffness of a relatively thinner NS laminates was matched with the standard wing skin design. Figure 3.2 contains a plot of the angle pairs, i.e., $\psi\ vs\ \phi$, and a plot of $\psi\ vs$ γ that matches the stiffness of a 16 ply, non-standard angled laminate to an 18-ply wing skin layup.

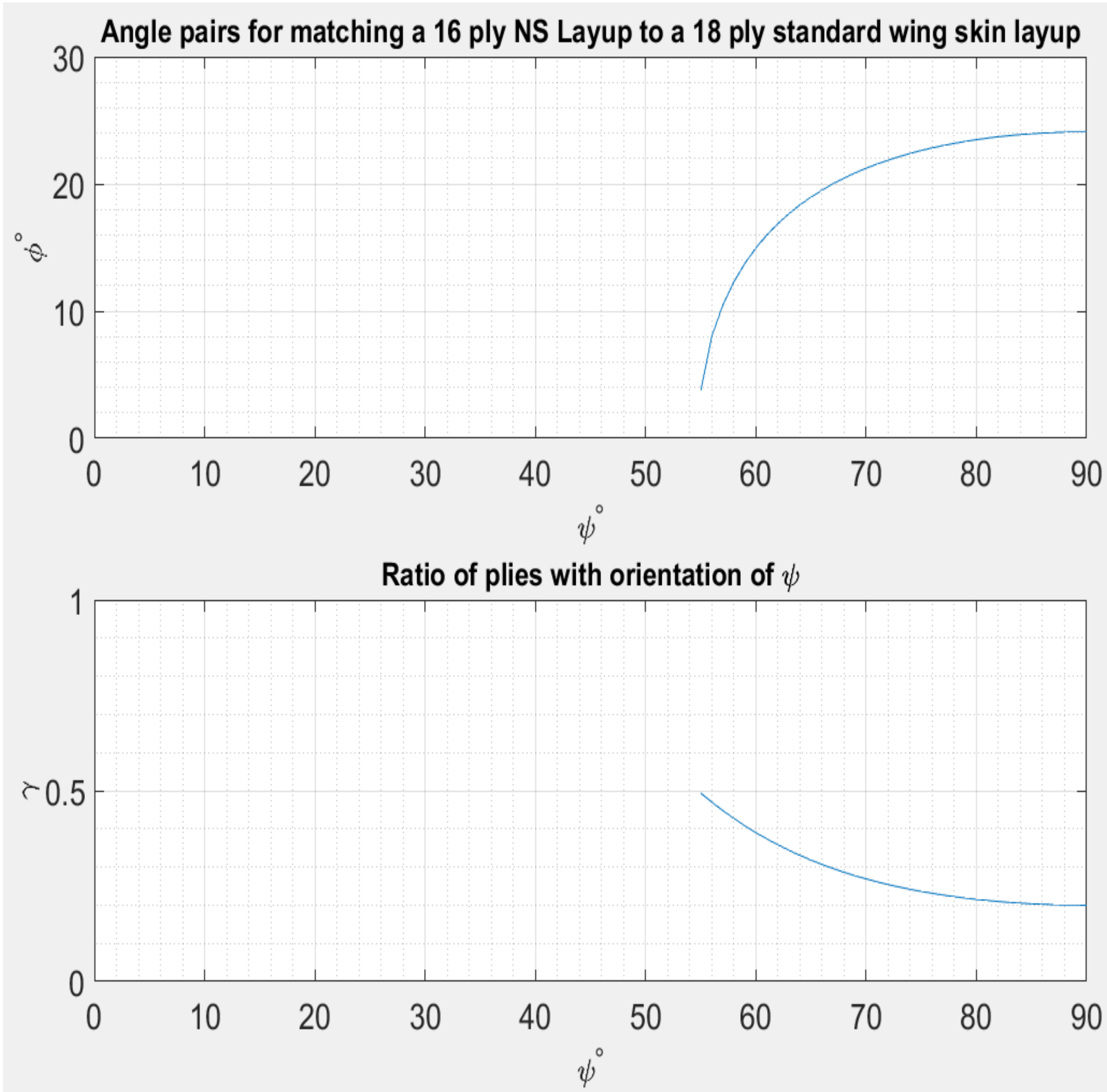

Figure 3.2 Designs for non-standard laminates made of 16 plies that match the stiffness of an 18 ply laminate

The solutions, i.e., the angle pairs ϕ, ψ and the thickness fractions corresponding to these angles described by the Figure 3.2, are the same as the solutions when the NS designs are assumed to have the same thickness as the standard designs shown in Figure 3.1. Hence, further variations of the number of NS layup plies were tested to check the variation in the range of possible laminate designs and the results are presented in the Figures 3.3 and 3.4. In Figure 3.3, the number of plies in the NS design were further reduced to determine if a larger difference between the number of plies in the NS and standard designs causes a shift in the solution. The solutions, i.e., the angle pairs $\phi,\ \psi$ and the thickness fractions corresponding to these angles, remain unchanged.

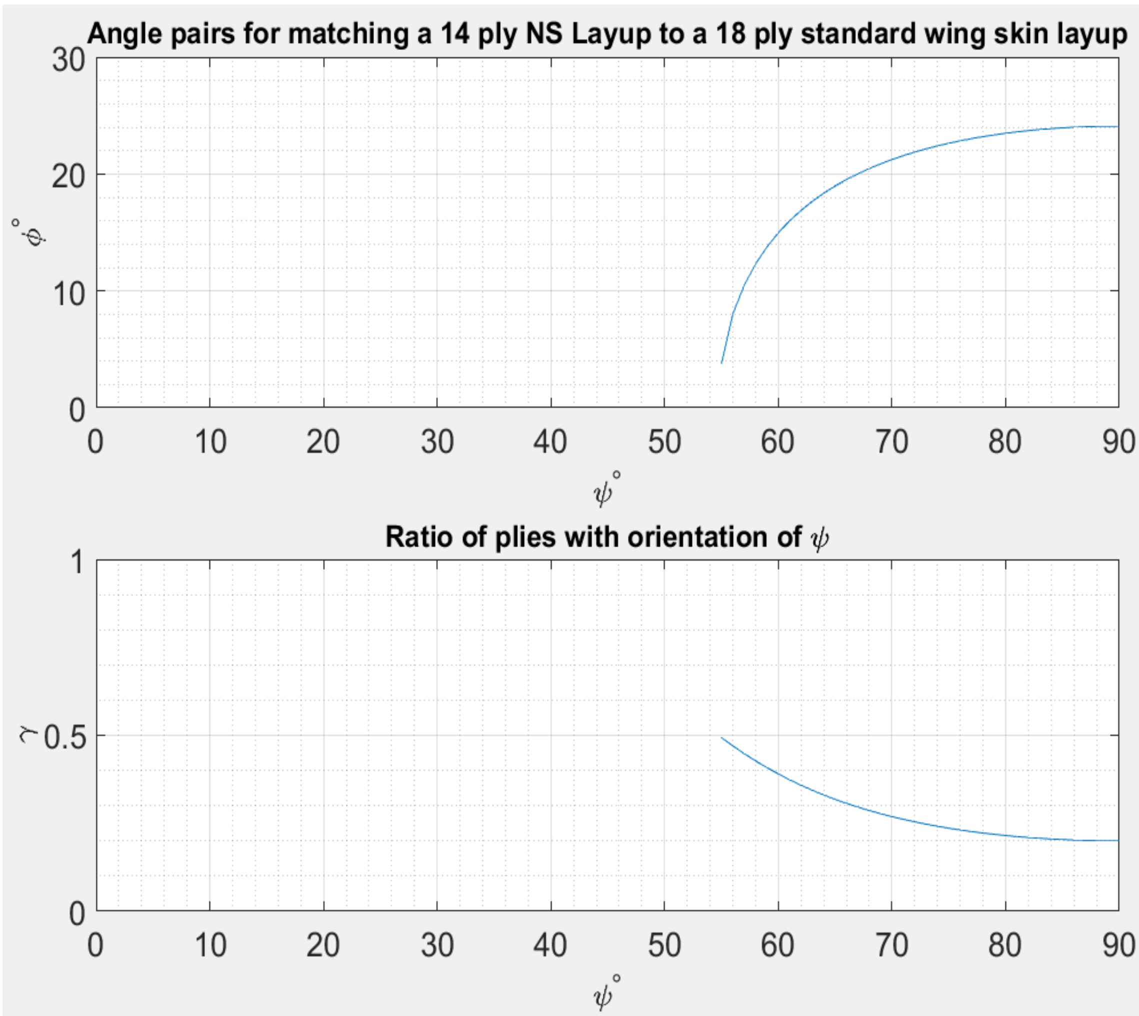

Figure 3.3 Designs for non-standard laminates made of 14 plies which match the stiffness of an 18 ply laminate

In Figure 3.4, the NS design was set to be thicker than the standard design. This was done to check if the solution changes when the NS design has a larger number plies as compared to the standard design. This exercise also resulted in the same solution as the original solution presented in Figure 3.1.

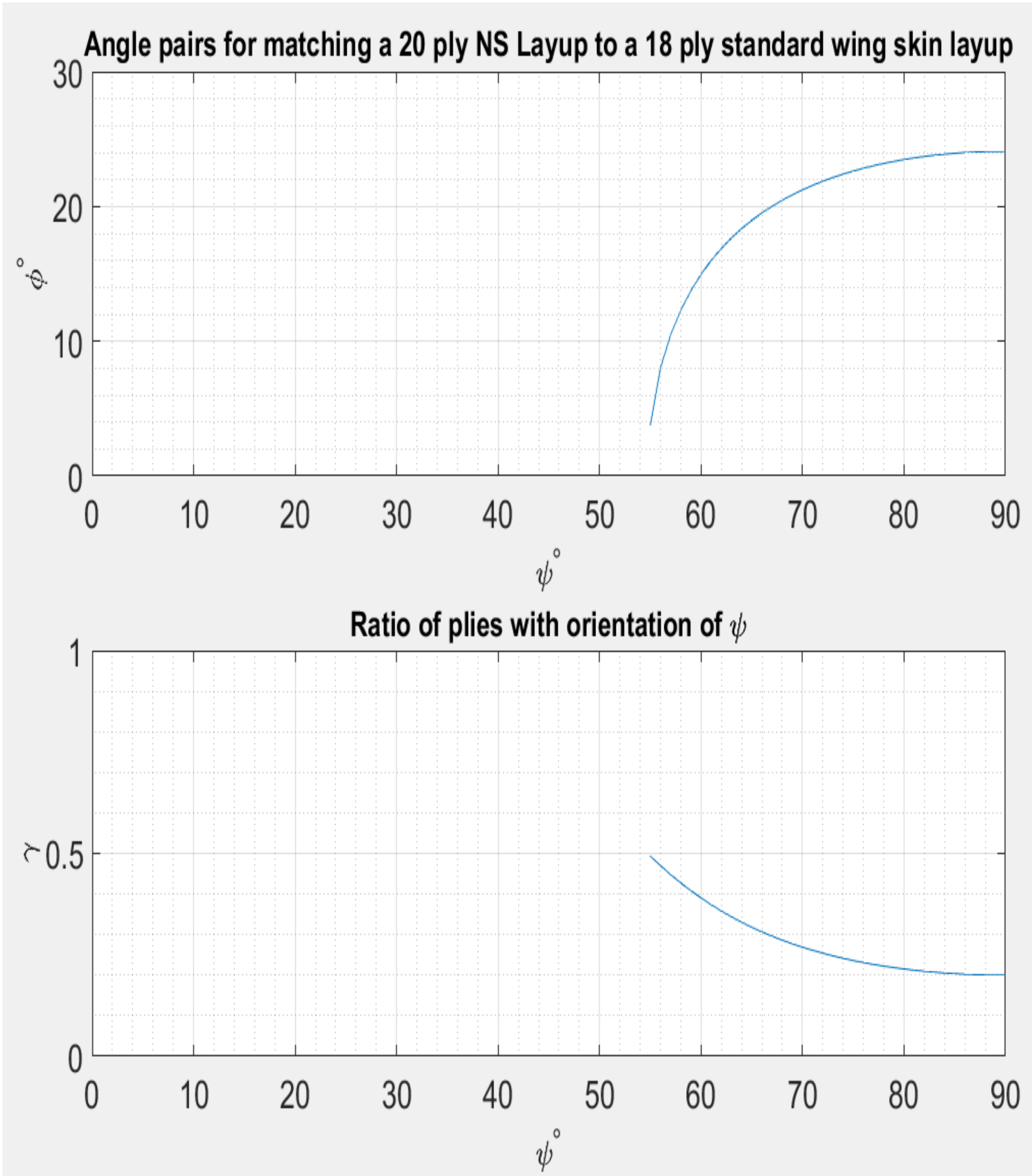

Figure 3.4 Designs for non-standard laminates made of 20 plies which match the stiffness of an 18 ply laminate

Every iteration results in the same set of solutions; hence, it can be concluded that the stiffness matching solutions are independent of the thickness of the NS designs. A proof of the independence of the stiffness matching solutions from the number of plies in the NS design is now presented in Section 3.5 of this chapter.

3.5 Independence of Solution from Ply Count

As seen above in Figures 3.2-3.4, the angle pairs and the angle ply ratios remain constant when the number of plies in the NS design are varied. The proof below describes why stiffness matching for laminates of different thickness was equivalent to stiffness matching of laminates with the same thickness resulting in the same solutions regardless of thickness of the non-standard angled laminate.

Equation 66 shows the condition that takes into account the thickness of both laminates so that the same stiffness is maintained when the standard angle and NS layups have different thicknesses.

$$[A^S] * \frac{n}{N} = [A^N] \tag{66}$$

Let the elements of a non-standard angled laminate with the same thickness as the standard design be denoted by $[A^{N1}]$ and the elements of non-standard angled laminate with different thickness be $[A^{N2}]$. Now taking A_{11}^S for the laminates to have the same stiffness, the conditions shown in Equations 67 and 68 must be met.

$$\begin{aligned} A_{11}^S = A_{11}^{N1} = \mathrm{N}\gamma(\mathrm{U}_1 + \mathrm{U}_2\cos(2\psi) + \mathrm{U}_3\cos(4\psi))(t_{ply}) \\ + \mathrm{N}(1-\gamma)(\mathrm{U}_1 + \mathrm{U}_2\cos(2\phi) + \mathrm{U}_3\cos(4\phi))(t_{ply}) \end{aligned} \tag{67}$$

$$\begin{aligned} A_{11}^{N2} = \mathrm{n}\gamma(\mathrm{U}_1 + \mathrm{U}_2\cos(2\psi) + \mathrm{U}_3\cos(4\psi))(t_{ply}) \\ + \mathrm{n}(1-\gamma)(\mathrm{U}_1 + \mathrm{U}_2\cos(2\phi) + \mathrm{U}_3\cos(4\phi))(t_{ply}) \end{aligned} \tag{68}$$

As discussed above, when two laminates have different ply counts, then the condition demonstrated by Equation 69 must be met for matched stiffness response.

$$A_{11}^{S}\frac{n}{N} = A_{11}^{N2} \tag{69}$$

Starting with Equation 67

$$A_{11}^{N1} = \mathrm{N}(\gamma(\mathrm{U}_1 + \mathrm{U}_2\cos(2\psi) + \mathrm{U}_3\cos(4\psi))(t_{ply})$$

$$+ (1-\gamma)(\mathrm{U}_1 + \mathrm{U}_2\cos(2\phi) + \mathrm{U}_3\cos(4\phi))(t_{ply}))$$

and dividing the entire equation by 'N' results in the following.

$$\frac{A_{11}^{N1}}{N} = \gamma(\mathrm{U}_1 + \mathrm{U}_2\cos(2\psi) + \mathrm{U}_3\cos(4\psi))(t_{ply})$$

$$+ (1-\gamma)(\mathrm{U}_1 + \mathrm{U}_2\cos(2\phi) + \mathrm{U}_3\cos(4\phi))(t_{ply})$$

Multiplying the numerator and denominator of the right-hand side of the equation by 'n' results in

$$\frac{A_{11}^{S}}{N} = \frac{\begin{array}{c}\mathrm{n}(\gamma(\mathrm{U}_1 + \mathrm{U}_2\cos(2\psi) + \mathrm{U}_3\cos(4\psi))(t_{ply}) + \\ (1-\gamma)(\mathrm{U}_1 + \mathrm{U}_2\cos(2\phi) + \mathrm{U}_3\cos(4\phi))(t_{ply}))\end{array}}{n}$$

On simplifying, Equation 70 results.

$$\frac{A_{11}^{S}}{N} = \frac{A_{11}^{N2}}{n} \tag{70}$$

Equation 70 is the same as Equation 69. Hence, the solution for performing stiffness matching for laminates with different thicknesses can be arrived at from the solution for laminates of the same thickness. This means that the solution for stiffness matching is independent of thickness and both ‘N’ and ‘n’ are arbitrary. Hence the solutions for stiffness matching for the same thickness laminates extends to any thickness.

This result gives one an enormous amount of flexibility; the same solution can be used to perform stiffness matching regardless of the number of plies within the NS design. This gives the designer the ability to incrementally alter the thickness of the laminate without affecting its stiffness. This was not possible with earlier standard designs.

3.6 Discussions on Stiffness Matching and NS designs

Based on the Figure 3.1, several symmetric physically realizable discreet layup designs can be created. The method detailed above and the method developed by Butler both assume that the thickness proportion of each NS angle is continuous. In reality, UD laminates have standardized and discrete ply thickness. This discretizes the possible thickness ratios for both angle pairs; hence, the entire range of theoretically possible designs are not physically realizable. In most cases, approximations must be made.

Butler’s method uses a continuous input for the standard designs, whereas the method presented in this thesis utilizes a discretized physically realizable input to more accurately represent a discrete layup. Neither method enforces any rules regarding symmetry or balance, which are important considerations when selecting a laminate design. Hence, these rules be taken into account when selecting a design from Figure 3.1.

Balancing standard angle designs requires that only the plies with orientations of ±45° be balanced, whereas 0° and 90° plies are inherently balanced.

As the conditions enforced only govern the in-plane stiffness, the out of plane stiffness, which is described by the [D] matrix, is not uniform across the range of NS designs. This results in variations in the out of plane performance even though the in-plane stiffness response remains the same. This variation of out of plane performance gives one the unique opportunity to tailor the laminates for improved buckling performance.

The method developed for stiffness matching above uses two angles to define the entire laminate, namely ϕ, ψ. Having fewer ply angles simplifies the layup process and makes homogenization of the laminate easier. Homogenization is the process in which the stacking sequence of the laminate is altered to disperse all angles uniformly throughout the laminate. Homogenization is shown in Figure 3.5, where the blue layers represent plies with orientation 0° and the yellow layers represent plies with orientation 90°. Homogenization helps make laminates tougher and stronger [1]. Furthermore, the homogenization of asymmetric laminates can lead to weight and cost savings [24].

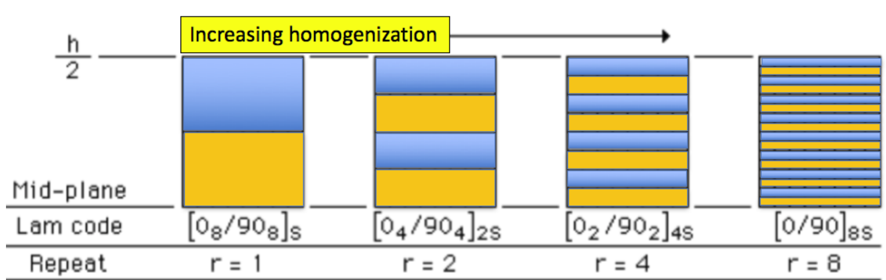

Figure 3.5 Homogenization of [0/90] with different ply thickness and repeats [1]

Any laminates with identical stiffness will exhibit the same stress-strain response when in service. This allows for the use of NS laminates to replace existing laminates without affecting the larger scale design of aircraft.

Stiffness matching also allows one to maintain the stiffness of a laminate regardless of total ply count. This property gives the designer much greater flexibility in terms of controlling stiffness when compared to standard angle composites.

Connections and joints are another area where composites continue to be treated as 'black aluminum.' Stiffness matching can be utilized to reduce the stiffness mismatch between parts with different layups and can be vital for improving the performance of joints, which have been noted to be very sensitive to stiffness mismatch [25].

3.7 Layups Chosen for Further Investigation

From Figure 3.1, three NS designs that match the stiffness of the standard wing skin layup were created. These designs will be used to compare the strength of NS layups with the standard wing skin layup in Chapters 4 and 5. Higher strength will result in potential weight savings.

The only rule imposed on these designs was symmetry about the mid plane of the laminate. Symmetry about the mid plane has been enforced because CLT yields large errors when analyzing asymmetrical laminates [33]. When a NS layup is defined, it is necessary to define the total number of plies, so that the number of plies of each NS angle can be determined. From Figure 3.1, if one chooses $\phi = 0^\circ$, then the complementary angle $\psi = 55^\circ$ and $\gamma = 0.4935$. Upon rounding γ to 0.5, the number of plies with angle ϕ, $N_\phi = 9$

and the number of plies with angle Ψ ,$N_{\psi} = 9$. This design, although physically realizable, cannot be symmetrical about the mid-plane. For symmetry about the mid plane in a laminate, the total number of plies for each angle must be even, therefore this NS design was rejected. Furthermore, designs with ϕ close to 0˚ would ostensibly perform very similarly to standard designs because 0˚ is a standard angle, whereas the corresponding NS angle ψ is in the range of 55˚ and is close to 45˚, which is also a standard angle. Hence, three designs from the curve in Figure 3.1 that allow for symmetry about the mid-plane were chosen and are presented in Tables 3.3-3.5.

Table 3.3: NS design #1

NS design #1	
Ply Number	Ply Orientation (Degrees)
1	14
2	-14
3	14
4	-14
5	14
6	60
7	-60
8	60
9	-60
10	-60
11	60
12	-60
13	60
14	14
15	-14
16	14
17	-14
18	14

Table 3.4: NS design #2

NS design #2	
Ply Number	Ply Orientation (Degrees)
1	19
2	-19
3	19
4	-19
5	19
6	-19
7	65
8	-65
9	65
10	65
11	-65
12	65
13	-19
14	19
15	-19
16	19
17	-19
18	19

Table 3.5: NS design #3

NS design #3	
Ply Number	Ply Orientation (Degrees)
1	23
2	-23
3	23
4	-23
5	23
6	-23
7	23
8	80
9	-80
10	-80
11	80
12	23
13	-23
14	23
15	-23
16	23
17	-23
18	23

It must be noted that apart from symmetry, the stacking sequence of the angles of the individual layers does not affect the in-plane stiffness of the designs. Optimization of the stacking sequence may be investigated in future studies. The strength of these designs will be compared to the standard wing skin design. The robustness of these designs under various loads will allow one to determine if NS designs present any advantages over standard designs.

3.8 Chapter Summary

A stiffness matching method was proposed and validated. The solutions of this method proved to be independent of the thickness of the NS designs. Three NS designs were developed. The strength of these designs is predicted in Chapter 4 and experimentally measured in Chapter 5.

CHAPTER 4

STRESS DISTRIBUTION AND FIRST PLY FAILURE METHOD

4.1 Stress Distributions in a Laminated Material

The ability to visualize the stress state of a laminate and to estimate its strength is vital when evaluating performance of a laminate design in the strength domain. These estimates help to reduce testing costs by allowing for an informed decision on which laminates should be fabricated for testing. In this chapter, the stress distribution developed within standard wing skin design and the NS designs shown in Tables 3.3-3.5 will be calculated for various types of loadings. These stress distributions will help one to understand if the NS designs are sufficiently robust when compared to standard angle designs. These stress distributions will be used to calculate the FPF loads for the standard wing skin and NS designs. These loads will be compared to determine which designs offer greater strength.

When a laminate is loaded in a given direction, different plies carry varying fractions of the total load. This is a result of the different stiffness of the plies within the laminate. Plies that exhibit greater stiffness in the loading direction carry a larger fraction of the load. Hence, a distribution of stresses is developed within the laminate. This is shown in Figure 4.1, where a uniform strain results in non-uniform stress distribution within the laminate. These stress distributions help in visualizing the effect of global loads on different plies and can be used to compare the safety of different laminates under the same loading.

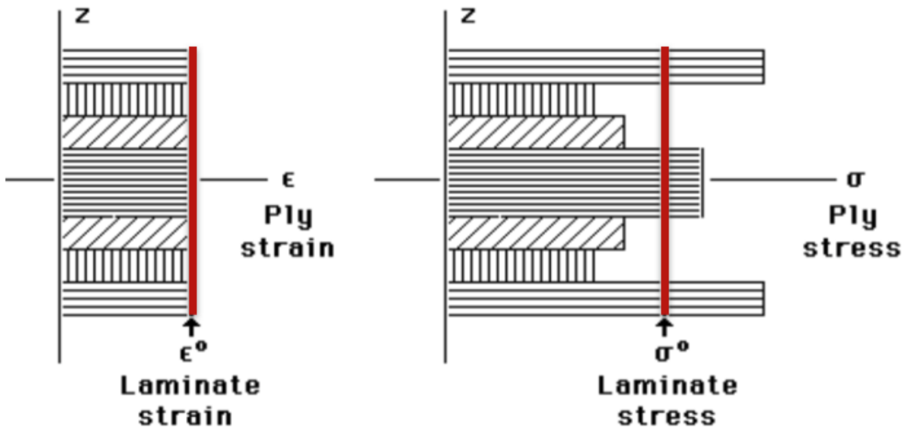

Figure 4.1 Stress and strain distributions in a symmetric laminate [1]

The variation of stresses within the laminate has a large bearing on how a laminate fails when loaded. The method used to plot these distributions will be extended to calculate First Ply Failure (FPF) loads in Section 4.2 for any laminate of interest. The FPF load is the theoretical load at which the weakest ply within the laminate fails. Furthermore, the progression of failure for a laminate can also be investigated by extending the FPF method. Therefore, these stress distributions form the basis to predict the strength of laminates. Based on these distributions, one can visualize the contribution of each ply to the load carrying capacity of the laminate. These distributions can be used to analyze which designs are more robust and to average the stress over the laminate more effectively. The standard wing skin designs will be compared to the NS designs in Tables 3.3-3.5 to determine which theoretical designs are more robust.

This distribution of stresses within a laminate under a mechanical load can be found using the constitutive relationships from CLT. The method for plotting these stress distributions when the laminates are subjected to in-plane loading is detailed below.

Initially, the mid-plane strains and curvatures for the laminate are found. As discussed in Section 2.1, according to CLT, Equation 38 describes the stress – strain relationship for laminates.

$$\begin{bmatrix} N \\ M \end{bmatrix} = \begin{bmatrix} A & B \\ B & D \end{bmatrix}. \tag{38}$$

Upon rearranging, Equation 71 results.

$$\begin{bmatrix} \epsilon \\ \kappa \end{bmatrix} = \begin{bmatrix} A' & B' \\ B' & D' \end{bmatrix} \begin{bmatrix} N \\ M \end{bmatrix} \tag{71}$$

To find $\begin{bmatrix} A' & B' \\ B' & D' \end{bmatrix}$, the intermediate matrices shown in Equations 72-75 are needed.

$$[A^*] = [A^{-1}] \tag{72}$$

$$[B^*] = -[A]^{-1}[B] \tag{73}$$

$$[C^*] = [B][A]^{-1} \tag{74}$$

$$[D^*] = [D] - [B][A]^{-1}[B] \tag{75}$$

Based on these matrices, $[A']$, $[B]'$ and $[D']$can be determined from Equations 76-78.

$$[A'] = [A^*] - [B^*][D^*]^{-1}[C^*] \tag{76}$$

$$[B'] = [B^*][D^*]^{-1} \tag{77}$$

$$[D'] = [D^*]^{-1} \tag{78}$$

For the case being considered, i.e., only in-plane loading, [M] =0, so there are no applied moments. Further, as only symmetric designs are considered, $[B] = 0$ and consequently $[B'] = 0$. These simplifications help to reduce computational time significantly.

Once the vector $\begin{bmatrix} \epsilon \\ \kappa \end{bmatrix}$, which gives the strains and curvatures at the mid plane of the laminate, has been calculated for the load case under consideration, one can find the stresses in the global co-ordinate system for individual plies, i.e., a general kth ply, using Equation 79

$$\begin{bmatrix} \sigma_x \\ \sigma_y \\ \tau_{xy} \end{bmatrix}^{[k]} = [\bar{Q}]^{[k]} \begin{bmatrix} \epsilon_x^0 \\ \epsilon_y^0 \\ \epsilon_{xy}^0 \end{bmatrix} + z^{[k]} \begin{bmatrix} \kappa_x \\ \kappa_y \\ \kappa_{xy} \end{bmatrix} \tag{79}$$

where $[\overline{Q}]$ is the transformed $[Q]$ matrix associated with the kth ply.

Once the vectors containing the stresses in each ply are known, this information can be used to visualize the stress state within the laminate to better understand the effect of a certain type of loading on the laminate of interest. Based on the method presented above, the theoretical stress distributions developed within a standard wing skin design will be compared to the NS designs (Tables 3.3-3.5) that match the stiffness of the standard wing skin design. These distributions will help one understand the individual contributions of different plies to the load carrying capacity of a laminate.

The load cases for which the stress distributions have been plotted were defined based on the loading experienced by composite specimen, using, for example tests, that follow ASTM D3039 [36] and ASTM D6641 [37]. As most ultimate strength testing is done by applying uniaxial loading on coupons, uniaxial loading along the so called "balancing axis," i.e., the global X and Y axes, has been considered. The primary load case of interest is when the laminate is loaded along the global X-axis, i.e., when Equation 80 is true.

$$\begin{bmatrix} N \\ M \end{bmatrix} = \begin{bmatrix} N_{xx} \\ 0 \\ 0 \\ 0 \\ 0 \\ 0 \end{bmatrix} \tag{80}$$

There is a large amount of data available for the failure strengths for various standard layups for this load case and is shown in Table 4.1 below, the significance of these strengths will be elaborated upon in Section 4.2. For the stress distribution calculations carried out below, the material properties of laminates manufactured from prepregs made of CYCOM 5320-1 resin with T650 fiber have been utilized [21]. In Chapter 5, the experimental Open Hole Compression (OHC) strengths of laminate designs shown in Tables 3.1 and 3.3-3.5, manufactured from CYCOM 53201-1 resin with T650 fiber are presented. Hence, one can utilize the stress distributions in Section 4.1 and the FPF predictions presented in Section 4.2 calculated according to the material properties of CYCOM 5320-1 resin with T650 fiber to identify correlations between the theoretical FPF predictions of the laminates presented in Tables 3.1, 3.3-3.5 and the experimental strengths presented in Chapter 5.

The theoretical stress distributions for when the standard wing skin laminate is loaded along the x axis, as shown in Table 3.1, is presented in Figure 4.2. The X axis of both sub-plots in Figure 4.2 represents the location of a ply within the laminate with the first ply being ‘1’. The angle associated with each ‘Ply Number’, i.e., the ply location, has been annotated at the top of the graph. Along the Y axis, the normal stress developed along the loading direction as a result of this load case has been normalized by different factors to help one better understand the stress state. In the first sub-plot, the stresses have been normalized by the gross stress, i.e., the average stress sustained by the entire laminate. This provides a sense of the fraction of the applied load carried by each ply.

In the second sub-plot in Figure 4.2, the stresses have been normalized by the minimum stress within the laminate. This provides a sense of the loads carried by each ply relative to each other.

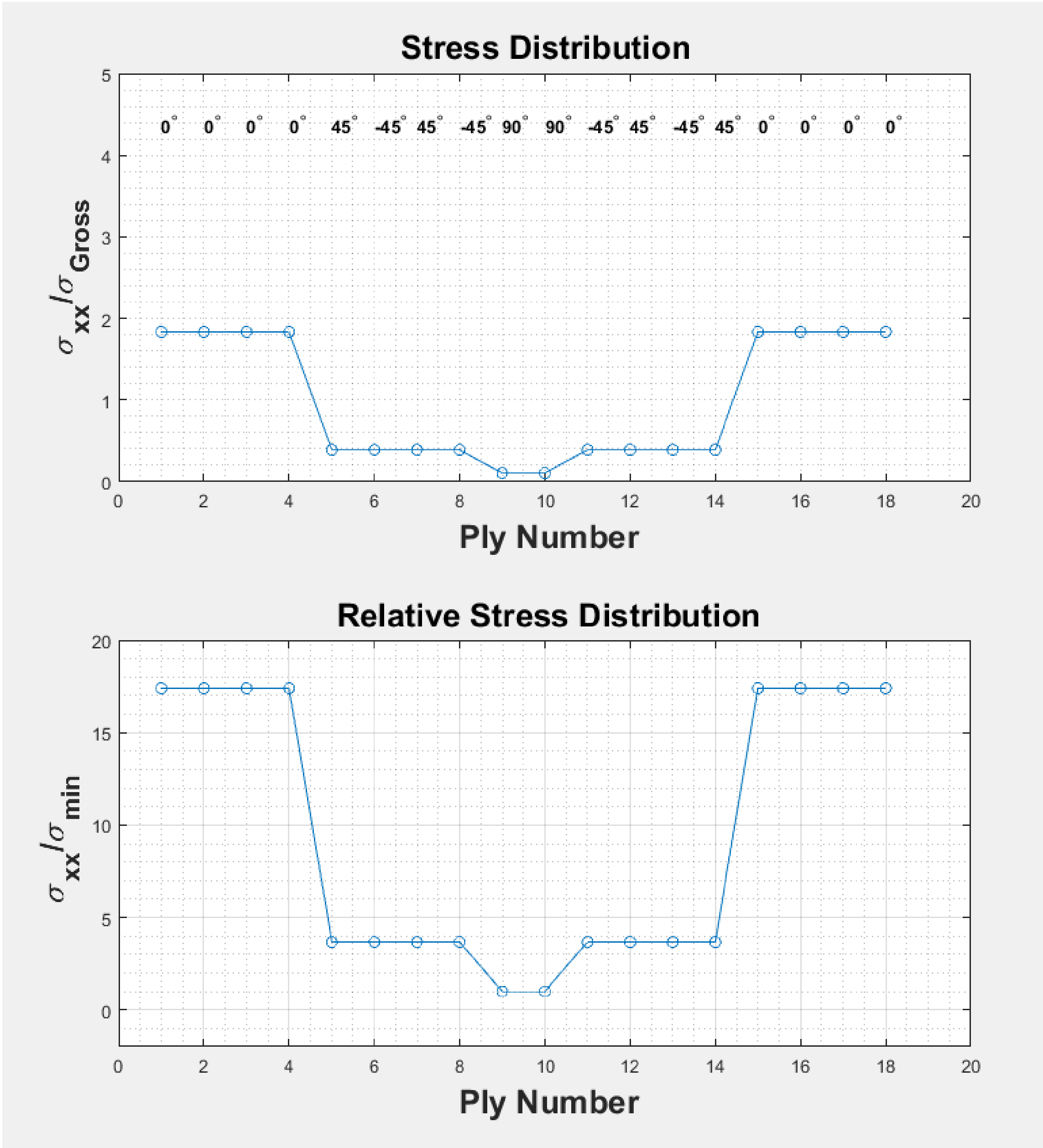

Figure 4.2 Stress distributions in a standard wing skin laminate

In Figure 4.2, one can observe that plies with angle 0° carry the majority of the applied loads. In comparison to the 0° plies, loads carried by the plies with angles of 45°, −45° and 90° are negligible. This is a result of the 0° plies exhibiting maximum stiffness in the loading direction, i.e., the X direction, while the other plies will be significantly more compliant. This stiffness gradient within the laminate results in the distribution of stress seen in Figure 4.2.

Furthermore, it can be seen that when the ply orientations for two adjacent plies is different, there is generally a large jump in the stress. To better visualize this discontinuity, a different approach was adopted. The stresses of neighboring plies were considered and are shown in Figure 4.3.

The larger normal stress between two adjacent plies at an interface was normalized by the relatively smaller stress to provide an idea of the stress discontinuity between layers. The normalized stress distributions were found to be independent of N_{xx}; hence, any arbitrary load along the x axis results in the same relative stress values. The x axis in Figure 4.3 represents the interface at which the stress discontinuity is being evaluated. For eighteen plies, seventeen interfaces need to be considered.

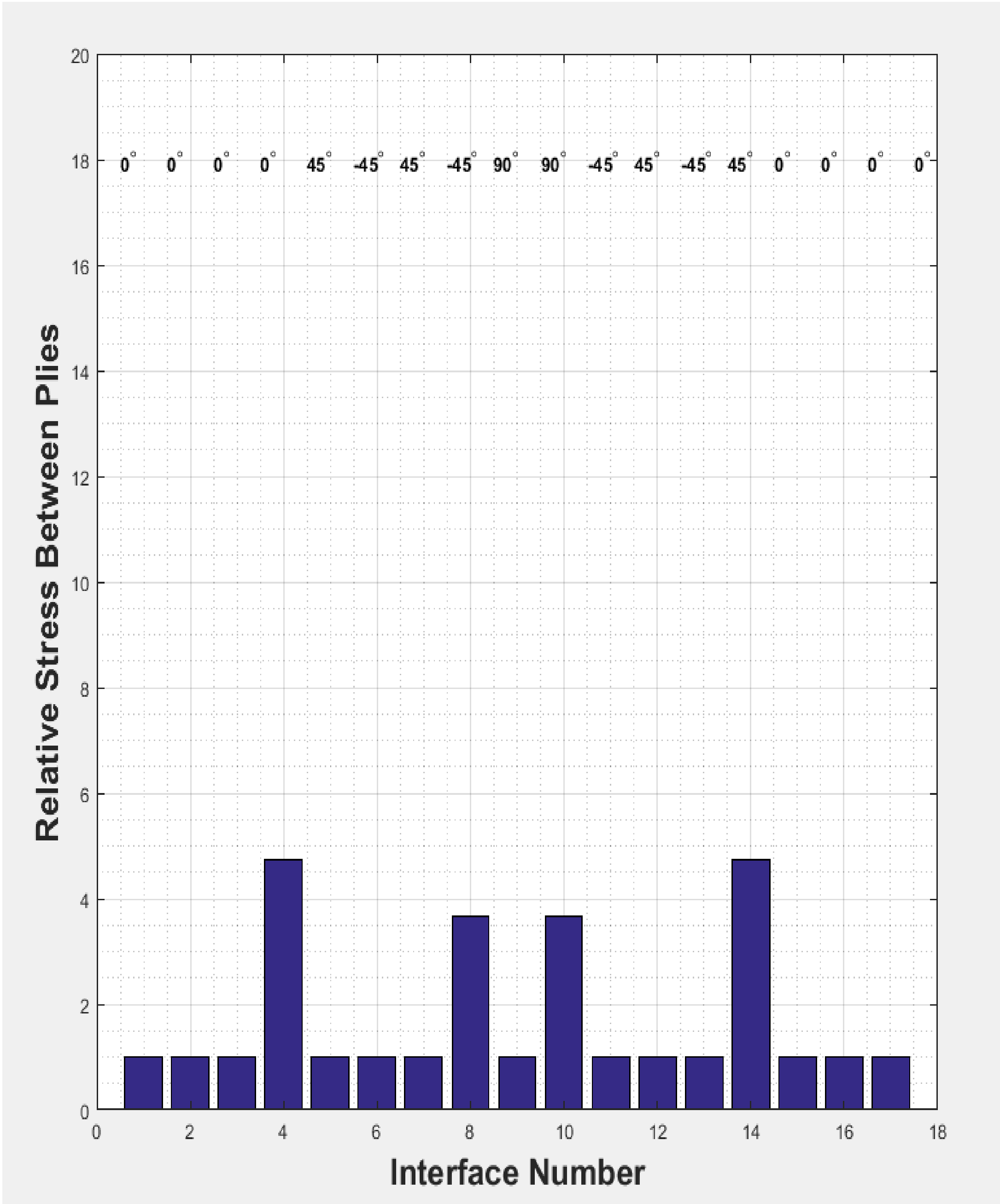

Figure 4.3 Stress discontinuity in a standard wing skin laminate when loaded along the X axis

The second load case loads the laminate along the global Y axis, i.e., when Equation 81 is true. This is of interest to determine if any gain or loss in the strength along x axis for the NS designs could be related to any change of strength in the y direction.

$$\begin{bmatrix} N \\ M \end{bmatrix} = \begin{bmatrix} 0 \\ N_{yy} \\ 0 \\ 0 \\ 0 \\ 0 \end{bmatrix} \tag{81}$$

For this case, when the laminate is loaded along the Y direction. The larger angles, i.e., 90˚, will exhibit much greater stiffness in the loading direction. The loading direction is aligned with the fiber direction of the 90˚ plies. This results in the 90˚ plies carrying a much greater proportion of load in comparison to the other plies, as shown in Figure 4.4. In a similar manner to Figure 4.2, the x axis of both sub plots represent the location of a ply within the laminate with the first ply being '1'. The angle associated with each 'Ply Number', i.e., ply location, has been annotated at the top of the graph. Along the y axis is the normal stress developed in the loading direction as a result of this load case. This normal stress has been similarly normalized to provide a better picture of the contributions of each ply.

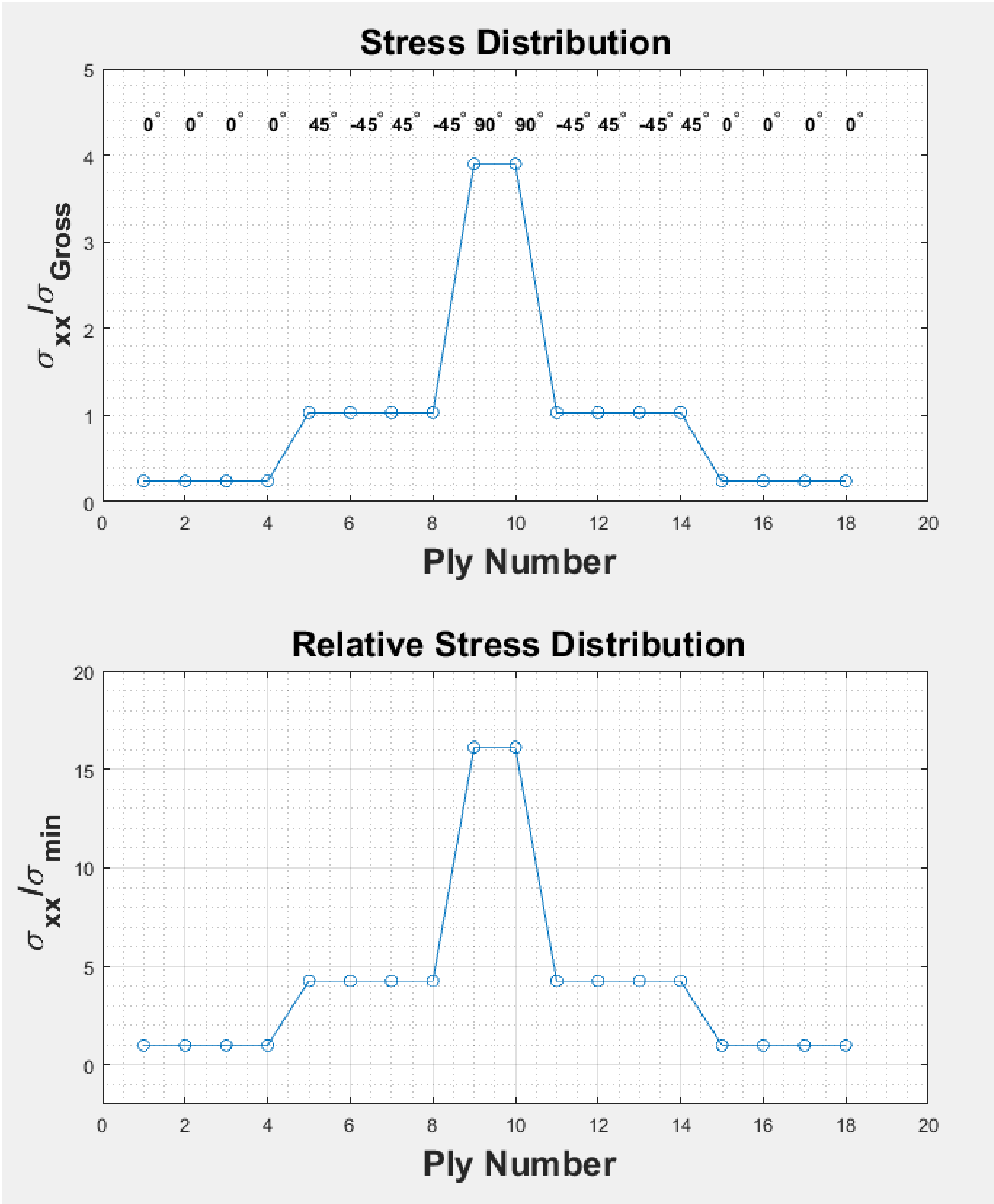

Figure 4.4 Stress distributions in a standard wing skin laminate when loaded along the Y direction

Now, in a similar manner to Figure 4.3, the stress discontinuity developed in the standard wing skin laminate when it is loaded in the y direction will be analyzed. The stress discontinuity is shown in Figure 4.5 and the axes follow the same scheme as Figure 4.3. Here, one can see the same trends observed before; there is a large stress discontinuity whenever there is a change in fiber orientation between adjacent plies and it is generally proportional to the difference in orientations between adjacent plies.

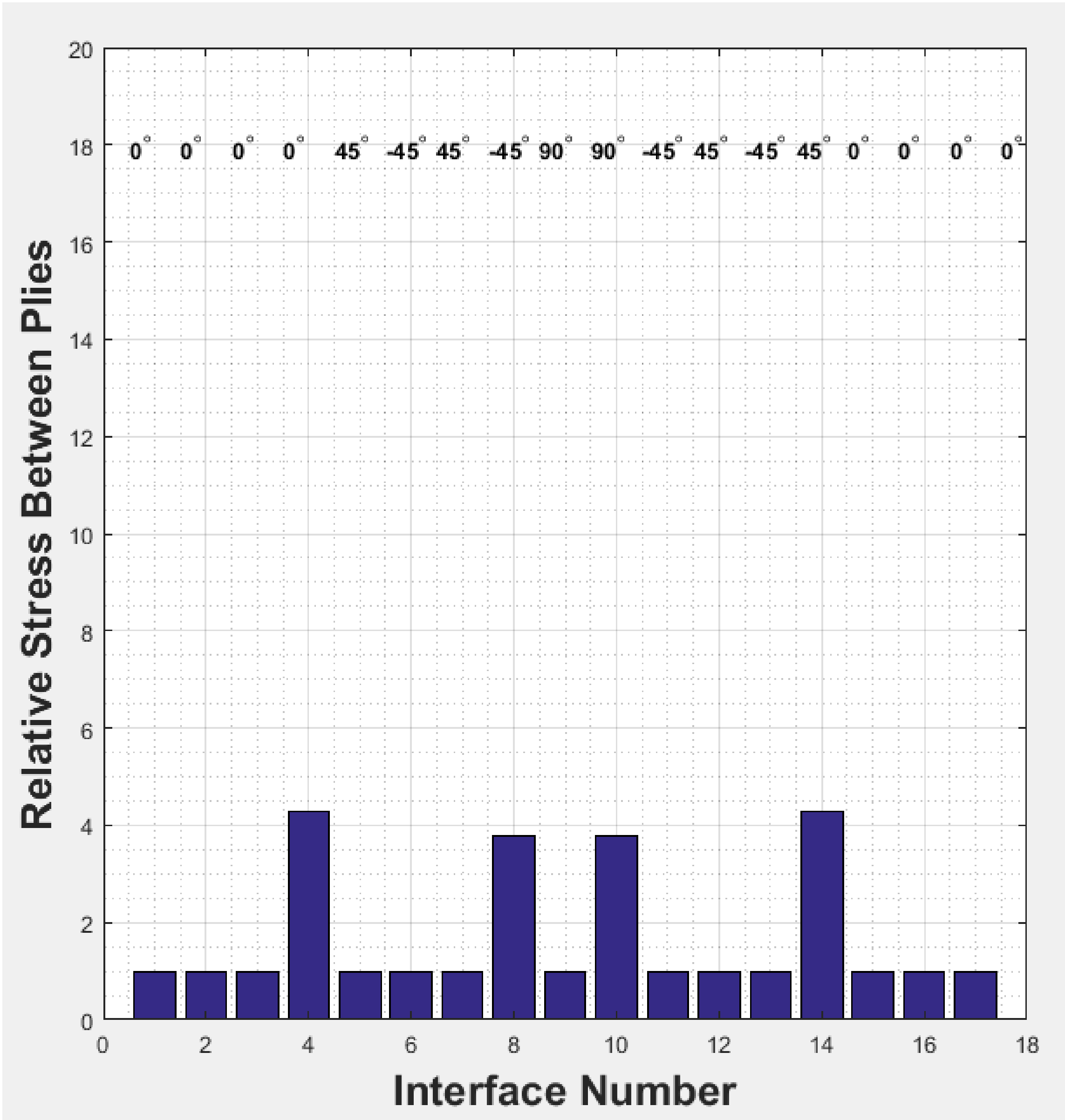

Figure 4.5 Stress discontinuity in a standard wing skin laminate when loaded along the Y direction

Similarly, these two classes of plots were used to analyze the NS designs. These plots can be used to compare the characteristics of the NS designs to the standard designs that acts as a benchmark and are presented below. The same treatment is applied to NS design #1 for loading along the x axis stress distributions and the resulting stress discontinuities have been plotted in Figure 4.6 and Figure 4.7, respectively.

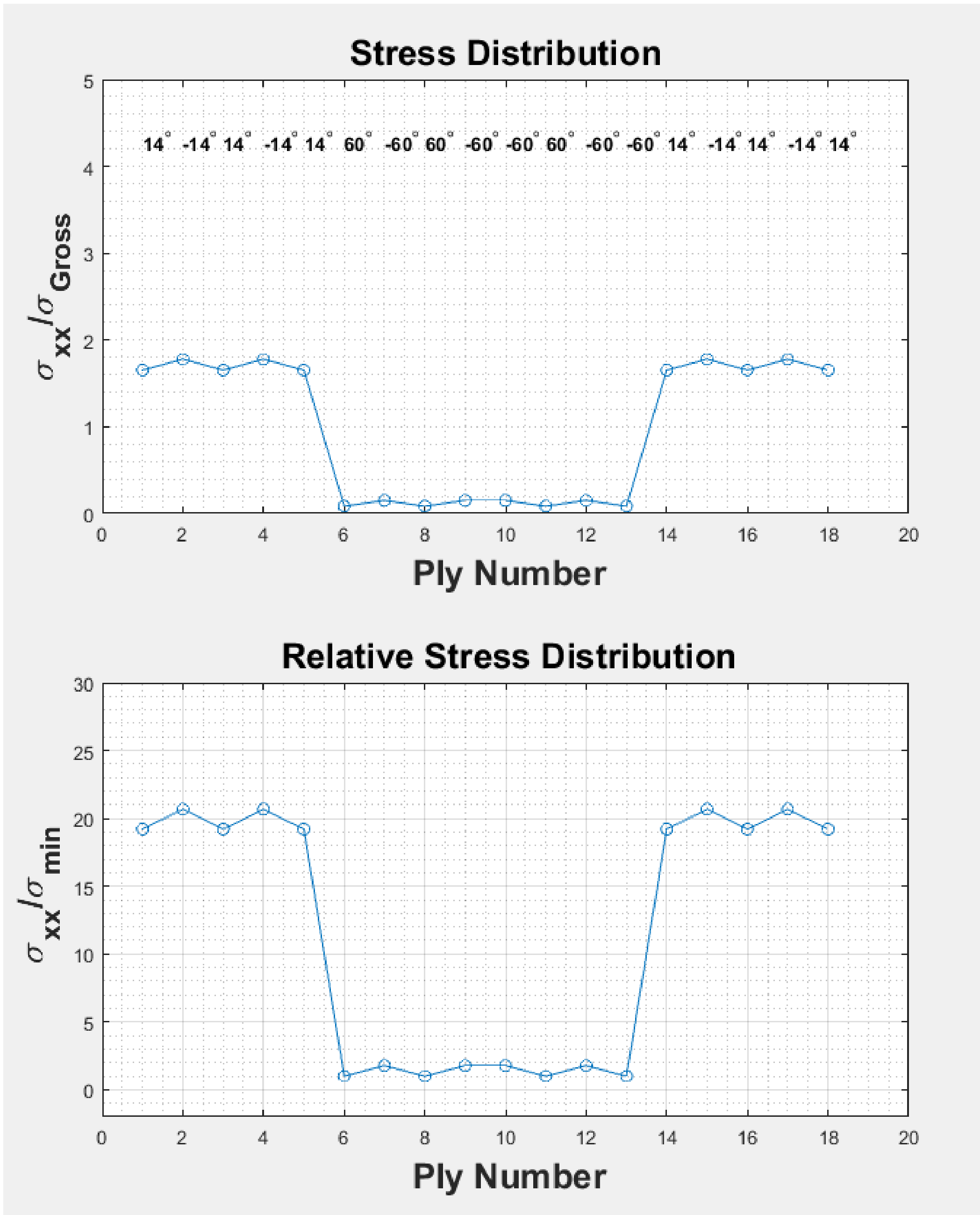

Figure 4.6 Stress distributions in NS design #1 when loaded along the X direction

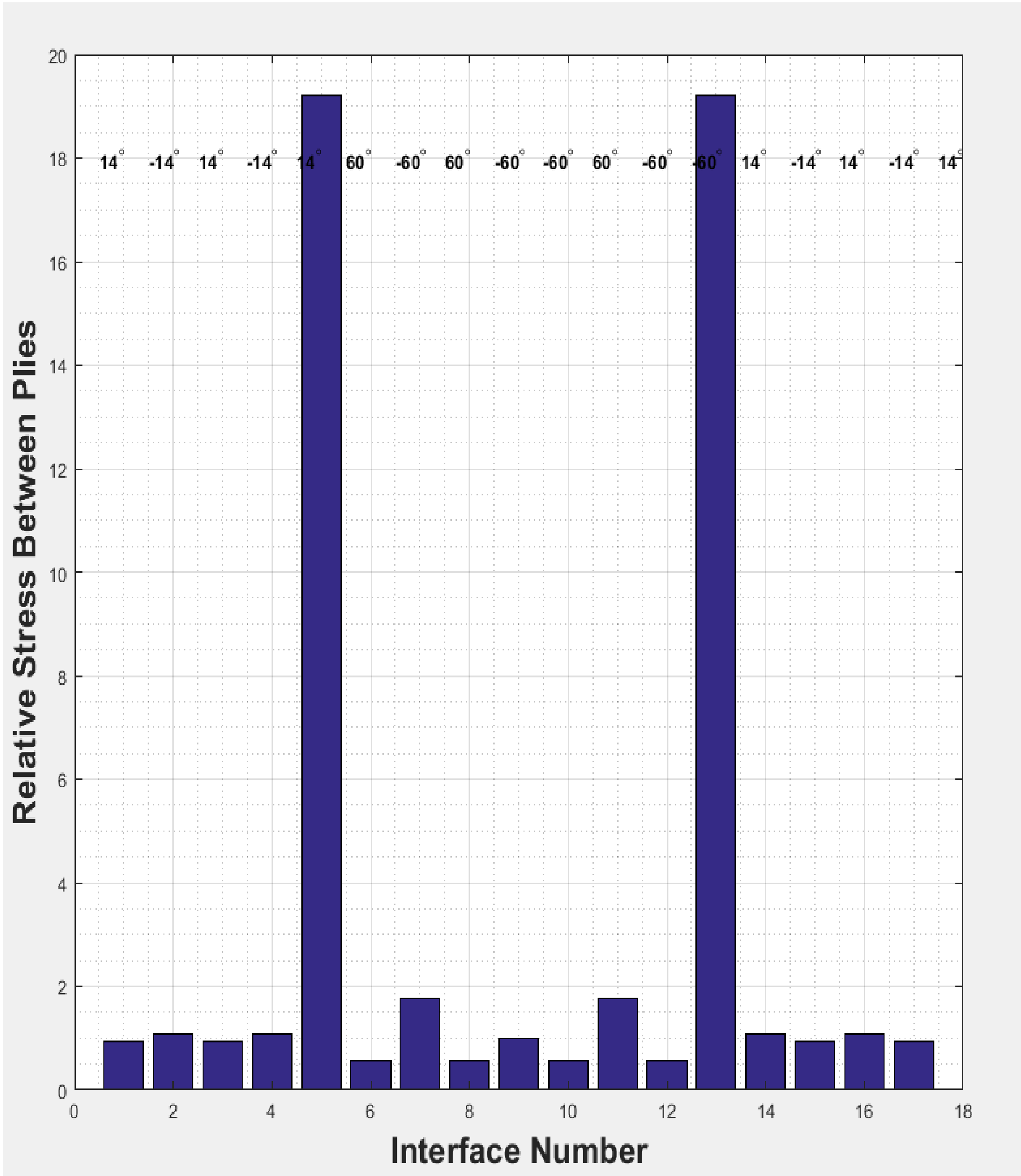

Figure 4.7 Stress discontinuity in NS design #1 when loaded along the X direction

In Figure 4.6 a large jump in stress can be seen when the ply angle changes from $\pm\phi$ to $\pm\psi$. This trend is repeated when the laminate is loaded in the Y direction. This is a result of $\pm\phi$ always being closer to 0˚ while $\pm\psi$ is generally closer to 90˚. Hence, trends of stress distribution and stress discontinuity observed in NS designs are similar to those seen in the standard wing skin layup.

However, the stress discontinuity for NS designs is different. In Figure 4.7, two rather large peaks are seen when compared to the peaks observed in the standard design. This difference can be explained by the nature of standard designs. In standard designs, the stress changes over two "steps"; the first is the transition when the ply angle changes from 0˚ to 45˚ and the second step is the transition 45˚ to 90˚. This reduces the mismatch of stresses over multiple steps. There are two major peaks in the stresses for the NS designs when the ply angle changes from $\pm\phi$ to $\pm\psi$.

Figure 4.8 and Figure 4.9 show the stress distributions and stress discontinuity when the NS design #1 is loaded in the Y direction.

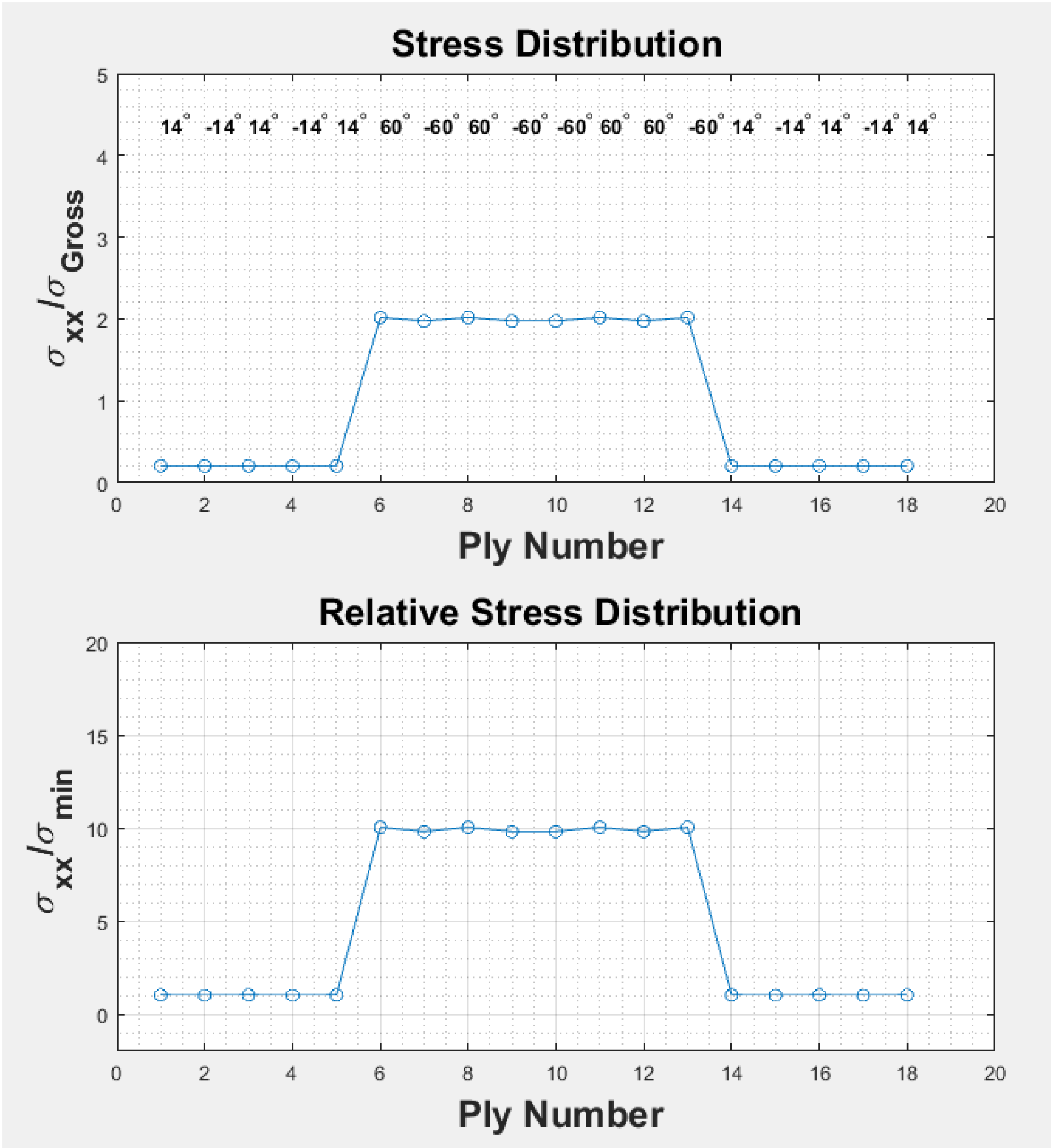

Figure 4.8 Stress distributions in NS design #1 when loaded along the Y direction

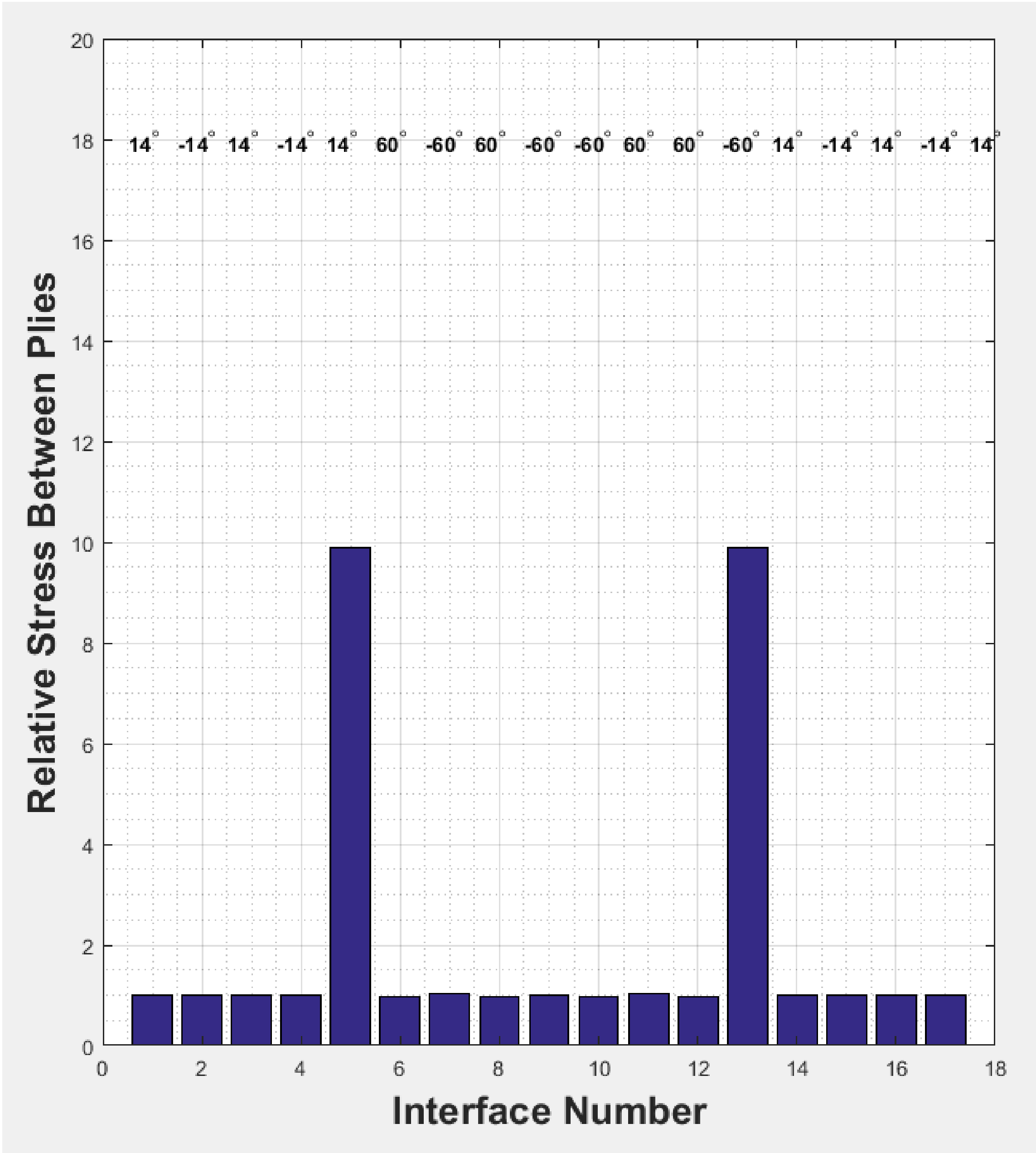

Figure 4.9 Stress discontinuity in NS design #1 when loaded along the Y direction

In general, the maximum value $\frac{\sigma_{xx}}{\sigma_{gross}}$ for the NS designs is lower than that seen in the standard designs. This indicates that the stress is more uniformly distributed over the entire laminate when compared to standard designs. This leads to the conclusion that the

NS designs will be more robust because the loads are more evenly distributed over more plies.

The stress distributions and stress discontinuity for the NS design #2 when loaded along the X axis are presented in Figure 4.10 and 4.11, respectively. The trends observed for NS design #1 are repeated.

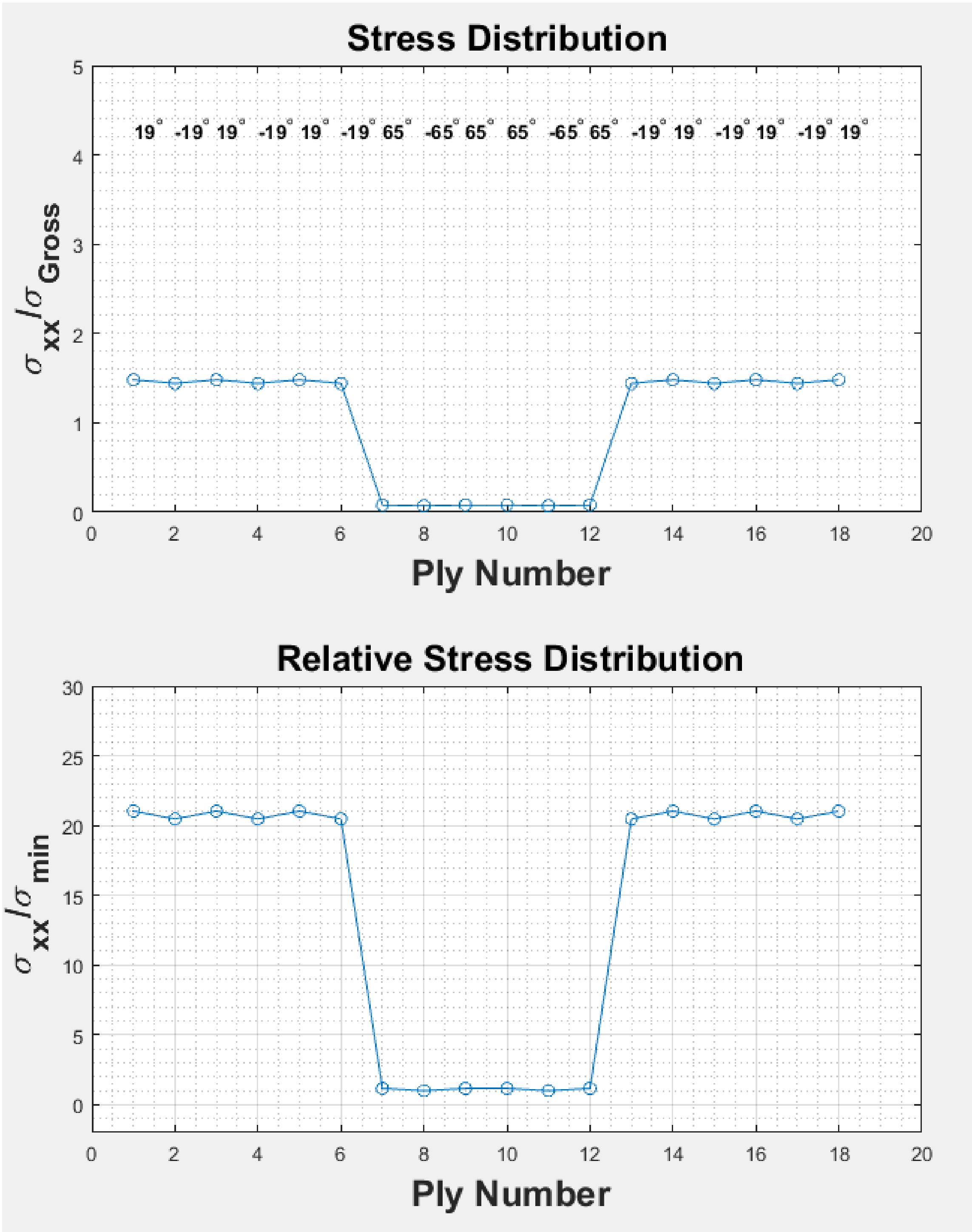

Figure 4.10 Stress distributions in NS design #2 when loaded along the X direction

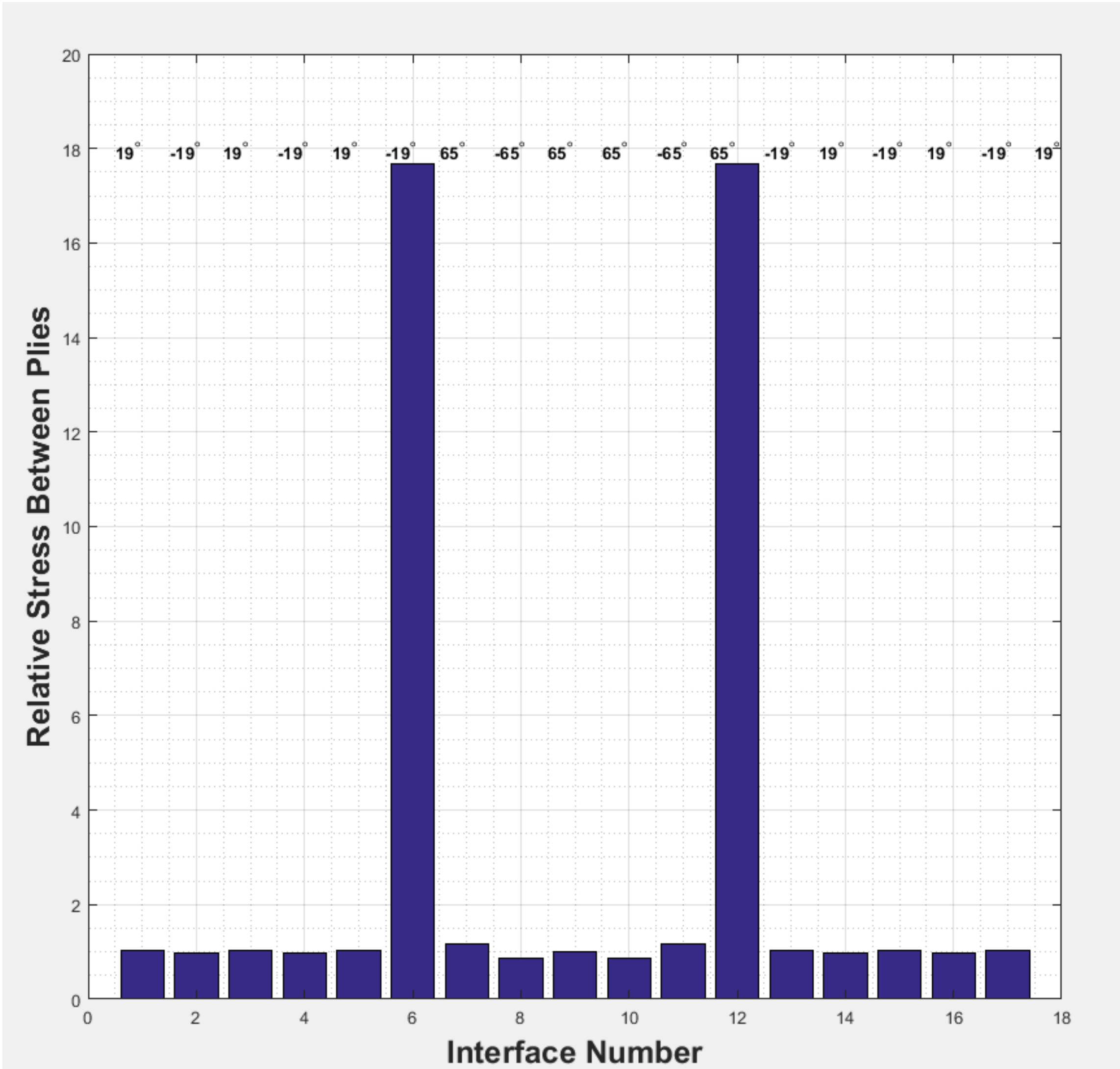

Figure 4.11 Stress discontinuity in NS design #2 when loaded along the X direction

The stress distributions and stress discontinuity for the NS design #2 when loaded along the Y axis are presented in Figure 4.12 and Figure 4.13, respectively. The trends when NS design #1 is loaded along the Y axis are repeated by NS design #2.

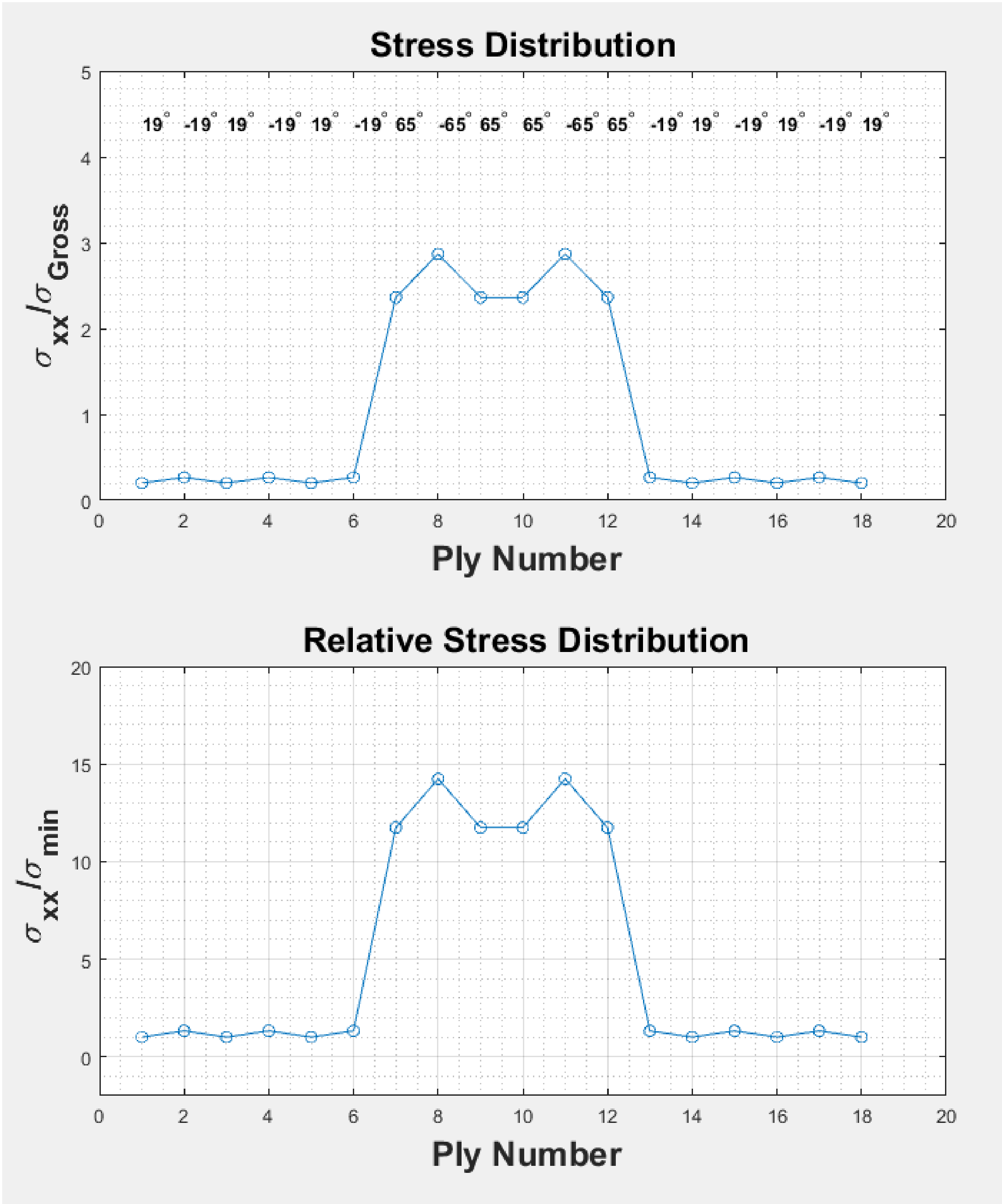

Figure 4.12 Stress distributions in NS design #2 when loaded along the Y direction

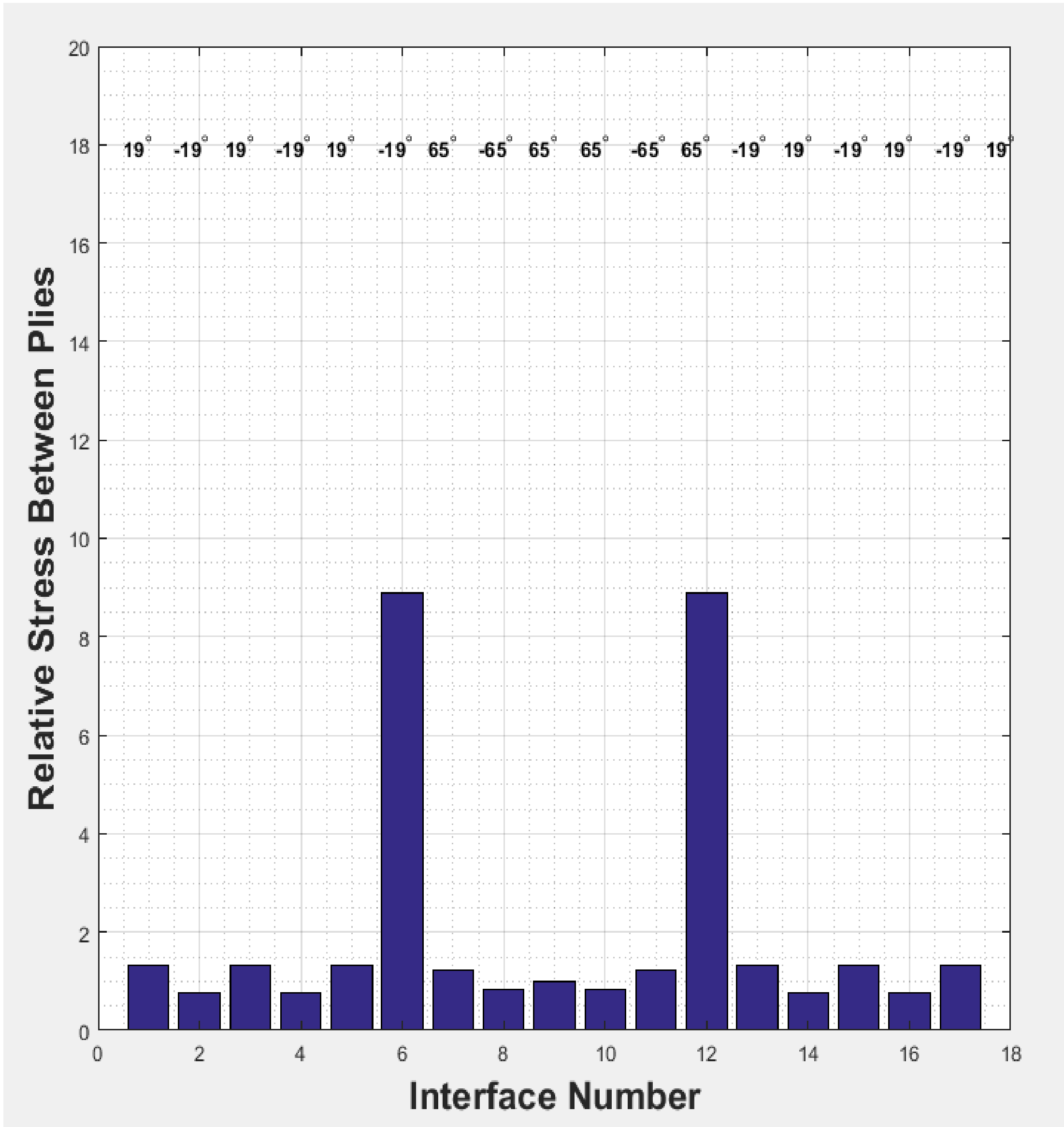

Figure 4.13 Stress discontinuity in NS design #2 when loaded along the Y direction

The stress distributions and stress discontinuity for the NS design #3 when loaded along the X axis are presented in Figure 4.14 and Figure 4.15, respectively. The trends seen for NS design #1 are again repeated. The lower maximum value of $\frac{\sigma_{xx}}{\sigma_{gross}}$ when compared to the standard design indicates that this design is more robust when compared to the standard design. This robustness results from a lower concentration of stress in the primary load bearing plies.

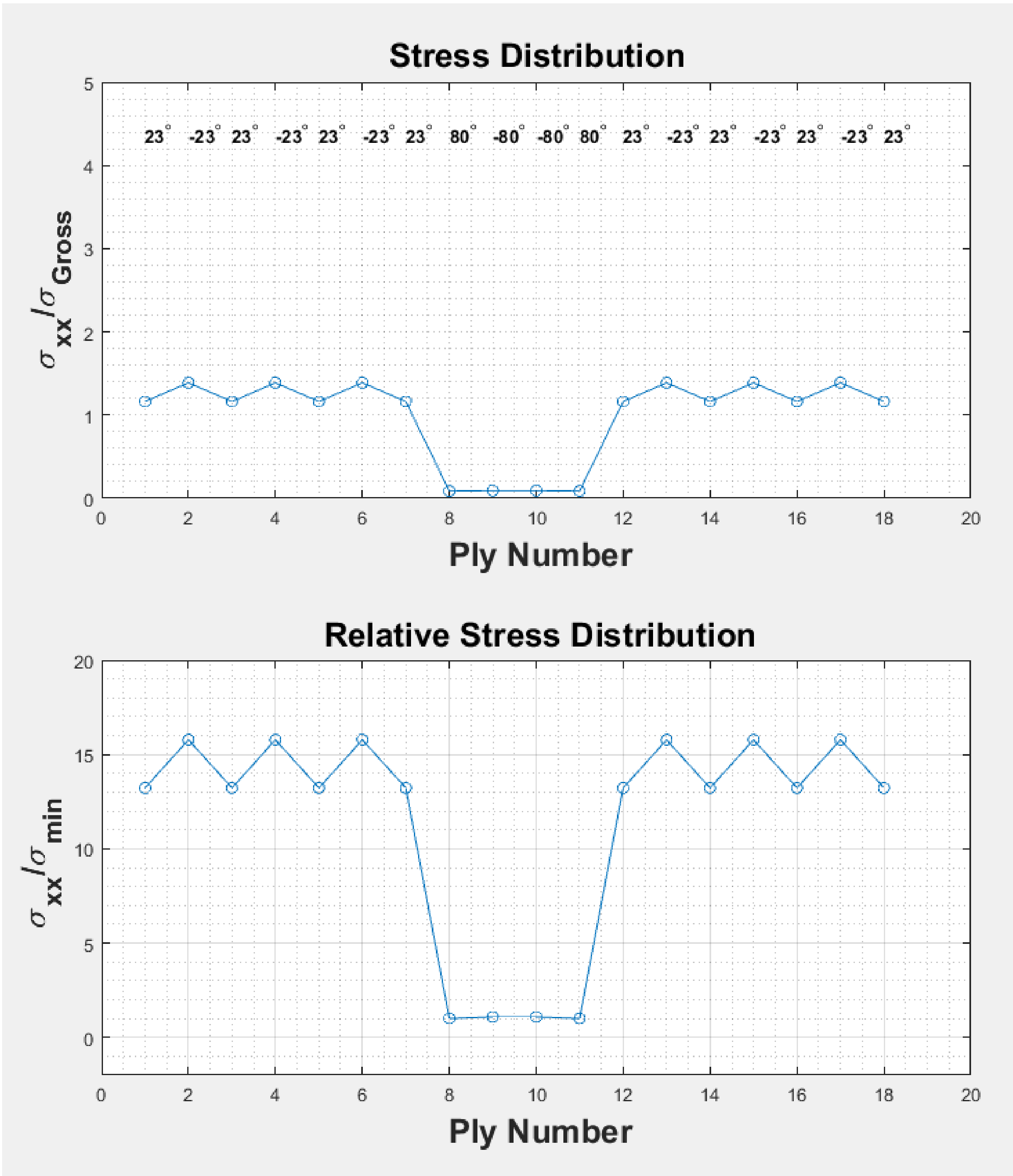

Figure 4.14 Stress distributions in NS design #3 when loaded along the X direction

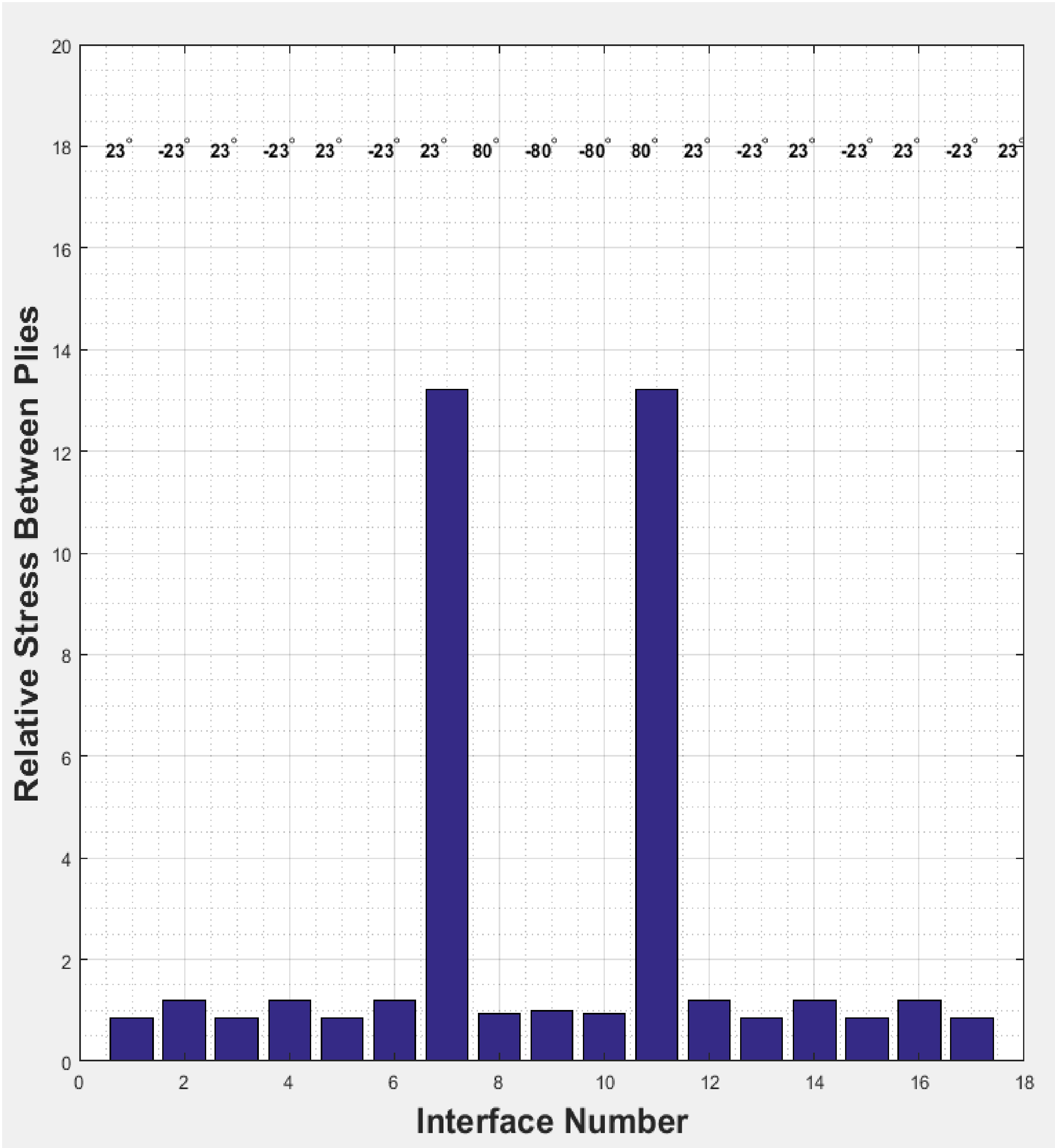

Figure 4.15 Stress discontinuity in NS design #3 when loaded along the X direction

The stress distributions and stress discontinuity for the NS design #3 when loaded along the Y axis are presented in Figure 4.16 and Figure 4.17, respectively. When compared to the standard wing skin design, the NS designs have more plies with higher angles, i.e., plies with angles closer to 90°; as a result, the stress is more evenly distributed when these NS laminates are loaded in the y direction as shown in Figure 4.16, which is representative of the stress state of all NS designs when loaded along the Y axis.

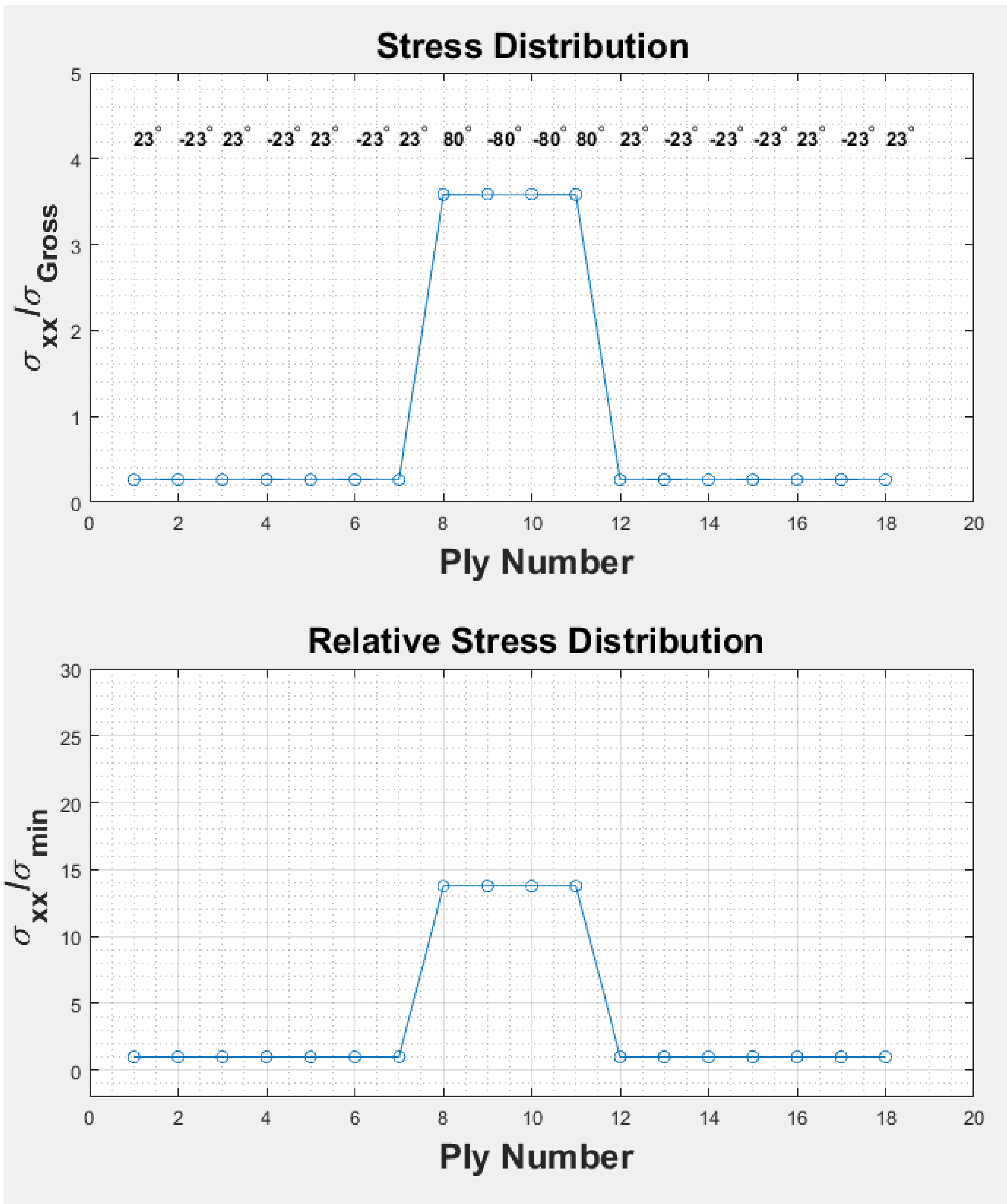

Figure 4.16 Stress distributions in NS design #3 when loaded along the Y direction

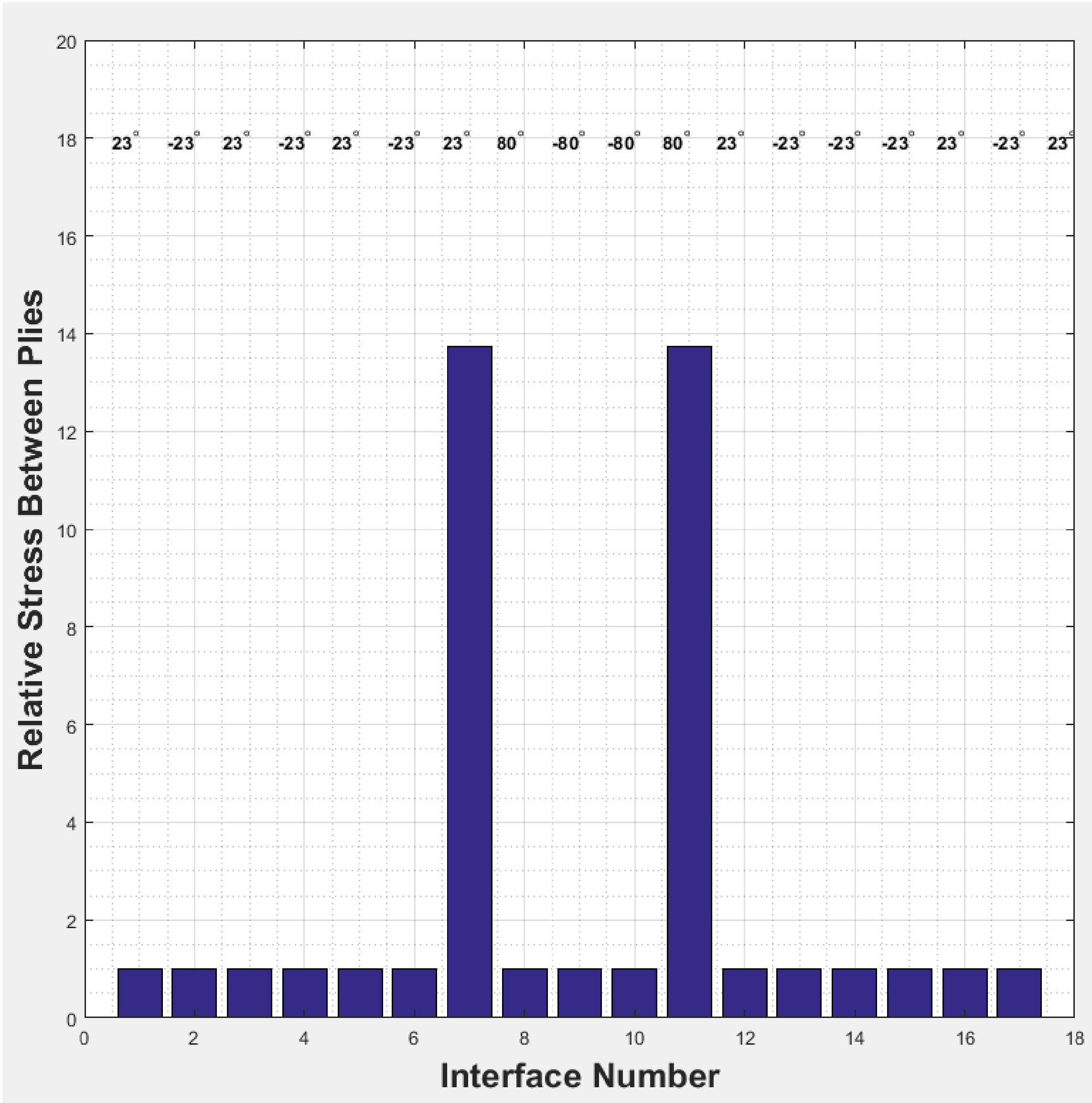

Figure 4.17 Stress discontinuity in NS design #3 when loaded along the Y direction

The stress distributions computed above can now be used to estimate the safe loads for the laminates of interest. The first ply failure (FPF) theory will be used in Section 4.2 to compare NS designs to a standard design. The theoretical safe loads for infinite un-notched plates will be computed. These are shown in the next section.

4.2 Methodology for Computing FPF Loads

First ply failure theory is the first approach used to estimate the strength of any laminate. It will provide an estimate of any gain or loss in strength by NS designs when compared to standard designs. Hence, one can predict if using NS angles while maintaining stiffness affects the strength of the laminates.

As a large number of operations are required, solving analytically for FPF loads can be quite complex. These operations are detailed below and draw upon many of the same operations used for computing the stress distributions presented in Section 4.1.

The loads applied to the laminate are used to define the [N] and [M] vectors. Then, based on these loads, the mid-plane strains of the laminate are found using Equation 71.

$$\begin{bmatrix} \epsilon \\ \kappa \end{bmatrix} = \begin{bmatrix} A' & B' \\ B' & D' \end{bmatrix} \begin{bmatrix} N \\ M \end{bmatrix} \tag{71}$$

These mid-plane strains are mapped to individual plies to find the stresses experienced by each ply in the global co-ordinate system. This operation is performed using Equation 79. It must be noted that ‘k’ represents the ply number associated with the ply of interest within the laminate.

$$\begin{bmatrix} \sigma_x \\ \sigma_y \\ \tau_{xy} \end{bmatrix}^{[k]} = [\bar{Q}]^{[k]} \begin{bmatrix} \epsilon_x^0 \\ \epsilon_y^0 \\ \epsilon_{xy}^0 \end{bmatrix} + z^{[k]} \begin{bmatrix} \kappa_x \\ \kappa_y \\ \kappa_{xy} \end{bmatrix} \tag{79}$$

Failure theories for composites generally require the knowledge of the stress states of all plies in their material co-ordinate systems. Hence, the ply stresses are transformed to the material co-ordinate system using the rotation matrix that was described earlier in Chapter 2 and is presented again here. Equations 42 and 43 are used to transform the global stresses in each ply to its material co-ordinate system.

$$\begin{bmatrix} \sigma_1 \\ \sigma_2 \\ \sigma_6 \end{bmatrix} = [T_1] \begin{bmatrix} \sigma_x \\ \sigma_y \\ \tau_{xy} \end{bmatrix} \tag{42}$$

$$[T_1] = \begin{bmatrix} m^2 & n^2 & 2mn \\ n^2 & m^2 & -2mn \\ -mn & mn & m^2 - n^2 \end{bmatrix} \tag{43}$$

The maximum stress criteria discussed in Chapter 2 is used to check for violations of the conditions represented by Equations 39-41.

$$-S_{Lc} < \sigma_{11} < S_{Lt} \tag{39}$$

$$-S_{Tc} < \sigma_{22} < S_{Tt} \tag{40}$$

$$-S_{LTs} < \tau_{12} < S_{LTs} \tag{41}$$

If and when the conditions shown by Equations 39-41 are violated, then FPF has occurred and the load is unsafe. To simplify the implementation of FPF, an iterative method has been used.

This method iteratively increases the load applied to the laminate. The ply stresses are calculated and then rotated to their individual material co-ordinate systems. Then, these stresses are compared to the failure criteria. Once a failure criteria is met, failure can be declared and an investigation of the failed plies and the failure mode can be undertaken.

For this work, the primary load case is loading along the X axis. This load case has been selected as there are extensive experimental data available in the literature.

The constitutive relationships used to define the stress-strain relationship assume infinite plate conditions. In general, the samples used for experimental testing are finite rectangular coupons. Therefore, these predictions are approximations and deviation from the experimental values is unavoidable. For this load case, the following equality is true.

$$\begin{bmatrix} N \\ M \end{bmatrix} = \begin{bmatrix} N_{xx} \\ 0 \\ 0 \\ 0 \\ 0 \\ 0 \end{bmatrix}$$

N_{xx} is increased over each iteration until a failure criterion is met. The step size of each iteration, i.e., the increments in which one increases N_{xx}, determines the accuracy of the loads at which theoretical FPF occurs.

This iterative method was implemented in a MATLAB code. Elastic constants for pre-pregs fabricated of CYCOM 5320-1 resin with T650 fiber reinforcement [21] are used to calculate the A, B, and D matrices for the layups being studied and are shown in Table 4.1.

Table 4.1: Elastic constants for CYCOM 5320-1 resin with T650 fiber reinforcement [21]

Type of Test	ASTM Standard	Elastic Constant	Mean Value
Tensile Longitudinal Modulus	D 3039-08	E_{11}^T	139 GPa
Tensile Transverse Modulus	D 3039-08	E_{22}^T	9.17 GPa
Shear Modulus	D3518-07	G_{12}	4.95 GPa
Major Poisson's Ratio	D3518-07	ν_{12}	0.33
Compressive Longitudinal Modulus	D6641-05	E_{11}^C	126 GPa
Compressive Transverse Modulus	D6641-05	E_{22}^C	8.55 GPa

To define the failure criteria for maximum stress failure theory shown in Equations 39-41, experimental values for the failure of the layup [0_8] in tension and compression were used to define S_{Lc} , S_{Lt}. Similarly, experimental values for the failure of the layup [90_8] in tension and compression were used to define S_{Tc} , S_{Tt}, and S_{LTs} was defined using shear strength tests carried out according to according to ASTM D3518-07 [38]. Tensile strengths were gathered from tests carried out according to ASTM D3039-08 [36].

Compressive strengths were gathered from tests carried out according to ASTM D6641-05 [37] and the data were obtained from [21] and are shown in Table 4.2.

Table 4.2: Failure criteria for Maximum Stress failure criterion [21]

Type of Test	ASTM Standard	Failure Criteria	Layup	Average Strength (MPa)
Tensile Strength	**D 3039-08**	S_{Lt}	$[0]_8$	**2061**
Tensile Strength	**D 3039-08**	S_{Tt}	$[90]_{16}$	**70**
Shear Strength	**D3518-07**	S_{LTs}	$[45/-45]_{4S}$	**56**
Compressive Strength	**D6641-05**	S_{Lc}	$[0]_{20}$	**1634**
Compressive Strength	**D6641-05**	S_{Tc}	$[90]_{20}$	**274**

As the FPF method only predicts when failure should start and not the entire progression of failure, it is generally found to be conservative when compared to the experimental data. The strengths of various layups made from CYCOM 5320-1 resin with T650 fiber reinforcement are presented in Table 4.3. These data will be compared with the FPF predictions of the layups shown in Table 4.3 to validate their accuracy. Next, the same method will be applied to the standard wing skin layup and the NS designs shown in Tables 3.3-3.5.

Table 4.3: Experimental strengths for various layups [21]

Type of Test	ASTM Standard	Layup	Average Strength (MPa)
Tensile Strength	D 3039-08	$[0]_8$	2061
Tensile Strength	D 3039-08	$[90]_{16}$	69.64
Tensile Strength	D 3039-08	$[45\ 0\ -45\ 90]_{2S}$	672
Tensile Strength	D 3039-08	$[45\ -45\ 0\ 45\ -45\ 90\ 45\ -45\ 45\ -45]_s$	466
Tensile Strength	D 3039-08	$[0\ 45\ 0\ 90\ 0\ -45\ 0\ 45\ 0\ -45]_s$	1055
Compressive Strength	D6641-05	$[0]_{20}$	1634
Compressive Strength	D6641-05	$[90]_{20}$	274
Compressive Strength	D6641-05	$[90\ 0\ 90]_7$	633
Compressive Strength	D6641-05	$[45\ 0\ -45\ 90]_{3S}$	666
Compressive Strength	D6641-05	$[45\ -45\ 0\ 45\ -45\ 90\ 45\ -45\ 45\ -45]_s$	498

The FPF loads for the standard layups under tensile loading along the X axis are presented in Table 4.4. On comparing them with the experimental values in Table 4.5, one observes that these initial predictions, with the exception of the layup with the laminate code $[90]_{16}$, are highly conservative.

Table 4.4: FPF Strengths for various layups under tension

Layup	FPF Prediction (MPa)	Failure Criteria	Failed Ply Angle (Degrees)
$[0]_8$	2061	S_{LT}	0
$[90]_{16}$	69.6	S_{Tt}	90
$[45\ 0\ -45\ 90]_{2S}$	443	S_{Tt}	90
$[45\ -45\ 0\ 45\ -45\ 90\ 45\ -45\ 45\ -45]_s$	317	S_{Tt}	90
$[0\ 45\ 0\ 90\ 0\ -45\ 0\ 45\ 0\ -45]_s$	712	S_{Tt}	90

When the predictions are compared to experimental values, one can observe that the FPF predictions grossly underestimate the strengths of the laminates in Table 4.5.

Table 4.5: FPF strengths vs experimental strengths

Layup	Average Strength (MPa)	FPF Prediction (MPa)	Error (%)
$[0]_8$	2061	2061	0
$[90]_{16}$	69.6	69.6	0
$[45\ 0\ -45\ 90]_{2S}$	673	443	-34
$[45\ -45\ 0\ 45\ -45\ 90\ 45\ -45\ 45\ -45]_s$	466	317	-32
$[0\ 45\ 0\ 90\ 0\ -45\ 0\ 45\ 0\ -45]_s$	1055	712	-32

It can be observed that whenever the layup has all four standard angles, then the predictions are highly conservative as the negative error demonstrates underestimation of the laminate strength. Hence, it was decided to continue loading the laminate in order to determine if less conservative predictions could be obtained when the next ply experiences stresses higher than the allowable stressed according to the maximum stress criterion. Much better agreement can be seen between the FPF predictions and experimental results as shown in Table 4.6. In Table 4.6, 'FPF 2' is the failure load when the failure of the 90˚ plies is ignored.

Table 4.6: FPF 2 Strengths vs experimental tensile strengths

Layup	Average Strength (MPa)	FPF Prediction 2 (MPa)	Error (%)
$[45\ 0\ {-45}\ 90]_{2S}$	673	764	14
$[45\ {-45}\ 0\ 45\ {-45}\ 90\ 45\ {-45}\ 45\ {-45}]_s$	466	417	-10
$[0\ 45\ 0\ 90\ 0\ {-45}\ 0\ 45\ 0\ {-45}]_s$	1055	1078	2

Table 4.7 presents the results for the FPF prediction of compressive behavior. Reasonable agreement between the FPF predictions and experimental is seen.

Table 4.7: Comparison of compressive FPF predictions vs experimental data

Layup	Average Strength (MPa)	FPF Prediction (MPa)	Error (%)
$[0]_{20}$	1634	1634	0
$[90]_{20}$	274	274	0
$[90\ 0\ 90]_7$	633	628	-0.75
$[45\ 0\ {-45}\ 90]_{3S}$	666	639	-4.01
$[45\ {-45}\ 0\ 45\ {-45}\ 90\ 45\ {-45}\ 45\ {-45}]_s$	498	394	-21

For standard designs, FPF has been shown to be conservative. FPF predicts the load at which the first ply should fail and not the progression of failure within the laminate to ultimate failure.

As the predictions from the MATLAB code have been seen to be reasonable in both tension and compression, the next section presents the use of FPF to predict the strengths of the standard wing skin design and the NS designs shown in Tables 3.3-3.5. Consequently, the FPF predictions are used to compare the theoretical strengths of the standard and NS designs.

4.3 FPF loads for Wing Skin Layups

The FPF predictions help one understand the possible failure mechanisms of the NS designs and provide an estimate of the strength of each design. Designs with higher strengths can be used to produce lighter structures. This analysis helps to identify the designs that are most likely to provide improved strength as compared to the existing standard design. Furthermore, testing layup strength according to ASTM standards is quite time consuming and expensive; hence, these methods may reduce the cost of obtaining optimal designs.

When the FPF predictions for the compressive strength of a standard wing skin layup are compared to the NS designs, it can be seen that two of the NS designs presented in Table 4.8 offer significant improvements. This can be explained by conclusions drawn from Figures 4.2-4.17. In Figures 4.2-4.17, one can observe that there are more primary load bearing plies in the NS designs, that the load is distributed over a larger number of plies, and hence a higher load can be sustained by the NS designs.

Table 4.8: Compressive strength FPF predictions for wing skin layups

Compressive Strength FPF Predictions			
Layup	FPF Prediction (MPa)	Failure Criteria	Failed Ply Angle
$[0\ 0\ 0\ 0\ 45\ -45\ 45\ -45\ 90]_S$	899	S_{LC}	0˚
$[23\ -23\ 23\ -23\ 23\ -23\ 23\ 80\ -80]_S$	1040	S_{LC}	23˚
$[19\ -19\ 19\ -19\ 19\ -19\ 65\ -65\ 65]_S$	1020	S_{LC}	19˚
$[14\ -14\ 14\ -14\ 14\ 60\ -60\ 60\ -60]_s$	882	S_{LC}	14˚

Similar trends are seen when the tensile strengths are estimated. However, the failure of the angles closer to 90° is seen and the S_{Tt} failure mode is observed, as shown in Table 4.9.

Table 4.9: Tensile strength FPF predictions for wing skin layups

Tensile Strength FPF Predictions			
Layup	FPF Prediction (MPa)	Failure Mode	Failed Ply Angle
$[0\ 0\ 0\ 0\ 45\ {-45}\ 45\ {-45}\ 90]_S$	660	S_{LT}	0°
$[23\ {-23}\ 23\ {-23}\ 23\ {-23}\ 23\ 80\ {-80}]_S$	657	S_{Tt}	80°
$[19\ {-19}\ 19\ {-19}\ 19\ {-19}\ 65\ {-65}\ 65]_S$	793	S_{Tt}	65°
$[14\ {-14}\ 14\ {-14}\ 14\ 60\ {-60}\ 60\ {-60}]_s$	781	S_{Tt}	60°

If NS layups are treated the same as standard layups as in Section 4.2, then the S_{Tt} failure mode should be ignored to give a more realistic load, because the laminate should fail when the primary load bearing plies fail. Hence, when the S_{Tt} failure mode is ignored, the predictions shown in Table 4.10 result.

Table 4.10: Tensile Strength FPF 2 predictions for wing skin layups

Tensile Strength FPF 2 Predictions			
Layup	FPF Prediction (MPa)	Failure Mode	Failed Ply Angle
$[0\ 0\ 0\ 0\ 45\ {-45}\ 45\ {-45}\ 90]_S$	660	S_{LT}	0°
$[23\ {-23}\ 23\ {-23}\ 23\ {-23}\ 23\ 80\ {-80}]_S$	1188	S_{LT}	23°
$[19\ {-19}\ 19\ {-19}\ 19\ {-19}\ 65\ {-65}\ 65]_S$	1168	S_{LT}	19°
$[14\ {-14}\ 14\ {-14}\ 14\ 60\ {-60}\ 60\ {-60}]_s$	1009	S_{LT}	14°

It can be seen in Tables 4.8 and 4.10 that the FPF predictions indicate that the NS layups will be significantly stronger compared to the standard layups in both tension and compression.

Based on results that indicate improved strength for NS designs when compared to the standard wing skin design, it was decided that physical testing of the NS designs should be carried out. Most airframe structures are prone to damage from incidents such as bird strikes and tool drops during their service life. Due to this damage, most structures fail at stresses much lower than their un-notched strengths, hence open hole compression testing provides valuable design data for composites with defects and cut outs [34]. These data can be used to design reliable and safe structures.

4.4 Chapter Summary

In this chapter, the stress distributions for the standard wing skin and NS designs that match the stiffness of the standard wing skin design were calculated. The results indicate that NS designs will be more robust than the standard design. The first ply failure loads for these designs were calculated. The NS designs were observed to be theoretically stronger than the standard wing skin design. Hence, OHC testing of these designs according to ASTM D6484 [17] are performed and presented in Chapter 5.

CHAPTER 5

OPEN HOLE COMPRESSION STRENGTH

It is common aerospace industry practice to develop notched design allowable strengths based on gross section stress to account for various stress concentrations, such as fastener holes, free edges, flaws, and damage not explicitly modeled in stress analysis [17].

The notched strength acts as the limiting design allowable for most structures. By comparing the OHC strength for NS composites to the standard design, one can determine if there is any improvement in the strength for NS designs over standard designs. This information can be directly used by designers in the future.

The compression test of a composite specimen can be considered a structural test having complex interactions between local failures and structural instabilities [18]. This amplifies the importance for the use of an easily repeatable standard test procedure.

The most widely used standard test procedure for Open Hole Compression (OHC) strength is ASTM D6484 [17]. It was developed by Boeing and is commonly referred to as the Boeing Open Hole Compression test method. This test was developed to evaluate the “effects of defects” in composites [12]. The coupon used for this test has the geometry shown in Figure 5.1.

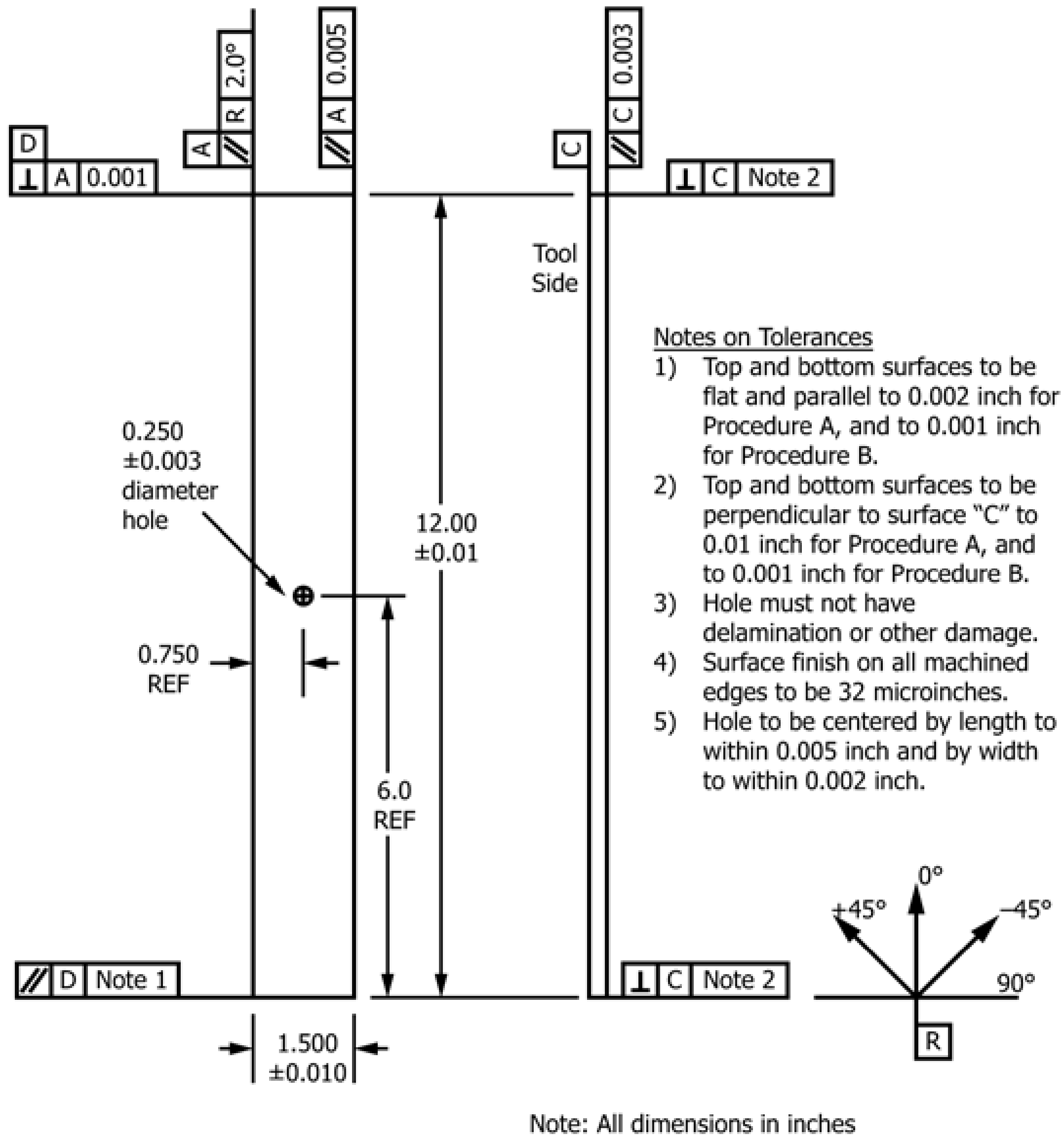

Figure 5.1 ASTM 6484 test specimen [17]

The fixture required to hold the specimen for this test is designed in such a way that the specimen faces are supported. This prevents buckling of the specimen and forces the failure to occur in ultimate compression [12]. Figure 5.2 details the fixture and its configuration when assembled around a standard specimen.

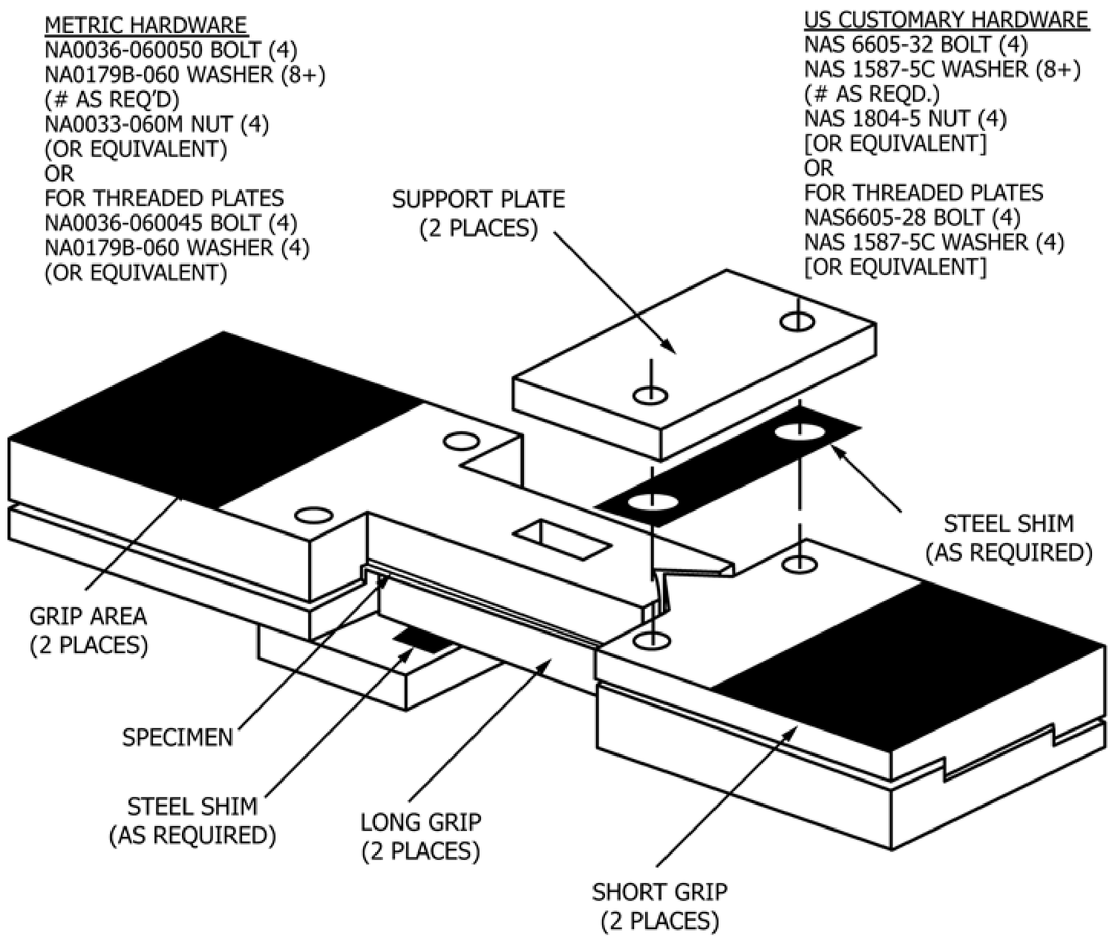

Figure 5.2 ASTM 6484 fixture [17]

5.1 Standard Test Procedure

A uniaxial compression test of a laminate is performed with a centrally located hole. The fixture is assembled around the sample. The standard specimen geometry ensures that, when the loaded face of the specimen sits flush with the loaded face of the fixture, the hole is centrally located within the fixture.

The four bolts that are used to attach the support plates to the grips should be torqued to a minimum of 60 lb-in. The bolts can be tightened further if required. The fixture is then placed between the compression platens as shown in Figure 5.6. Then, the assembly is loaded at a rate of 1mm/min until failure.

5.2 Deviations from Standard Test Procedure

Due to manufacturing and machining constraints, there are several areas where deviations from the standard were found to be unavoidable. The standard prescribes coupons which are 12 in. (305 mm) long while the coupon size was limited to a length of 11 in. (280 mm) due to the size of the available prepreg. The width of the coupon was not modified but the tolerance for the width of the coupons was also larger than that prescribed ±0.01in. The tolerances were greater than specified by the standard as a result of limited resources available for accurate machining of the coupons. The upper deviation was found to be +0.0295 in. (0.75 mm) while the lower deviation was found to be -0.0165in (0.41 mm) with the average deviation being 0.016 in (0.4 mm).

The 12-inch length of the coupons results in a mixture of end loading directly from the platen and shear loading from the grips. If shorter coupons are used, then they will not be in contact with the platens and hence experience pure shear loading via the grips.

An alternate testing procedure for the same standard utilizes hydraulic grips to clamp the fixture. For this case, the loading is transferred to coupons purely through shear. In a study conducted by ASTM [17], the results from the two types of loading were compared. The results show that both procedures produce nearly the same results. Hence, the shorter coupons which are loaded through shear should produce the same results as a standard test. Therefore, the results presented here for 11-inch long coupons should be nearly the same as if 12-inch long coupons were used.

The standard has been designed for standard angle laminates. As non-standard angle laminates were tested, unexpected failure modes were observed, which will be discussed at the conclusion of this chapter.

As the coupons were smaller than the standard coupons, a different method for aligning the hole of the coupon with the center of the fixture had to be utilized. Markings were made on each coupon relative to the central hole and these markings were used to center the hole in the window of the fixture.

Once the coupon is centered, on both grips the bolts in the fixture are tightened with a torque wrench. It was observed that a higher torque than the minimum recommended 60 lb-in prevented any slippage of the coupon within the fixture. The torque used for all reported tests was 120 lb-in. A torque wrench was used to ensure uniform torque on all bolts. A minimum of four bolts can be used. To reduce the wear of bolts, eight bolts were used for the reported set of tests.

Based on these procedures various layups were tested to compare the notched strength of the laminate designs described in this work. The testing is described in the next section.

5.3 Layups Tested

Two standard angled designs along with three NS designs were fabricated for testing; the layups are shown in Table 5.1. Within the standard angle layups, the first design is based on the wing skin layups as presented by Butler et al. is shown in Table 5.1 and is denoted as layups L1 and L3. To check the validity of the tests carried out using the modified coupon with dimensions described in Section 5.2, a second standard angle layup with coupons based on the modified dimension shown in Section 5.2 was tested. This layup is shown in Table 5.1 and is denoted as layup L7. The OHC strength of layup L7 according to ASTM D6484 [17] is available in the literature and is compared with the strengths found is the experimental results reported in Section 5.4. The NS layups have been selected to evenly cover the range of possible designs so that any variation of failure strengths and failure modes within the range can be identified.

Initially, samples from Solvay Cytec Cycom 5320-1 resin with IM7 Unitape Pre-pregs were fabricated. A production run for two panels with six samples per panel was conducted. The first panel was the standard wing skin laminate denoted as L1 shown in Table 5.1. The second design was the third NS design detailed in Table 3.5. These samples were tested according to ATSM D6484 [17]. As this limited test run did not generate enough data for conclusive results, a second more comprehensive production run was carried out. For this set of samples, Solvay Cytec Cycom 5320-1 resin with T650 Unitape Pre-pregs were used. The standard wing skin layup as well as all of the discrete NS designs were fabricated. Table 5.1 outlines the layups tested in this work.

Table 5.1: Layups tested

Layup ID	Layup	Fiber Type
L1	$[0\ 0\ 0\ 0\ 45\ -45\ 45\ -45\ 90]_S$	IM7
L2	$[23\ -23\ 23\ -23\ 23\ -23\ 23\ 80\ -80]_S$	IM7
L3	$[0\ 0\ 0\ 0\ 45\ -45\ 45\ -45\ 90]_s$	T650
L4	$[23\ -23\ 23\ -23\ 23\ -23\ 23\ 80\ -80]_S$	T650
L5	$[19\ -19\ 19\ -19\ 19\ -19\ 65\ -65\ 65]_S$	T650
L6	$[14\ -14\ 14\ -14\ 14\ 60\ -60\ 60\ -60]_S$	T650
L7	$[45\ 0\ -45\ 90]_{4S}$	T650

5.3.1 Sample manufacturing process:

Plies of length 11 inches and width 5 inches were cut from a roll of prepreg material made from CYCOM 5320-1 resin with T650 fibres, such that the fibers were oriented along the required angles and laid up on an aluminium mold by hand. A vacuum bag was then assembled over the uncured plates. The uncured plates were packaged under a layer of bleeder followed by a layer of breather and a porous membrane, over which a vacuum bag was placed and sealed using sealant tape. A packaged plate is shown in Figure 5.3.

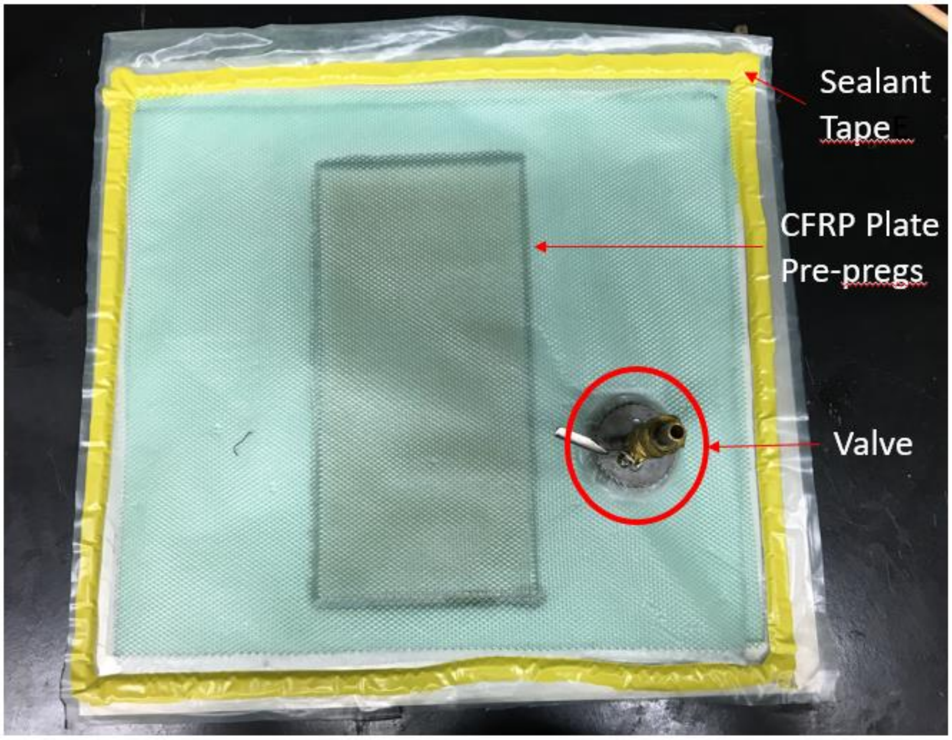

Figure 5.3 Assembled Package

A vacuum was then pulled using a WELCH DUOSEAL 1402 vacuum pump through a valve in the package. The plates were then cured in a HAF0 1600 series convection oven. The curing cycle shown in Figure 5.4 was used for all tested layups. After the first two curing steps the vacuum bag was removed and a free standing curing step was carried out.

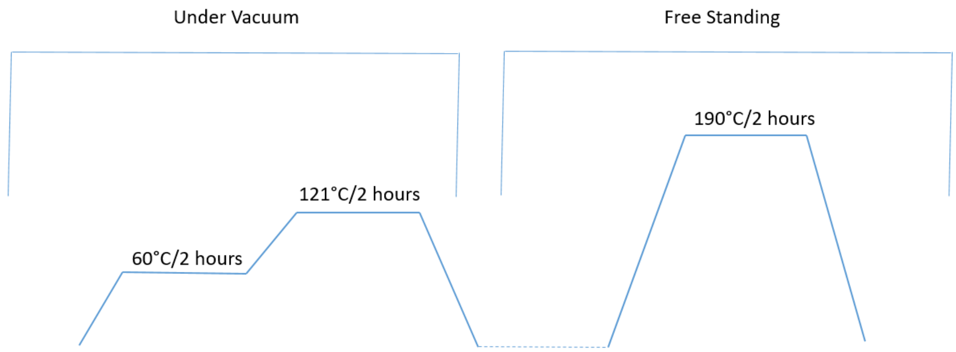

Figure 5.4 Curing cycle used for this study

5.4 Experimental Setup

An OHC fixture manufactured by Wyoming Test Fixtures for ASTM D6484 [17] was utilized for this study and is shown in Figure 5.5. The test frame utilized was a hydraulic static test SATEC UNIDRIVE frame rated to a maximum force of approximately 400,000N and is shown in Figure 5.6 As specified by ASTM D6484 [17], displacement control loading was applied to all specimens. The standard loading rate of 1mm/min was maintained for all tests [17]. The frame was computer controlled. A break detector protocol in the test frame controller was used to detect a rapid drop in load with displacement. When a break was detected, i.e., a drop of load of 25% from the peak load, the loading was stopped and the peak load was recorded. The only data recorded from each test was the peak load.

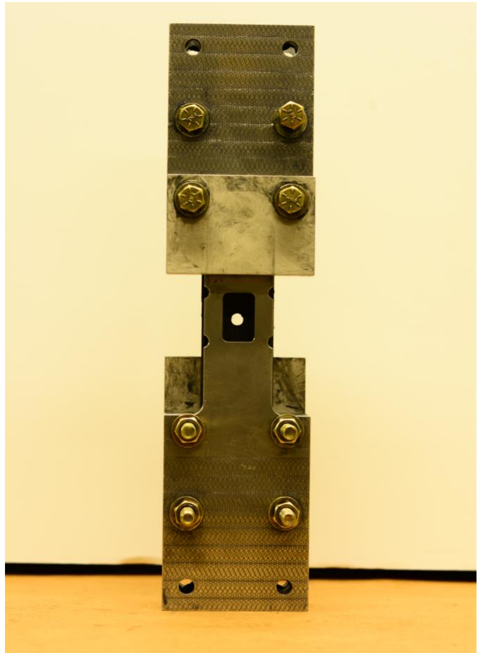

Figure 5.5: OHC test fixture

Figure 5.6 SATEC UNIDRIVE Hydraulic Testing frame

5.5 Results

The dominant failure mechanism in the OHC test is local fiber micro buckling failure of 0˚ plies, based on the loss of stability of the fibers in the matrix phase. Subsequently, the final failure occurs as a result of inter-laminar delamination, kink band broadening, and fiber fracture [18].

In the standard wing skin layup samples, i.e., L1 and L3, a crack is seen to propagate perpendicular to the primary loading direction. Extensive delamination was observed surrounding the hole. These observations are consistent with [18]. The failure mechanism for layup L3 is shown in Figure 5.7. The cracks observed in Figure 5.7 are representative for the failure modes observed in all samples of layups L1 and L3 tested in this thesis.

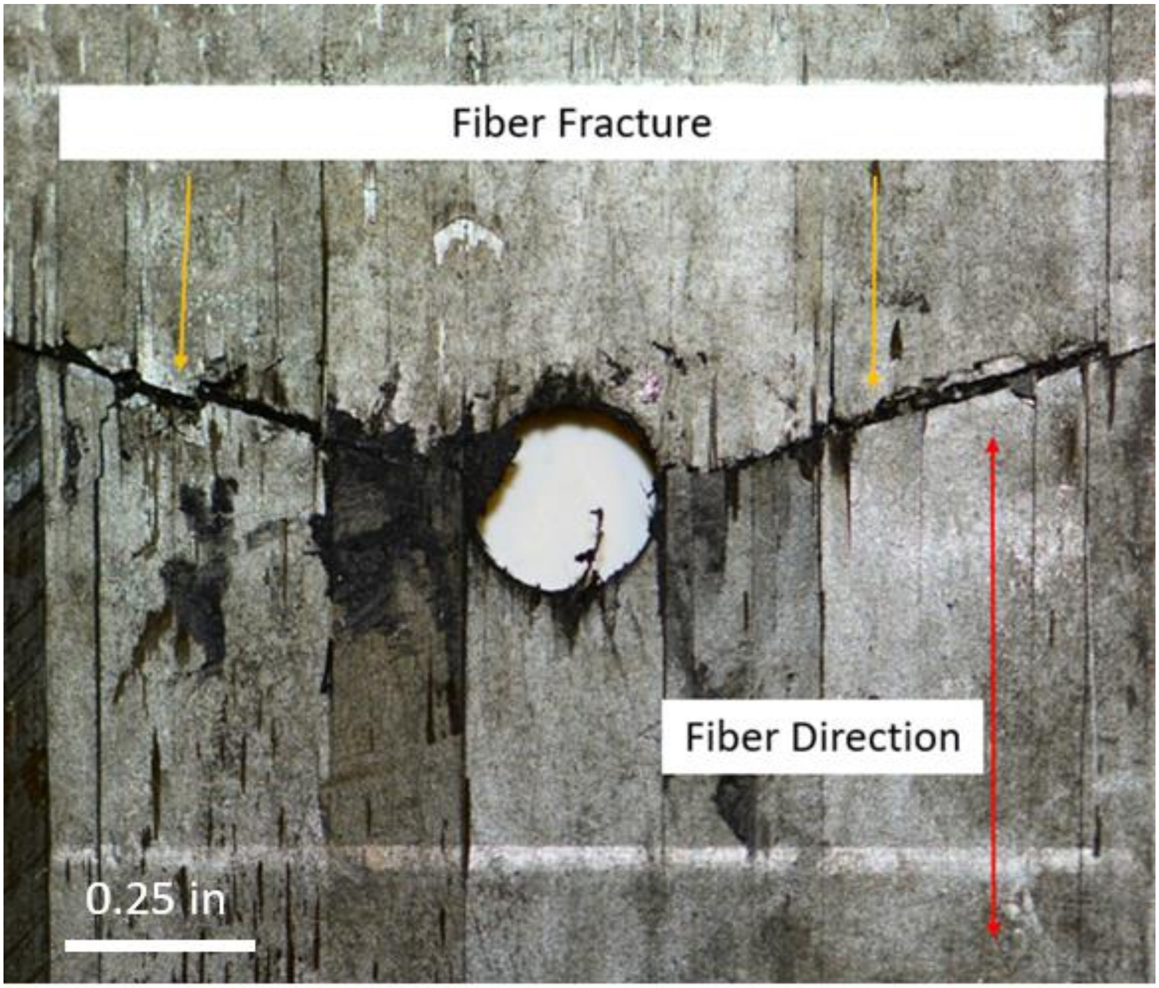

Figure 5.7 Failure Mechanism for layups L1 and L3

In the NS designs, the cracks primarily run along the direction of either the $+\phi$ or $-\phi$ directions, i.e., the lower angle which, in this configuration, is closest to the surface of the laminate. It is shown in Section 4.1 that these plies carry a majority of the load. In Figure 5.8, one can see the crack propagate along the $+\phi$ direction in layup L5. The same type of failure has been seen for all NS layups, i.e., layups L2 and L4-L6.

.

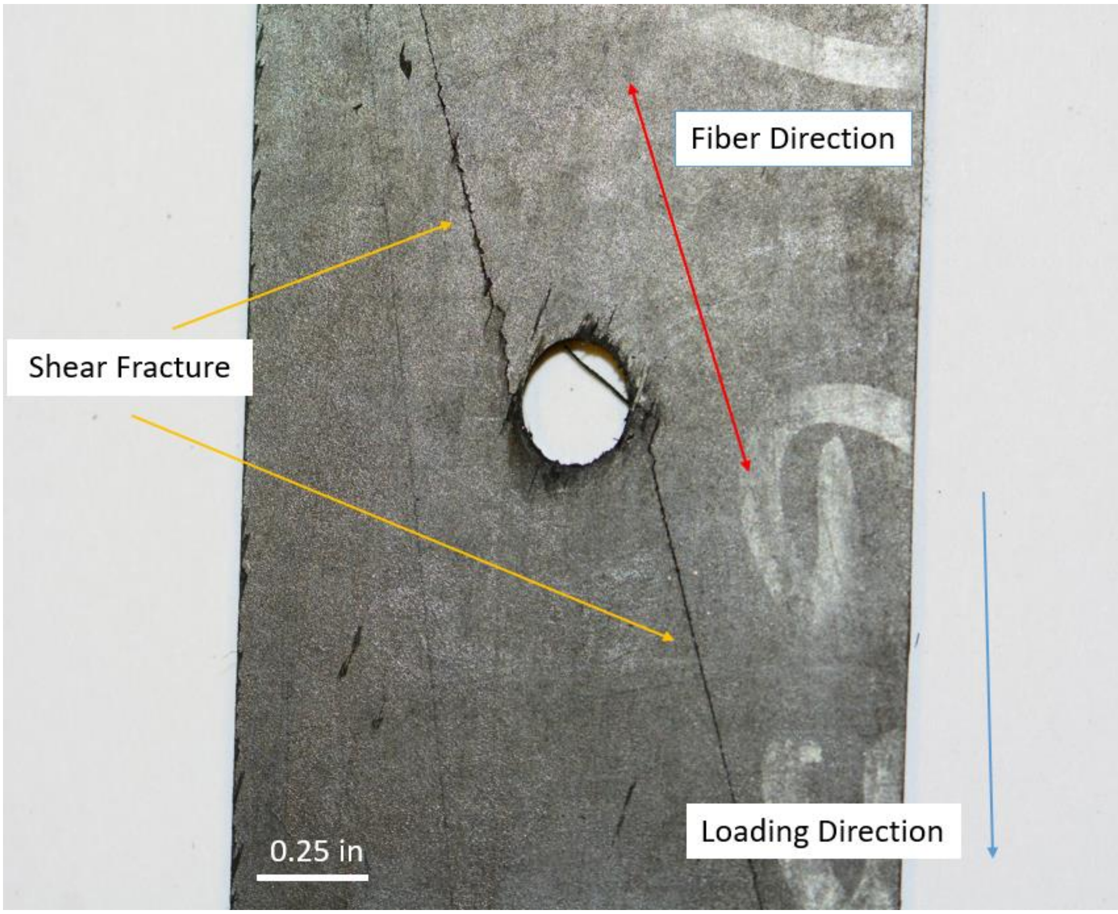

Figure 5.8 Failure mechanism for layup L5

The cracks that occur in the $-\phi$ layers sometimes propagate towards the surface ply, i.e., the ply with a fiber orientation of $+\phi$. This propagation of cracks from sub surface plies to the surface plies was frequently observed in layups L2, and L4-L6 and is shown in Figure 5.9 for layups L2 and L4.

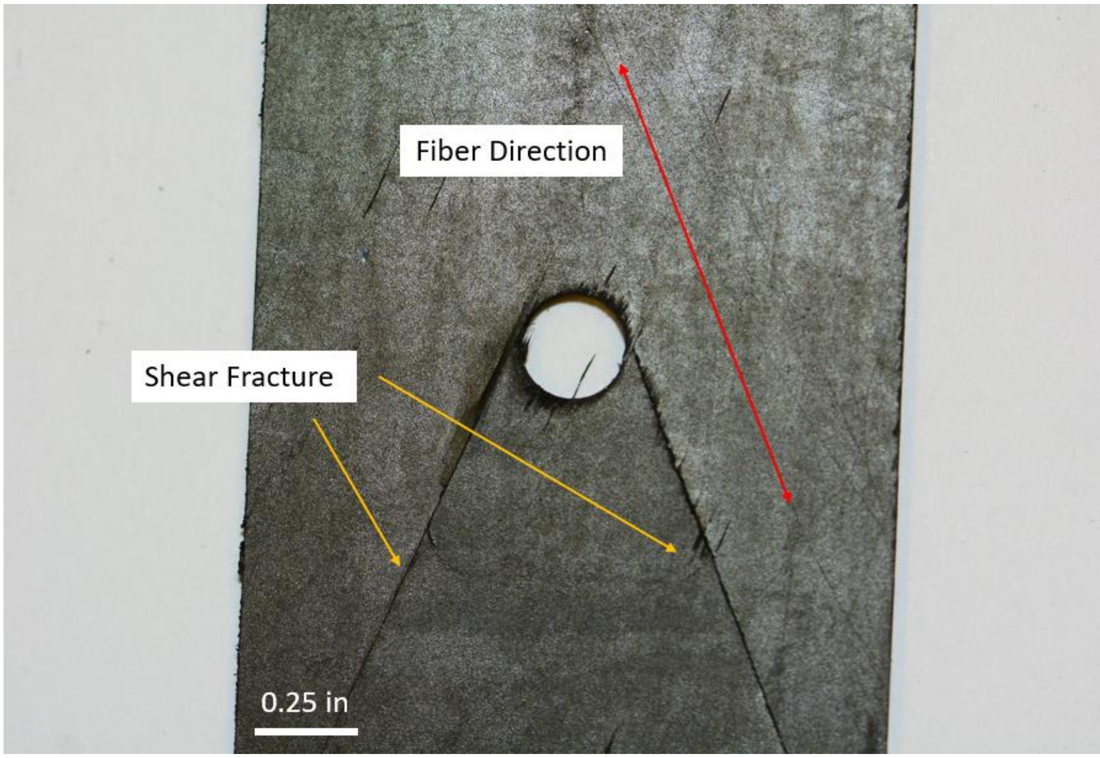

Figure 5.9 Failure mechanism for layups L2 and L4

As these cracks propagate along the fiber directions and not perpendicular to it, the failures observed in the NS angles are not fiber micro buckling but rather they are matrix failures. The NS designs were significantly weaker than the standard wing skin design. The OHC strengths of the layups tested are presented in Table 5.2. The failure load for each reported test is presented in Appendix D.

Table 5.2 Average OHC strength for selected layups

Layup ID	Layup	Fiber Type	Average Failure Stress (MPa)	Standard Deviation (MPa)
L1	$[0\ 0\ 0\ 0\ 45\ {-45}\ 45\ {-45}\ 90]_S$	IM7	425	40
L2	$[23\ {-23}\ 23\ {-23}\ 23\ {-23}\ 23\ 80\ {-80}]_S$	IM7	302	12
L3	$[0\ 0\ 0\ 0\ 45\ {-45}\ 45\ {-45}\ 90]_s$	T650	446	12
L4	$[23\ {-23}\ 23\ {-23}\ 23\ {-23}\ 23\ 80\ {-80}]_S$	T650	310	11
L5	$[19\ {-19}\ 19\ {-19}\ 19\ {-19}\ 65\ {-65}\ 65]_S$	T650	321	12
L6	$[14\ {-14}\ 14\ {-14}\ 14\ 60\ {-60}\ 60\ {-60}]_S$	T650	312	21
L7	$[45\ 0\ {-45}\ 90]_{4S}$	T650	314	7

The OHC strength for layup L7 is according to [21] is 349 MPa. Hence, the strength measured by the experiments is within 10% of the strength reported in the literature. The difference can be for many reasons. The plates manufactured for this study were fabricated by hand-layup. Hence, variations in ply angles can never be completely eliminated. The machining of the coupons from the plates adds another process which leads to a possible buildup of tolerances which affect the orientation of fibers with respect to the loading direction.

5.5 Discussion

The standard wing skin design has significantly higher OHC strength than the NS designs. To determine the relative strengths of designs with identical stiffness, the strengths of layups L3-L6 are normalized by the strength of the standard wing skin design L3. A reduction of approximately thirty percent can be seen for most NS designs. These relative strengths are shown in Table 5.3.

Table 5.3 Relative OHC strengths

Layup	Average Max Strength (MPa)	Strength relative to Standard Angled Layup
$(0_4,\pm45_4,90_1)_S$	447	1.00
$(23\ -23\ 23\ -23\ 23\ -23\ 23\ 80\ -80)_S$	310	0.70
$(19\ -19\ 19\ -19\ 19\ -19\ 65\ -65\ 65)_s$	322	0.72
$(14\ -14\ 14\ -14\ 14\ 60\ -60\ 60\ -60\ )_S$	312	0.70

This reduction in OHC strength can be attributed to the fact that the failure modes for standard and NS designs are different. As observed Figures 5.7-5.9, the failure mode for standard designs is dominated by fiber micro buckling. In compression, standard layups always fail starting with the micro buckling of the 0° plies followed by the delamination of off-axis plies [22].

The NS designs do not exhibit any noticeable fiber micro-buckling. The cracks observed in the NS designs run along the ply orientations indicating a matrix failure. This explains the relative weakness of the NS designs as the matrix is a much weaker constituent of the composite than the fiber reinforcement.

The standard for testing OHC, ASTM D6484 [17], has been designed for layups consisting of the four standard angles. The 0° fibers run continuously between both grips of the OHC fixture, as a result the primary load bearing plies have continuous fibers running between both grips, this has been shown in Figure 5.10. Failure occurs when local instability at an edge causes a micro buckle that grows into ultimate failure [22]. In this work, the hole at the center of the coupon is the edge at which crack nucleation takes place. The crack then propagates perpendicular the fiber orientation of the 0˚ plies.

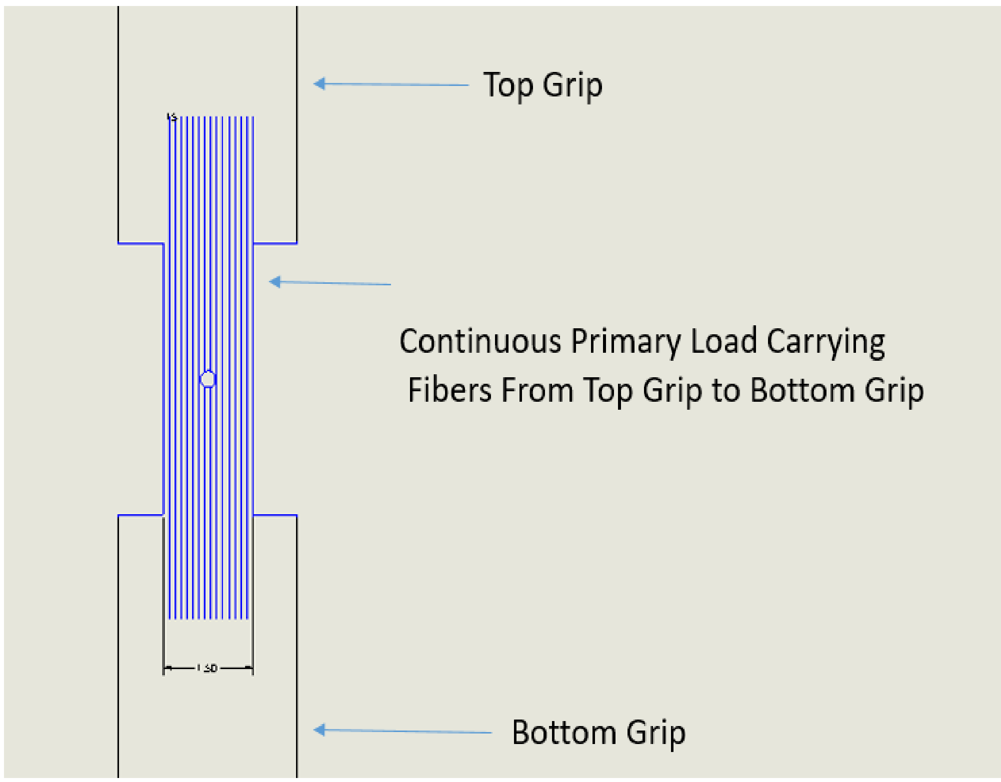

Figure 5.10 Primary load bearing fibers for standard layup specimen under OHC

The cracks in the NS design are observed to initiate at the point of maximum stress concentration. However, contrary to standard designs, in NS designs cracks propagate along the ply fiber orientations to the coupon edges as shown by Figures 5.7-5.9.

The primary load carrying plies in NS designs are off-axis plies when their orientation is not 0˚. Hence, unlike the 0˚ plies, all of the fibers originating from the top grip do not run continuously till the bottom grip, this results in fiber discontinuity, as shown in Figure 5.11. The geometry of the coupons is unfavorable to test the actual performance of NS layups. The width of the unsupported gage section is 1.5 in (38 mm) while its length is approximately 4 in (102 mm). This is will not affect standard angled laminates as the 0° plies will run continuously from the top grip to the bottom. Only fibers around the hole will experience fiber discontinuity.

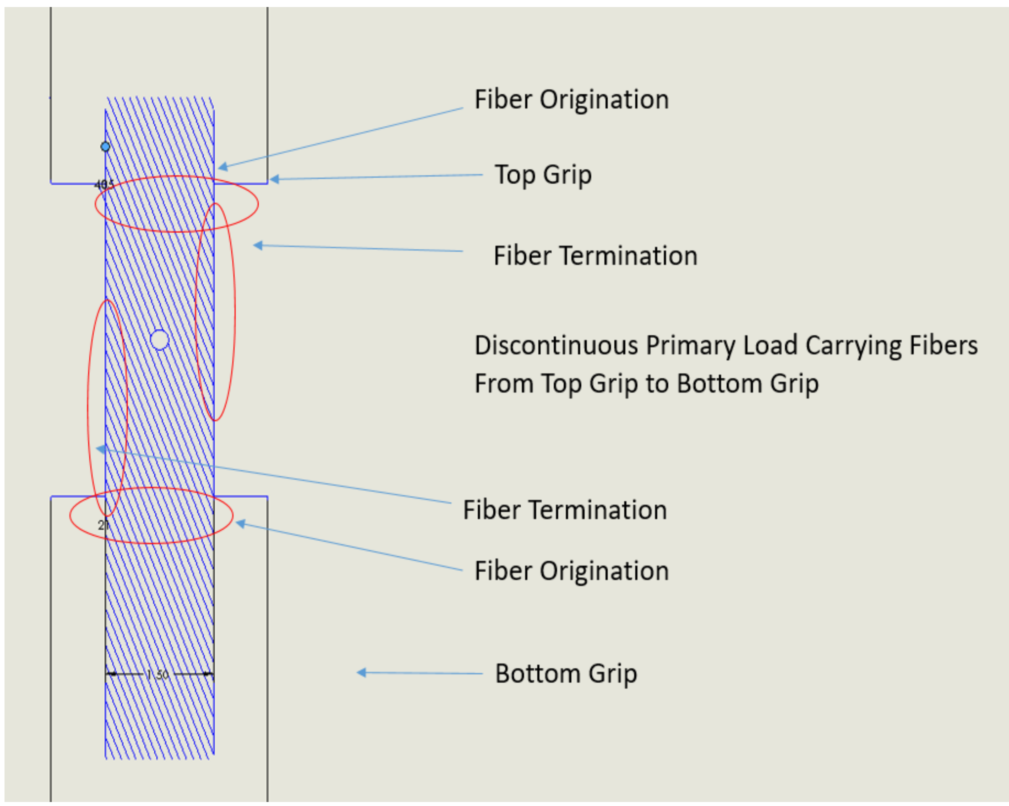

Figure 5.11 Primary Load bearing fibers for NS layups under OHC

However, the primary load carrying plies have off axis orientations for NS designs, this leads to fiber discontinuity shown in Figure 5.11. This fiber discontinuity between grips allows shear failure to occur before catastrophic micro-buckling failure. The singularity associated with the free edge of laminated test specimens causes a stress concentration, especially when a laminate contains plies with fibers in varying orientations. The strength of full-sized components may be misrepresented by narrow test specimens [39]. The narrow aspect ratio of this gage section is hence vital and affects the test results for NS designs more significantly than standard layups.

5.6 Summary

The results of OHC testing on standard angle and NS designs shown in Table 5.1 have been presented. Deviations resulting from manufacturing and machining constraints from the OHC testing standard ASTM D6484 [17] were reported. The modified testing procedure was validated against available data from the literature [21]. The NS designs tested exhibit a different failure mode than the standard wing skin design. A possible cause for premature failure of NS designs was identified to be the lack of fiber continuity in the NS designs. The recommendations to alter the tests carried out for representative strengths for NS designs are presented in Chapter 6.

CHAPTER 6

CONCLUSIONS AND FUTURE WORK

6.1 Conclusions

A theoretical and experimental study of the behavior of Non-Standard angled laminates was conducted. A stiffness matching method based on the ‘A’ matrix in composite laminate theory was developed. This method helps one to compute the range of possible non-standard laminates that have the same in-plane stiffness as an input laminate. The non-standard layups computed consist of a pair of NS angles. The range of theoretically possible NS designs that match the in-plane stiffness for a standard wing skin layup was computed based on this method. The validity of this method was validated using the method developed by Butler et al. [7]. The validity of these solutions was verified by a mathematical proof for laminates with dissimilar ply counts. It was seen that the angle pairs and thickness fractions of each NS angle are independent of the laminate ply count. This helps in maintaining stiffness regardless of laminate thickness, which was not possible with earlier standard designs. Based on this result, these layups can be used to mitigate stiffness mismatch between parts in an assembly, which is a crucial concern when two parts are mechanically joined. It is clear that in terms of stiffness NS designs provide much greater flexibility over standard designs. The ability to reduce stiffness mismatch between different components will greatly benefit complex assemblies.

As the range of possible solutions is a continuous domain, a number of physically realizable discrete designs were extracted from this range. It was observed that when laminate design rules such as symmetry and balance are applied to this range, the number of possible designs is reduced to a finite set of solutions. This makes NS designs more amenable to optimization, as the number of designs is now limited and a more detailed analysis for a few selected designs can be carried out.

The failure loads for a set of un-notched standard layups were estimated based on first ply failure theory. As good agreement was seen with available data, this method was applied to the standard wing skin layup. Then, the same method was applied to NS designs. According to this method a significant improvement in FPF strength in the NS designs over the standard wing skin design was seen.

OHC testing according to ASTM D6484 [17] for standard and NS designs was performed. This allows one to compare the maximum safe loads for both standard and NS wing skin layups. Here it was seen that the failure mechanism for standard angle composites was dominated by micro buckling of the 0° fibers, whereas in NS designs a different failure mode was seen. The NS designs failed in shear, with cracks in the matrix along the fibers of the primary load bearing plies observed. As a result, the NS designs failed at lower loads than standard designs. In most cases a reduction of approximately thirty percent was observed when compared to the standard design. In NS designs, the fibers of the primary load bearing plies do not run continuously between both grips. This results in the fibers transferring loads to neighboring fibers via the matrix. Therefore, matrix failure occurs before local instability of fibers can cause fiber failure, i.e., micro-buckling. Fiber continuity within the standard specimens leads to the micro-buckling. As the gage section for OHC testing according to ASTM D6484 [17] is narrow, it tends to favor layups with 0° plies while any off-axis plies make only a secondary contribution to the strength of the laminate. Therefore, even though the results of this study indicate that standard designs are more resilient under compression, alternate testing methods should be investigated.

6.2 Future Work

Additional work is needed to gain a more thorough understanding of NS laminate design. Alternate formulations for stiffness matching with constraints to ensure balance and symmetry in the laminates should be developed as laminates that do not maintain stiffness and balance are not accurately modeled by CLT. Aircraft structures are often subjected to complex 3-D loads; hence, the effects on the out of plane stiffness must also be considered in future studies.

Traditionally, testing of standardized coupons has been used to gather material data. These data are used to design components with more complex geometries. This mapping of data from coupons to complex structures has been convenient and accurate for standard angles. But this may not be the case for NS designs. Hence, the dependence of the strengths on the coupon geometry must be studied.

The laminate stacking sequence has an important effect on strength. When 0^{o} fibers are placed on the surface of a coupon, they buckle more easily due to reduced support and the laminate loses compressive strength [29]. The layups used for this study all have lower angles on the surface and higher angles in the center. The effect of the stacking sequence and homogenization of the layups should also be studied to discern any possible gain of strength with change in the stacking sequence. Homogenization results in stronger and tougher laminates [1]. This work focused on the OHC strength, which, as discussed in

Section 1.2, limits the allowable stress for most structural applications. However, there is a wide variety of tests that must be performed to obtain a more complete picture of the response of these laminates. Tests such as Open Hole Tension and un-notched strengths testing are required. Data from these tests will allow for accurate FEM modeling of complex structures made from NS laminates.

The trends seen in the predicted FPF loads for un-notched laminates have not been repeated in notched specimen tested. Hence, further work is required to build a model that can accurately predict the strength of notched NS designs. Currently most strength predictions rely on the un-notched strength as well as the characteristic length of the defect [26]. As the characteristic length for the specimen tested is constant, one requires information on the un-notched strengths of the NS designs. Based on the un-notched strengths, on should be able to check the validity of commonly used criteria for NS designs.

APPENDIX A

MATLAB code for implementing stiffness matching formulation when both standard and NS designs have the same thickness.

```
clc;
clearvars;
% Uni Directional Tape Properties
%E11 is Youngs Modulus in X E22 is Youngs Modulus in Y Units GPa
%G12 is in plane Shear Modulus Units GPa
%u12 is major Poissons Ratio
%u21 is minor possons Ratio
E11=138.584;
E22=9.170;
G12=4.950;
u12=0.326;
u21=(u12*E22)/E11;
%Stiffness matrix of one ply i.e. a Lamina is Q Matrix
Q=zeros(3);
denom=1-(u12*u21);
Q(1,1)=E11/denom;
Q(1,2)=(u12*E22)/denom;
Q(2,1)=(u12*E22)/denom;
Q(2,2)=E22/denom;
Q(3,3)=G12;
%Calculation of Stiffness invariants to be used later
U1=(1/8)*(3*Q(1,1)+3*Q(2,2)+2*Q(1,2)+4*Q(3,3));
U2=(1/2)*(Q(1,1)-Q(2,2));
U3=(1/8)*(Q(1,1)+Q(2,2)-2*Q(1,2)-4*Q(3,3));
U4=(1/8)*(Q(1,1)+Q(2,2)+6*Q(1,2)-4*Q(3,3));
U5=(1/8)*(Q(1,1)+Q(2,2)-2*Q(1,2)+4*Q(3,3))
% Thetadb is the array with the stacking Sequence
%NPlies is the number of plies in stackup
% hply is the height of one ply

%h_ply units in mm
h_ply=0.14;
thetadb=[0 0 0 0 45 -45 45 -45 90 90 -45 45 -45 45 0 0 0 0 ];
Nplies=length(thetadb);
%calculation of Qbar i.e. rotated stiffnes of a lamina
A=zeros(3);
for i=1:Nplies
    Qbar=zeros(3);
    theta =(thetadb(i)*pi)/180;
    m=cosd(thetadb(i));
    n=sind(thetadb(i));

Qbar(1,1)=(m^4)*Q(1,1)+2*(m^2)*(n^2)*(Q(1,2)+2*Q(3,3))+(n^4)*Q(2,2);
    Qbar(1,2)=(m^2)*(n^2)*(Q(1,1)+Q(2,2)-
4*Q(3,3))+((m^4)+(n^4))*Q(1,2);
    Qbar(1,3)=(m^3)*n*(Q(1,1)-Q(1,2)-2*Q(3,3))+m*(n^3)*(Q(1,2)-
Q(2,2)+2*Q(3,3));
```

```
    Qbar(2,1)=Qbar(1,2);

Qbar(2,2)=(n^4)*Q(1,1)+2*(m^2)*(n^2)*(Q(1,2)+2*Q(3,3))+(m^4)*Q(2,2);
    Qbar(2,3)=m*(n^3)*(Q(1,1)-Q(1,2)-2*Q(3,3))+(m^3)*n*(Q(1,2)-
Q(2,2)+2*Q(3,3));
    Qbar(3,1)=Qbar(1,3);
    Qbar(3,2)=Qbar(2,3);
    Qbar(3,3)=(m^2)*(n^2)*(Q(1,1)-2*Q(1,2)+Q(2,2))+(((m^2)-
(n^2))^2)*Q(3,3);
    A=A+Qbar*h_ply;
end
%Exx is the Laminate Youngs modulus in X units in MPa
%Eyy is the Laminate Youngs modulus in Y units in MPa
%Gxy is the Laminate Shear modulus in X units in MPa
Exx= (A(1,1)-((A(1,2)^2)/A(2,2)))/(Nplies*h_ply);
Eyy= (A(2,2)-((A(1,2)^2)/A(1,1)))/(Nplies*h_ply);
Gxy=A(3,3)/((Nplies*h_ply));
uxy=A(1,2)/A(2,2);
% Starting to Figure out Non Standard Ply angles and Percentages
%A matrices define the in Plane response
%Stiffness as can be seen above depends on the A matrices and overall
%laminate thickness
%as We will be using different thickness of laminates
%We need to scale the A matrix of the non standard Laminate to get the
same
%Exx Eyy Gxy A_ns is the A matrix for thinner non standard plate
%Nplies_ns are the number of plies in the non standard plate
Nplies_ns=18;
A_ns=A
Exx_ns= (A_ns(1,1)-((A_ns(1,2)^2)/A_ns(2,2)))/(Nplies_ns*h_ply);
Eyy_ns= (A_ns(2,2)-((A_ns(1,2)^2)/A_ns(1,1)))/(Nplies_ns*h_ply);
Gxy_ns=A_ns(3,3)/((Nplies_ns*h_ply));
uxy_ns=A_ns(1,2)/A_ns(2,2);

%choose first non standard angle in degrees
% psi is defined , we solve for gamma and phi,psi in degree
gammadb=zeros(1,91);
phidb=zeros(1,91);
psidb=zeros(1,91)
for i = 55:90

psi=i
psidb(i+1)=psi;
%a is cos(2phi) b is cos(4phi)
%change Nplies to non standard plate Nplies

syms gamma a

sol =
solve([(Nplies_ns*U1+gamma*Nplies_ns*U2*cosd(2*psi)+gamma*Nplies_ns*U3*
cosd(4*psi)+Nplies_ns*(1-gamma)*U2*cos(2*a)+Nplies_ns*(1-
gamma)*U3*cos(4*a))*h_ply==A_ns(1,1),(Nplies_ns*U1-
gamma*Nplies_ns*U2*cosd(2*psi)+gamma*Nplies_ns*U3*cosd(4*psi)-
Nplies_ns*(1-gamma)*U2*cos(2*a) +Nplies_ns*(1-
gamma)*U3*cos(4*a))*h_ply==A_ns(2,2),a>=-
1,a<=1,gamma>=0,gamma<=1],[gamma,a])
```

```
solution_existence= size(sol.gamma);
b=radtodeg(vpa(sol.a));
if solution_existence>0
gammadb(i+1)=vpa(abs((sol.gamma(1))));
phi_in_rad=vpa(sol.a(1));
phidb(i+1)=abs(radtodeg(phi_in_rad))
end


end
subplot(2,1,1);

plot(psidb(56:91),phidb(56:91))
xlabel('\psi^\circ')
ylabel('\phi^\circ')
title( 'Angle pairs for matching a 18 ply NS Layup to a 18 ply standard
wing skin layup')
grid on
axis([0 90 0 30])
subplot(2,1,2);
plot(psidb(56:91),gammadb(56:91))
title('Ratio of plies with orientation of \psi')
xlabel('\psi^\circ')
ylabel('\gamma')
axis([0 90 0 1])
grid on
```

APPENDIX B

MATLAB code for implementing stiffness matching formulation when standard and NS designs have different thickness.

```
clc;
clearvars;
% Uni Directional Tape Properties
%E11 is Youngs Modulus in X E22 is Youngs Modulus in Y Units GPa
%G12 is in plane Shear Modulus Units GPa
%u12 is major Poissons Ratio
%u21 is minor possons Ratio
E11=121.200;
E22=2.300;
G12=5.515;
u12=0.3;
u21=(u12*E22)/E11;
%Stiffness matrix of one ply i.e. a Lamina i.e. Q Matrix or C matix in
%Butler&Andy Paper
Q=zeros(3);
denom=1-(u12*u21);
Q(1,1)=E11/denom;
Q(1,2)=(u12*E22)/denom;
Q(2,1)=(u12*E22)/denom;
Q(2,2)=E22/denom;
Q(3,3)=G12;
%Calculation of Stiffness invariants to be used later
U1=(1/8)*(3*Q(1,1)+3*Q(2,2)+2*Q(1,2)+4*Q(3,3));
U2=(1/2)*(Q(1,1)-Q(2,2));
U3=(1/8)*(Q(1,1)+Q(2,2)-2*Q(1,2)-4*Q(3,3));
U4=(1/8)*(Q(1,1)+Q(2,2)+6*Q(1,2)-4*Q(3,3));
U5=(1/8)*(Q(1,1)+Q(2,2)-2*Q(1,2)+4*Q(3,3))
% Theta is the array with the stacking Sequence Use only Balanced ans
% Symmetric and Balanced Stacking Sequences ONLY
%NPlies is the number of plies in stackup
% hply is the height of one ply

%h_ply units in mm
h_ply=0.14;
thetadb=[0 0 0 0 45 -45 45 -45 90 90 -45 45 -45 45 0 0 0 0 ];
Nplies=length(thetadb);
%calculation of Qbar i.e. rotated stiffnes of a lamina
A=zeros(3);
for i=1:Nplies
    Qbar=zeros(3);
    theta =(thetadb(i)*pi)/180;
    m=cosd(thetadb(i));
    n=sind(thetadb(i));

Qbar(1,1)=(m^4)*Q(1,1)+2*(m^2)*(n^2)*(Q(1,2)+2*Q(3,3))+(n^4)*Q(2,2);%so
mething wrong
```

```
    Qbar(1,2)=(m^2)*(n^2)*(Q(1,1)+Q(2,2)-
4*Q(3,3))+((m^4)+(n^4))*Q(1,2);
    Qbar(1,3)=(m^3)*n*(Q(1,1)-Q(1,2)-2*Q(3,3))+m*(n^3)*(Q(1,2)-
Q(2,2)+2*Q(3,3));
    Qbar(2,1)=Qbar(1,2);

Qbar(2,2)=(n^4)*Q(1,1)+2*(m^2)*(n^2)*(Q(1,2)+2*Q(3,3))+(m^4)*Q(2,2);
    Qbar(2,3)=m*(n^3)*(Q(1,1)-Q(1,2)-2*Q(3,3))+(m^3)*n*(Q(1,2)-
Q(2,2)+2*Q(3,3));
    Qbar(3,1)=Qbar(1,3);
    Qbar(3,2)=Qbar(2,3);
    Qbar(3,3)=(m^2)*(n^2)*(Q(1,1)-2*Q(1,2)+Q(2,2))+(((m^2)-
(n^2))^2)*Q(3,3);
    A=A+Qbar*h_ply;
end
%Exx is the Laminate Youngs modulus in X units in MPa
%Eyy is the Laminate Youngs modulus in Y units in MPa
%Gxy is the Laminate Shear modulus in X units in MPa
Exx= (A(1,1)-((A(1,2)^2)/A(2,2)))/(Nplies*h_ply);
Eyy= (A(2,2)-((A(1,2)^2)/A(1,1)))/(Nplies*h_ply);
Gxy=A(3,3)/((Nplies*h_ply));
uxy=A(1,2)/A(2,2);
% Starting to Figure out Non Standard Plys angles and Percentages
%A matrices define the in Plane response
%Stiffness as can be seen above depens on the A matrices and overall
%laminate thickness
%as We will be using different thickness of laminates
%We need to scale the A matrix of the non standard Laminate to get the
same
%Exx Eyy Gxy A_ns is the A matrix for thinner non standard plate
%Nplies_ns are the number of plies in the non standard plate
Nplies_ns=20;
A_ns=(A*Nplies_ns)/Nplies;
Exx_ns= (A_ns(1,1)-((A_ns(1,2)^2)/A_ns(2,2)))/(Nplies_ns*h_ply);
Eyy_ns= (A_ns(2,2)-((A_ns(1,2)^2)/A_ns(1,1)))/(Nplies_ns*h_ply);
Gxy_ns=A_ns(3,3)/((Nplies_ns*h_ply));
uxy_ns=A_ns(1,2)/A_ns(2,2);

%choose first non strandard angle in degrees
% psi is defined , we solve for gamma and phi,psi in degree
gammadb=zeros(1,91);
phidb=zeros(1,91);
psidb=zeros(1,91)
for i = 55:90

psi=i
psidb(i+1)=psi;
%a is cos(2phi) b is cos(4phi)
%change Nplies to non standard plate Nplies

syms gamma a

sol =
solve([(Nplies_ns*U1+gamma*Nplies_ns*U2*cosd(2*psi)+gamma*Nplies_ns*U3*
cosd(4*psi)+Nplies_ns*(1-gamma)*U2*cos(2*a)+Nplies_ns*(1-
gamma)*U3*cos(4*a))*h_ply==A_ns(1,1),(Nplies_ns*U1-
```

```
gamma*Nplies_ns*U2*cosd(2*psi)+gamma*Nplies_ns*U3*cosd(4*psi)-
Nplies_ns*(1-gamma)*U2*cos(2*a) +Nplies_ns*(1-
gamma)*U3*cos(4*a))*h_ply==A_ns(2,2),a>=-
1,a<=1,gamma>=0,gamma<=1],[gamma,a])
solution_existence= size(sol.gamma);
b=radtodeg(vpa(sol.a));
if solution_existence>0
gammadb(i+1)=vpa(abs((sol.gamma(1))));
phi_in_rad=vpa(sol.a(1));
phidb(i+1)=abs(radtodeg(phi_in_rad))
end


end
subplot(2,1,1);

plot(psidb(56:91),phidb(56:91))
xlabel('\psi^\circ')
ylabel('\phi^\circ')
title( 'Angle pairs for matching a 18 ply NS Layup to a 18 ply standard
wing skin layup')
grid on
axis([0 90 0 30])
subplot(2,1,2);
plot(psidb(56:91),gammadb(56:91))
title('Ratio of plies with orientation of \psi')
xlabel('\psi^\circ')
ylabel('\gamma')
axis([0 90 0 1])
grid on
```

APPENDIX C

MATLAB code used to calculate the stress distribution and FPF loads.

```
%Damage Criterion for Composites
%First Need to Calculate A B D for all reqd matrices to find strains
%After strains of LAMINATE move to ply-wise i.e. LAMINA level stresses
%Iso-strain for all plies assumed
%Values verified against examples 3.5-3.12 in PK Mallick book
clc;
clearvars;
% Uni Directional Tape Properties
%E11 is Youngs Modulus in X E22 is Youngs Modulus in Y Units GPa
%G12 is in plane Shear Modulus Units GPa
%u12 is major Poissons Ratio
%u21 is minor possons Ratio
E11=138.58;
E22=9.17;
G12=4.9504;
u12=0.326;
u21=(u12*E22)/E11;
%Stiffness matrix of one ply i.e. a Lamina i.e. Q Matrix or C matix in
%Butler&Andy Paper
Q=zeros(3);
denom=1-(u12*u21);
Q(1,1)=E11/denom;
Q(1,2)=(u12*E22)/denom;
Q(2,1)=(u12*E22)/denom;
Q(2,2)=E22/denom;
Q(3,3)=G12;
%Calculation of Stiffness invariants to be used later
U1=(1/8)*(3*Q(1,1)+3*Q(2,2)+2*Q(1,2)+4*Q(3,3));
U2=(1/2)*(Q(1,1)-Q(2,2));
U3=(1/8)*(Q(1,1)+Q(2,2)-2*Q(1,2)-4*Q(3,3));
U4=(1/8)*(Q(1,1)+Q(2,2)+6*Q(1,2)-4*Q(3,3));
U5=(1/8)*(Q(1,1)+Q(2,2)-2*Q(1,2)+4*Q(3,3));
% Theta is the array with the stacking Sequence Use only Balanced ans
% Symmetric and Balanced Stacking Sequences ONLY
%NPlies is the number of plies in stackup
% hply is the height of one ply

%h_ply units in mm
h_ply=0.14;
thetadb=[23 -23 23 -23 23 -23 23 80 -80 -80 80 23 -23 23 -23 23 -23 23]
Nplies=length(thetadb);
Qdb=zeros(3,3,Nplies);
h      = Nplies * h_ply;
for i = 1:Nplies;
  zbar(i) = - (h + h_ply)/2 + i*h_ply;
end;
%calculation of Qbar i.e. rotated stiffnes of a lamina
A=zeros(3);
B=zeros(3);
```

```
D=zeros(3);
for i=1:Nplies
    Qbar=zeros(3);
    theta =(thetadb(i)*pi)/180;
    m=cosd(thetadb(i));
    n=sind(thetadb(i));

Qbar(1,1)=(m^4)*Q(1,1)+2*(m^2)*(n^2)*(Q(1,2)+2*Q(3,3))+(n^4)*Q(2,2);%so
mething wrong
    Qbar(1,2)=(m^2)*(n^2)*(Q(1,1)+Q(2,2)-
4*Q(3,3))+((m^4)+(n^4))*Q(1,2);
    Qbar(1,3)=(m^3)*n*(Q(1,1)-Q(1,2)-2*Q(3,3))+m*(n^3)*(Q(1,2)-
Q(2,2)+2*Q(3,3));
    Qbar(2,1)=Qbar(1,2);

Qbar(2,2)=(n^4)*Q(1,1)+2*(m^2)*(n^2)*(Q(1,2)+2*Q(3,3))+(m^4)*Q(2,2);
    Qbar(2,3)=m*(n^3)*(Q(1,1)-Q(1,2)-2*Q(3,3))+(m^3)*n*(Q(1,2)-
Q(2,2)+2*Q(3,3));
    Qbar(3,1)=Qbar(1,3);
    Qbar(3,2)=Qbar(2,3);
    Qbar(3,3)=(m^2)*(n^2)*(Q(1,1)-2*Q(1,2)+Q(2,2))+(((m^2)-
(n^2))^2)*Q(3,3);
     Qdb(:,:,i)=Qbar;
    A=A+Qbar*h_ply;
    B=B+Qbar*h_ply*zbar(i);
    D = D + Qbar * (h_ply * zbar(i)^2  + h_ply^3 / 12);
end


%Exx is the Laminate Youngs modulus in X units in MPa
%Eyy is the Laminate Youngs modulus in Y units in MPa
%Gxy is the Laminate Shear modulus in X units in MPa
Exx= (A(1,1)-((A(1,2)^2)/A(2,2)))/(Nplies*h_ply);
Eyy= (A(2,2)-((A(1,2)^2)/A(1,1)))/(Nplies*h_ply);
Gxy=A(3,3)/((Nplies*h_ply));
uxy=A(1,2)/A(2,2);
% Finding the Reqd matrices from ABD
%Chaning units of A ,B to N-m ,D is fine
% Defining Failiure criteria
%Units in MPA
S11_max_Compression=1889.1639;
S22_max_Compression=69.63706677643123;
S12_max=93;
A=A*1000000;
B=B*1000;

Ai=inv(A);
D_star=D-(B*Ai*B);
D1=inv(D_star);
B1=-Ai*B*inv(D_star);
C1=-inv(D_star)*B*Ai;
A1=Ai+Ai*B*inv(D_star)*B*Ai;
N=zeros(3,1);
%Nxx is N(1)
N(1)=00;
%Nyy is N(2)
```

```
N(2)=0;
% e is the strains
%z_mid_plane_ply is the z co-ordinate of the midplane of each ply units
in
%meters


a=0;
z_mid_plane_ply= (-h/2 +h_ply/2)/1000;
while (a<1)
e=A1*N;
k=C1*N;
edb=zeros(3,1,Nplies);

for i=1:Nplies
    edb(:,:,i)=A1*N+z_mid_plane_ply*k;
    %h_ply converted to meters
    z_mid_plane_ply=z_mid_plane_ply+h_ply/1000;
end

% calculating Plywise stresses
stressdb=zeros(3,1,Nplies);
%stress units in GPa
for i=1:Nplies
    stressdb(:,:,i)= Qdb(:,:,i)*edb(:,:,i);

end
%converting stresses to MPa
stressdb=stressdb*1000;
%stresses in material co-ordinate systems

stress_mat=zeros(3,1,Nplies);
for i=1:Nplies

stress_mat(1,1,i)=stressdb(1,1,i)*(cosd(thetadb(i))^2)+stressdb(2,1,i)*
(sind(thetadb(i))^2)+2*stressdb(3,1,i)*cosd(thetadb(i))*sind(thetadb(i)
);

stress_mat(2,1,i)=stressdb(1,1,i)*(sind(thetadb(i))^2)+stressdb(2,1,i)*
(cosd(thetadb(i))^2)-
2*stressdb(3,1,i)*cosd(thetadb(i))*sind(thetadb(i));
    stress_mat(3,1,i)=(-
stressdb(1,1,i)+stressdb(2,1,i))*sind(thetadb(i))*cosd(thetadb(i))+stre
ssdb(3,1,i)*((cosd(thetadb(i)))^2-(sind(thetadb(i)))^2);

    if  stress_mat(1,1,i)>=S11_max_Compression

        fprintf('Failure Occured At Load');
        disp(N);
        e='Failed Ply Angle  ';
        disp(e)
        disp(thetadb(i))
        e='Failed Ply Number  ';
        disp(e);
        disp(i);
```

```
        f='Failure Mode is S11';
        sigma= N/(h_ply*Nplies*1000)
        disp(f);
        a=a+1

    elseif stress_mat(2,1,i)>=S22_max_Compression

        e='Failure Ocuured At Load';
        disp(e);
        disp(N)
        fprintf('Failed Ply is ')
        disp(thetadb(i))
        a=a+1
        f='Failure Mode is S22';
        sigma= N/(h_ply*Nplies*1000)
        disp(f);

    elseif abs(stress_mat(3,1,i))>=S12_max

        e='Failure Occured At Load';
        disp(e)
        disp(N)
        fprintf('Failed Ply Has the angle ')
        disp(thetadb(i))
        a=a+1
        sigma= N/(h_ply*Nplies*1000)
        f='Failure Mode is S12';
        disp(f);
    end
end
 N(1)=N(1)+100;
end
sigma= N/(h_ply*Nplies*1000)
Global_stress_X=zeros(1,Nplies);
for i=1:Nplies
    Global_stress_X(i)=stressdb(1,1,i);
end
Global_stress_X=Global_stress_X/sigma(1)

ply_location=linspace(1,Nplies,Nplies);
subplot(2,1,1);
plot(ply_location,Global_stress_X,'-o')
xlabel('\bf Ply Number')
ylabel('\bf\sigma_{xx}/\sigma_{Gross}')
title('Stress Distribution')
grid minor
axis([0 20 0 5])
str ={{'\bf23^\circ'},{'\bf-23^\circ'},{'\bf23^\circ'},{'\bf-
23^\circ'},{'\bf23^\circ'},{'\bf-
23^\circ'},{'\bf23^\circ'},{'\bf80^\circ'},{'\bf-80^\circ'},{'\bf-
80^\circ'},{'\bf80^\circ'},{'\bf23^\circ'},{'\bf-
23^\circ'},{'\bf23^\circ'},{'\bf-23^\circ'},{'\bf23^\circ'},{'\bf-
23^\circ'},{'\bf23^\circ'}} ;
%annotation('textbox',dim,'String',str);

Relative_Global_stress_x=Global_stress_X/min(Global_stress_X)
```

```
subplot(2,1,2);
plot(ply_location,Relative_Global_stress_x,'-o')
title('\bf Relative Stress Distribution')
xlabel('\bf Ply Number')
ylabel('\bf  \sigma_{xx}/\sigma_{min} ')
axis([0 20 -2 20 ])
yc=48
text([1 2 3 4 5 6 7 8 9 10 11 12 13 14 15 16 17 18 ],[yc yc yc yc yc yc
yc yc yc yc yc yc yc yc yc yc yc yc  ],str)
grid on
grid minor
subplot(2,1,2)
Stress_Mismatch=zeros(1,Nplies-1)

figure
for i=1:(Nplies/2)
Stress_Mismatch(i)= abs(Global_stress_X(i)/Global_stress_X(i+1));
end
for i=(Nplies/2):Nplies-1
Stress_Mismatch(i)= abs(Global_stress_X(i+1)/Global_stress_X(i));
end


Interface = linspace(1,17,17)
bar(Stress_Mismatch)
bc=18
text([0.5 1.5 2.5 3.5 4.5 5.5 6.5 7.5 8.5 9.5 10.5 11.5 12.5 13.5 14.5
15.5 16.5 17.5 ],[bc  bc bc  bc bc  bc bc  bc bc  bc bc  bc bc  bc bc
bc bc  bc  ],str)
xlabel('Interface Number')
ylabel('Relative Stress Between Plies')
grid on
axis([0 18 0 20 ])
grid minor
```

APPENDIX D

Sample Number	Layup	Fiber Type	Sample Width (mm)	Sample Thickness (mm)	Gross Failure Stress[1] MPa	Density[2] g/cm^3
1	$(0\ 0\ 0\ 0\ 45\ -45\ 45\ -45\ 90)_S$	T650	38.3	2.54	447.37	1.53
2	$(0\ 0\ 0\ 0\ 45\ -45\ 45\ -45\ 90)_S$	T650	38.3	2.54	445.61	
3	$(0\ 0\ 0\ 0\ 45\ -45\ 45\ -45\ 90)_S$	T650	38.6	2.54	422.7	
4	$(0\ 0\ 0\ 0\ 45\ -45\ 45\ -45\ 90)_S$	T650	38.6	2.54	440.15	
5	$(0\ 0\ 0\ 0\ 45\ -45\ 45\ -45\ 90)_S$	T650	38.6	2.54	458.03	
6	$(0\ 0\ 0\ 0\ 45\ -45\ 45\ -45\ 90)_S$	T650	38.6	2.54	465.25	
7	$(0\ 0\ 0\ 0\ 45\ -45\ 45\ -45\ 90)_S$	IM7	37.6	2.54	438.3	1.54
8	$(0\ 0\ 0\ 0\ 45\ -45\ 45\ -45\ 90)_S$	IM7	38.6	2.54	473.08	
9	$(0\ 0\ 0\ 0\ 45\ -45\ 45\ -45\ 90)_S$	IM7	38.6	2.54	455.11	
10	$(0\ 0\ 0\ 0\ 45\ -45\ 45\ -45\ 90)_S$	IM7	38.3	2.54	439.06	
11	$(0\ 0\ 0\ 0\ 45\ -45\ 45\ -45\ 90)_S$	IM7	38.6	2.54	382.76	
12	$(0\ 0\ 0\ 0\ 45\ -45\ 45\ -45\ 90)_S$	IM7	38.6	2.54	361.81	
13	$(19\ -19\ 19\ -19\ 19\ -19\ 65\ -65\ 65)_S$	T650	38.9	2.54	325.59	1.53
14	$(19\ -19\ 19\ -19\ 19\ -19\ 65\ -65\ 65)_S$	T650	38.3	2.54	346.54	
15	$(19\ -19\ 19\ -19\ 19\ -19\ 65\ -65\ 65)_S$	T650	38.6	2.54	314.48	
16	$(19\ -19\ 19\ -19\ 19\ -19\ 65\ -65\ 65)_S$	T650	38.6	2.54	312.88	
17	$(19\ -19\ 19\ -19\ 19\ -19\ 65\ -65\ 65)_S$	T650	38.6	2.54	316.71	
18	$(19\ -19\ 19\ -19\ 19\ -19\ 65\ -65\ 65)_S$	T650	38.6	2.54	315.61	
19	$(23\ -23\ 23\ -23\ 23\ -23\ 23\ 80\ -80)_S$	T650	38.9	2.54	320.17	1.55
20	$(23\ -23\ 23\ -23\ 23\ -23\ 23\ 80\ -80)_S$	T650	38.9	2.54	320.98	
21	$(23\ -23\ 23\ -23\ 23\ -23\ 23\ 80\ -80)_S$	T650	38.6	2.54	310.97	
22	$(23\ -23\ 23\ -23\ 23\ -23\ 23\ 80\ -80)_S$	T650	38.9	2.54	290.01	

[1] Calculated according to ASTM D6484 [17]
[2] Density tested according to ASTM 792-00 [40] using a METTLER TOLEDO AG245 analytical balance

23	(23 -23 23 -23 23 -23 23 80 -80)$_S$	T650	38.6	2.54	304.76	
24	(23 -23 23 -23 23 -23 23 80 -80)$_S$	T650	38.1	2.54	315.68	
25	(14 -14 14 -14 14 60 -60 60 -60)$_S$	T650	38.9	2.54	299.65	1.54
26	(14 -14 14 -14 14 60 -60 60 -60)$_S$	T650	37.9	2.54	318.01	
27	(14 -14 14 -14 14 60 -60 60 -60)$_S$	T650	37.9	2.54	295.2	
28	(14 -14 14 -14 14 60 -60 60 -60)$_S$	T650	38.1	2.54	297.74	
29	(14 -14 14 -14 14 60 -60 60 -60)$_S$	T650	37.9	2.54	354.76	
30	(14 -14 14 -14 14 60 -60 60 -60)$_S$	T650	38.6	2.54	305.11	
31	(23 -23 23 -23 23 -23 23 80 -80)$_S$	IM7	38.3	2.54	294.25	1.55
32	(23 -23 23 -23 23 -23 23 80 -80)$_S$	IM7	38.1	2.54	286.76	
33	(23 -23 23 -23 23 -23 23 80 -80)$_S$	IM7	38.3	2.54	291.34	
34	(23 -23 23 -23 23 -23 23 80 -80)$_S$	IM7	38.3	2.54	318.91	
35	(23 -23 23 -23 23 -23 23 80 -80)$_S$	IM7	38.6	2.54	314.48	
36	(23 -23 23 -23 23 -23 23 80 -80)$_S$	IM7	38.3	2.54	309.47	
37	$(45,0,-45,90)_{4s}$	T650	38.1	4.318	308.59	1.54
39	$(45,0,-45,90)_{4s}$	T650	38.3	4.318	315.86	
40	$(45,0,-45,90)_{4s}$	T650	38.6	4.318	307.95	
41	$(45,0,-45,90)_{4s}$	T650	37.8	4.318	325.21	

REFERENCES

[1] Tsai, S., Daniel, J., Sihn, S., Arteiro, A. and Rainsberger, R. (2017). Fiber-Composite Laminates Theory and practice of analysis, design and automated layup. Stanford, CA: Stanford University, 2017.

[2] Dodwell, T., Butler, R. and Rhead, A. (2016). Optimum Fiber Steering of Composite Plates for Buckling and Manufacturability. AIAA Journal, 54(3), pp. 1146-1149.

[3] Composites.ugent.be. (2018). Home Made Composites (HomMaCom) - What are composites? [Online] Available at: http://www.composites.ugent.be/home_made_composites/what_are_composites.html [Accessed 25 Jan. 2018].

[4] Aly, A. (2017). The manufacturing and integration of fluidic oscillators for composite aircraft structures. Master's. Georgia Institute of Technology.

[5] Pradhan, B. and Santra, M. (1984). Hole reinforcement for reducing SCF in uniaxially loaded FRP composite plates containing central circular holes. Fibre Science and Technology, 21(2), pp. 149-160.

[6] Dang, T., Hallet, S., Kim, B., Cahain, Y., Butler, R. and Liu, W. (2014). Modelling of as manufactured geometry for prediction of impact and compression after impact behaviour of variable angle tow laminates. Journal of Composite Materials, 49(12), pp.1423-1438.

[7] Nielsen, M., Johnson, K., Rhead, A. and Butler, R. (2017). Laminate design for optimised in-plane performance and ease of manufacture. Composite Structures, 177, pp. 119-128.

[8] Gibson, R. (2011). Principles of Composite Material Mechanics, Third Edition. Hoboken: CRC Press.

[9] Liu, Y., Zwingmann, B. and Schlaich, M. (2015). Carbon Fiber Reinforced Polymer for Cable Structures—A Review. Polymers, 7(10), pp. 2078-2099.

[10] Lee, D. and Suh, N. (2006). Axiomatic design and fabrication of composite structures. New York: Oxford University Press.

[11] Mallick, P. (1993). Fiber-reinforced composites. New York: M. Dekker.

[12] Compositesworld.com. (2017). Open-hole compression testing. [Online] Available at: https://www.compositesworld.com/articles/open-hole-compression-testing [Accessed 7 Nov. 2017].

[13] Compositesworld.com. (2017). A400M wing assembly: Challenge of integrating composites. [Online] Available at: https://www.compositesworld.com/articles/a400m-wing-assembly-challenge-of-integrating-composites [Accessed 18 Nov. 2017].

[14] Reddy, J. and Pandey, A. (1987). A first-ply failure analysis of composite laminates. Computers & Structures, 25(3), pp. 371-393.

[15] Irisarri, F., Bassir, D., Carrere, N. and Maire, J. (2009). Multiobjective stacking sequence optimization for laminated composite structures. Composites Science and Technology, 69(7-8), pp. 983-990.

[16] Hahn, H. and Tsai, S. (1974). On the Behavior of Composite Laminates after Initial Failures. Journal of Composite Materials, 8(3), pp. 288-305.

[17] D6484/D6484M-09 Standard Test Method for Open-Hole Compressive Strength of Polymer Matrix Composite Laminates. , (2009). West Conshohocken, PA: ASTM International.

[18] Elhajjar, R. and Shams, S. (2014). Compression testing of continuous fiber reinforced polymer composites with out-of-plane fiber waviness and circular notches. Polymer Testing, 35, pp. 45-55.

[19] Amacher, R., Cugnoni, J., Botsis, J., Sorensen, L., Smith, W. and Dransfeld, C. (2014). Thin ply composites: Experimental characterization and modeling of size-effects. Composites Science and Technology, 101, pp. 121-132.

[20] Iarve, E., Kim, R. and Mollenhauer, D. (2007). Three-dimensional stress analysis and Weibull statistics based strength prediction in open hole composites. Composites Part A: Applied Science and Manufacturing, 38(1), pp. 174-185.

[21] National Institute for Aviation Research (2017). Solvay Cytec Cycom 5320-1 T650 Unitape Qualification Material Property Data Report. National Center for Advanced Materials Performance.

[22] Berbinau, P., Soutis, C., Goutas, P. and Curtis, P. (1999). Effect of off-axis ply orientation on 0°-fibre microbuckling. Composites Part A: Applied Science and Manufacturing, 30(10), pp. 1197-1207.

[23] Wu, Z., Weaver, P., Raju, G. and Chul Kim, B. (2012). Buckling analysis and optimisation of variable angle tow composite plates. Thin-Walled Structures, 60, pp. 163-172.

[24] Arteiro, A., Catalanotti, G., Xavier, J. and Camanho, P. (2013). Notched response of non-crimp fabric thin-ply laminates. Composites Science and Technology, 79, pp. 97-114.

[25] Burns, L., Mouritz, A., Pook, D. and Feih, S. (2012). Bio-inspired design of aerospace composite joints for improved damage tolerance. Composite Structures, 94(3), pp. 995-1004.

[26] Khechai, A., Tati, A., Guerira, B., Guettala, A. and Mohite, P. (2018). Strength degradation and stress analysis of composite plates with circular, square and rectangular notches using digital image correlation. Composite Structures, 185, pp. 699-715.

[27] Stone, D. (2008). The influence of ply orientation on the open-hole tension strength of composite laminates. Master's. Washington State University.

[28] Soden, P., Kaddour, A. and Hinton, M. (2004). Recommendations for designers and researchers resulting from the world-wide failure exercise. Composites Science and Technology, 64(3-4), pp. 589-604.

[29] Vankan, W., Tijs, B., de Jong, G., de Frel, H. and Singh, N. (2016). Strength of notched and un-notched thermoplastic composite laminate in biaxial tension and compression. Journal of Composite Materials, 50(25), pp. 3477-3500.

[30] Rast, J. (2009). Characterizing the Fatigue Damage in Non-Traditional Laminates of Carbon Fiber Composites Using Radiography. Master's. Georgia Institute of Technology.

[31] Progressive Failure Analysis Methodology for Laminated Composite Structures. (1999). Hampton Virginia: NASA, p. 4.

[32] Staab, G. (2015). Laminar composites. Butterworth-Heinemann.

[33] Sun, C. and Chin, H. (1988). Analysis of asymmetric composite laminates. AIAA Journal, 26(6), pp 714-718.

[34] Saeed, M., Chen, Z., Chen, Z. and Li, B. (2014). Compression behavior of laminated composites subjected to damage induced by low velocity impact and drilling. Composites Part B: Engineering, 56, pp. 815-820.

[35] Tsai, S. and Wu, E. (1971). A General Theory of Strength for Anisotropic Materials. Journal of Composite Materials, 5(1), pp. 58-80.

[36] D3039/D3039M-17 Standard Test Method for Tensile Properties of Polymer Matrix Composite Materials. (2017). West Conshohocken, PA: ASTM International.

[37] D6641/D6641M-16e1 Standard Test Method for Compressive Properties of Polymer Matrix Composite Materials Using a Combined Loading Compression (CLC) Test Fixture. (2016). West Conshohocken, PA: ASTM International.

[38] D3518/D3518M-13 Standard Test Method for In-Plane Shear Response of Polymer Matrix Composite Materials by Tensile Test of a ±45° Laminate. (2013). West Conshohocken, PA: ASTM International.

[39] Reinarz, A., Dodwell, T., Fletcher, T., Seelinger, L., Butler, R. and Scheichl, R. (2018). Dune-composites – A new framework for high-performance finite element modelling of laminates. Composite Structures, 184, pp .269-278.

[40] ASTM D792-00 Standard Test Methods for Density and Specific Gravity (Relative Density) of Plastics by Displacement, ASTM International, West Conshohocken, PA, 2000.